Ordered mono- and multi-layers from nanographene derivatives

Dissertation

zur Erlangung des akademischen Grades
Doctor rerum naturalium
(Dr. rer. nat.)
im Fach Chemie
eingereicht an der

Mathematisch-Naturwissenschaftlichen Fakultät I
Humboldt-Universität zu Berlin

von
Frau Min Ai (M. Sc.)
geboren am 25.11.1977 in Jiangxi

Präsident der Humboldt-Universität zu Berlin:

Prof. Dr. Dr. h. c. Christoph Markschies

Dekan der Mathematisch-Naturwissenschaftlichen Fakultät I:
Prof. Dr. Lutz-Helmut Schön

Prof. Dr. Jürgen P. Rabe

Prof. Dr. Klaus Rademann

Prof. Dr. Paolo Samorì

eingereicht am: 06.11.2009
Tag der mündlichen Prüfung : 20.11.2009

Zusammenfassung

Die vorliegende Dissertation berichtet über die Untersuchung von selbst-aggregierten Einfach- und Mehrfachschichten aus Nanographenen-Derivate mit Hilfe der Rastertunnelmikroskopie (RTM) an Fest-Flüssig-Grenzflächen. Die π-Konjugation bringt einzigartige elektronische Eigenschaften mit sich, so dass die Nanographen-Derivate viel versprechende Bausteine für eine molekulare und organische Elektronik sind, da sie maßgeschneidert und kostengünstig prozessiert werden können, und leicht und flexibel sind. Für elektronische Anwendungen ist es notwendig, die Nanographene in ultradünnen Filmen mit geordneten supramolekularen Strukturen zu organisieren.

Nanostrukturen werden für Nanographene-Derivate auf hoch orientiertem pyrolytischem Graphit (HOPG) untersucht, wie zum Beispiel alkylierte Hexi-*peri*-hexabenzocoronene (HBCs) unterschiedlicher Symmetrie und dreiecksförmige polyzyklische aromatische Kohlenwasserstoffe (PAK). Es zeigt eine erstaunliche Vielfalt von supramolekularen Strukturen, z.B. Zick-Zack-, Blumen- oder Honigwaben-Muster. Eine faszinierende Besonderheit besteht in den Honigwaben Strukturen, die sich durch Selbstaggregation dreieckiger alkylierter Phenyl-PAKs bilden, und die damit Nanotemplate für Gastmoleküle darstellen.

In vielen Fällen bilden Nanographene-Derivate nicht nur Monoschichte sondern auch Multischichten auf Graphit. Die Selbstorganisation von Doppelschichten aus einer HBC-Stern-Verbindung bietet das Potenzial für Baustelemente in der organischen Elektronik, zum Beispiel für Nanodrähte. Die alkylierten Phenyl-HBCs bilden polykristalline Strukturen sowohl in der "face-on"-Anordnung in Monoschichten auf Graphit wie in der "edge-on"-Anordnung in Multischichten, die sich in einem äußeren elektrischen Feld bilden. Beides kann nützlich sein, da für die mögliche Anwendung in einer Photovoltaik-Zelle die "face-on"-Orientierung auf Oberflächen erforderlich ist, während für organische Feldeffekt-Transistoreneine "edge-on" Nanostruktur benötigt wird.

RTM

Nanographene

HBC

PAK

Nanotemplate

Abstract

This thesis reports on the investigation of self-assembled mono- and multilayers from nanographene derivatives via scanning tunneling microscopy (STM) at solid-liquid interfaces. Because of the unique electronic properties associated with their π-bonded topology, nanographenes are promising building blocks for molecular and organic electronics, which provide the possibility of tunability together with low-cost processing, light weight, and flexibility. For the application in electronics it is necessary to organize nanographenes in ultrathin films with well-ordered supramolecular structures.

Nanostructures of monolayers on Highly Oriented Pyrolytic Graphite (HOPG) are studied for different nanographene derivatives, such as alkylated hexa-*peri*-hexabenzocoronenes (HBCs) with different symmetries, and triangle-shaped polycyclic aromatic hydrocarbons (PAHs). They exhibit a surprising diversity of supramolecular structures, for example zigzag, flower-like or honeycomb shapes. A fascinating peculiarity provides the honeycomb structures which are self-assembled from triangle-shaped alkylated phenyl PAHs, which provide nanotemplates to accommodate guest molecules.

In many cases, nanographene derivatives not only form monolayers but also multilayers on HOPG. Star-shaped HBC molecules self organize into bilayers in polar solvents, which exhibit the potential for the formation of building blocks of organic electronics, for instance nanowires. The alkylated phenyl HBCs form polycrystalline structures both in the “face-on” arrangement in a monolayer on HOPG, and “edge-on” in multilayers within an external electric field. Both may be useful for potential applications, since in a photovoltaic cell, the “face-on” orientation on surfaces is required, while for the purpose to be applied in organic field-effect transistors, the “edge-on” nanostructure on the electrodes is necessary.

STM

Nanographene

HBC

PAH

nanotemplate

Table of Contents

Zusammenfassung 2
Abstract 4
Abbreviations and symbols 1
1 Introduction 3
2 Background 4
2.1 Organic and molecular electronics 4
2.1.1 Organic electronics 4
2.1.2 Molecular electronics 9
2.2 Nanotemplates 10
2.3 Nanographenes 15
2.3.1 Electronic devices based on nanographenes 15
2.3.2 Synthesis of polycyclic aromatic hydrocarbon derivatives 17
2.4 Self-assembly of molecules at surfaces 24
2.4.1 Physisorption 25
2.4.2 Dynamics from physisorption 26
2.4.3 Chemisorption 26
2.5 Scanning probe microscopy 28
2.5.1 Scanning tunneling microscopy 28
2.5.1.1 Basic principle of scanning tunneling microscopy 29
2.5.1.2 Operating modes 30
2.5.1.3 Theory of scanning tunneling microscopy 32
2.5.1.4 Scanning tunneling microscopy of molecules on surfaces 32
2.5.2 Scanning force microscopy 33
2.5.2.1 Fundamental principles of Scanning force microscopy 34
2.5.2.2 Interacting forces 34
3 Experimental section 37
3.1 Scanning tunneling microscopy 37
3.1.1 Sample preparation 38
3.2 Scanning force microscopy 39
3.3 Image processing 40
4 Results and Discussion 41
4.1 Self-assembled 2D monolayer from one substance 41
4.1.1 HBC self-assembly influenced by the position of $C_{12}H_{25}$-substituents 41
4.1.2 Triangle-shaped nanographene derivatives 45
4.2 Self-assembled 2D monolayers from two substances 56
4.2.1 Non-covalent electron donor/ electron acceptor coadsorption 56
4.2.2 Chicken-wire nanostructures selection for guest molecules 64
4.3 Investigation of molecular multilayers 70
4.3.1 HBC-amine bilayer 70
4.3.2 Star-shaped nanographene derivative ordering with solvent 76
4.3.3 Alkylated phenyl-HBC nanostructure at an interface and on a surface 81
5 Conclusions and Outlooks 86
6 References 89
A Acknowledgements 100
B Lebenslauf 102
C Publications 103
D Erklärung 104

Abbreviations and symbols

BDA	4-4'-biphenyl dicarboxylic acid
2D	Two-dimensional
DBA	Dehydrobenzoannulene
EMLs	Emissive layers
ETLs	Electron transport layers
FIB	Focussed ion beam
ΔG	Change of Total free energy
ΔH	Change of Enthalpy
HBC	Hexabenzocoronene
HOMO	Highest Occupied Molecular Orbital
HOPG	Highly Oriented Pyrolytic Graphite
HTL	Hole transport layer
ITO	Indium tin oxide
I(*V*)	Current-voltage characteristic
LB	Langmuir-Blodgett
LUMO	Lowest Unoccupied Molecular Orbital
OFET	Organic Field-Effect Transistor
OLED	Organic Light-Emitting Diode
PAH	Polycyclic Aromatic Hydrocarbon
PEDOT	Poly(ethylene-dioxythiophene)

PSS	Poly(styrene sulfonic acid)
PTCDI	Perylene tetracarboxylic diimide
PTFE	Poly(tetrafluoroethylene)
Δ S	Change of Entropy
SFM	Scannning Force Microscopy
STM	Scanning Tunneling Microscopy
6T	α-sexithiophene
TDA	4, 1', 4', 1"-terphenyl-1, 4"-dicarboxylic acid
TSB35	1,3,5-tris[(E)-2-(3,5-didecyloxyphenyl)-ethenyl]-benzene
UHV	Ultrahigh vacuum
V	Bias voltage
ϕ	Average work function between the two electrodes.
Ψ	Electron wave functions

1 Introduction

Organic and molecular electronics have been attractive in last decades, since organic molecules provide the possibilities of easy tunability together with low-cost processing, and organic materials have been successfully explored for the application in electronic devices. Organic electronic devices are organic light-emitting diodes (OLEDs)[1], organic field-effect transistors (OFETs)[2], organic photovoltaic cells [3] and organic semiconductor lasers[4]. In order to miniaturize electronics, molecular electronics with few molecules or a single molecule may become a solution with advantages[5]. Polycyclic aromatic hydrocarbons with extended π-conjugation in the plane and π-π stack formation provide the possibility to be integrated into some organic and molecular devices.

The invention of scanning probe microscopy by Binnig, Rohrer, Gerber and Weibel [6,7] led into a new age of investigations of organic and molecular electronics. In particular, scanning tunneling microscopy (STM) allows to image molecular patterns and measure electronic properties of ultrathin films. The two dimensional molecular arrangement will play a very important role for electronics, for instance with regard to the key property of charge mobility. Self-assembled nanotemplates open a new route by the bottom-up approach to design organic and molecular electronic properties via host-guest systems.

In this thesis, nanostructures formed by various PAHs derivatives are investigated. The text is organized as follows: Chapter 2 focuses on scientific background. At first organic electronics, molecular electronics and nanotemplates will be presented, and then nanographene will be introduced, and the general principles of molecular self-assembly on surfaces will be covered. Furthermore, the principles of scanning probe microscopy will be presented with a special focus on scanning tunneling microscopy. Chapter 3 is dedicated to the experimental part: sample preparation, equipment and image processing. Chapter 4 presents the results and discussion. It covers two-dimensional self-assembled monolayers formed by homo-molecules and hetero-molecules. Moreover, multilayers are introduced. Chapter 5 reports conclusions and gives outlooks for further work.

2 Background

2.1 Organic and molecular electronics

2.1.1 Organic electronics

The early discoveries of conducting and semiconducting organic polymers in the 1970s have in the meantime led to promising applications in the field of organic electronics [8]. Along these lines, organic chemists have pursued various π-conjugated systems as active components for electronic and optoelectronic devices. Some of the devices reach the consumer market. The most successful is the organic light emitting device, which is currently used in long lived and highly efficient color displays. Not far behind organic light emitting devices are organic thin film transistors and strong efforts are devoted to low cost and efficient organic solar cells. Ultimately, some more exotic devices, e.g. organic lasers and memories, may become commercial. The organic materials used in electronic and optoelectronic devices may be divided into three groups: small molecules, dendrimers [9] and polymers.

1) Organic Light Emitting Diodes (OLEDs)
Electrically stimulated light emission from organic molecular crystals was published by Bernanose *et. al* in 1953 [2]. In 1987 the first thin film heterojunction OLED based on a fully organic heterojunction of a hole transporting and an electron transporting material was developed by Tang and Van Slyke [10]. Since then the scientific research in the field of OLEDs has developed enormously [2,11], leading to first commercial devices. In 1997, the Japanese company Pioneer introduced a car stereo with an OLED display. Nowadays, commercially mostly passive matrix displays with display diagonals up 3.8 in. have been addressed. Meanwhile, larger demonstrators with display diagonals up to 40 in. have been presented [2].

A standard OLED is comprised of a transparent, high work function anode (usually glass coated with electrically conductive indium tin oxide (ITO)), an organic hole injection and

transport layer, an organic emission and electron transport layer, and a reflective cathode with low work function, like MgAg or Al (Figure 2.1).

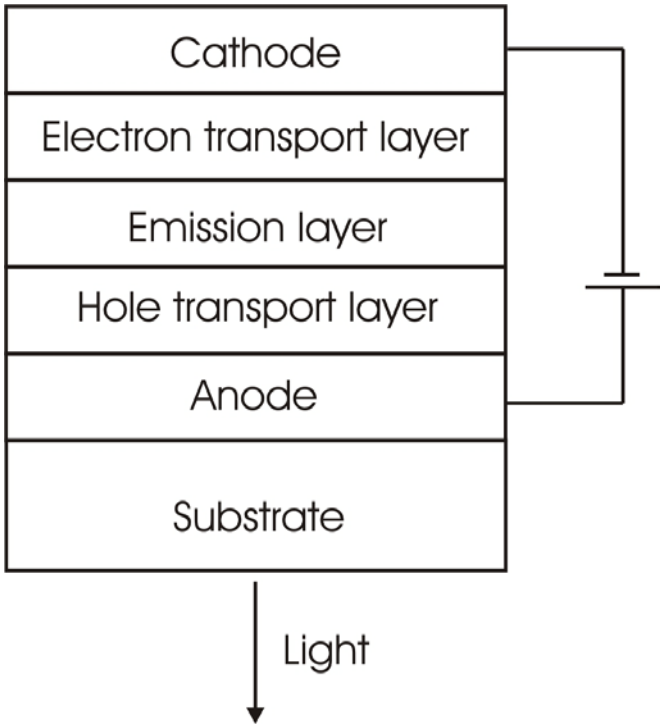

Figure 2.1: Schematic structure of a standard OLED [2].

2) Organic Field-Effect Transistors (OFETs)

Since the first FETs based on polymer [12] and small molecule [13] semiconductors were reported, the interest in OFETs has risen for both technological and scientific reasons. Due to the relatively low charge carrier mobilities OFETs will not directly compete with inorganic transistors (silicon or gallium arsenide) in their current fields of application, but organic transistors and circuits are interesting because they have the potentional to serve in inexpensive and flexible electronic circuits. The possible applications are radio frequency identification tags [14] and flexible displays [15].

A field-effect transistor requires several layers: a thin semiconducting layer, which is separated from a gate electrode by the insulating gate dielectric; source and drain electrodes separated by a distance and in contact with the semiconducting layer, depicted in Figure 2.2. The organic semiconducting layer is usually vacuum sublimed, spin-coated, or drop-cast depending on the materials. The gate electrode can be a metal or a conducting polymer. As gate dielectrics, inorganic insulators, such as SiO_2, Al_2O_3 and Si_3N_4, or polymeric insulators, for example, poly(methylmethacrylate) or poly(4-vinylphenol) are commonly used. The

source and drain electrodes, which inject charges into the semiconductor, are usually high work function metals such as gold, but conducting polymers such as poly(ethylene-dioxythiophene) doped with polystyrenesulfonic acid (PEDOT:PSS) are used as well.

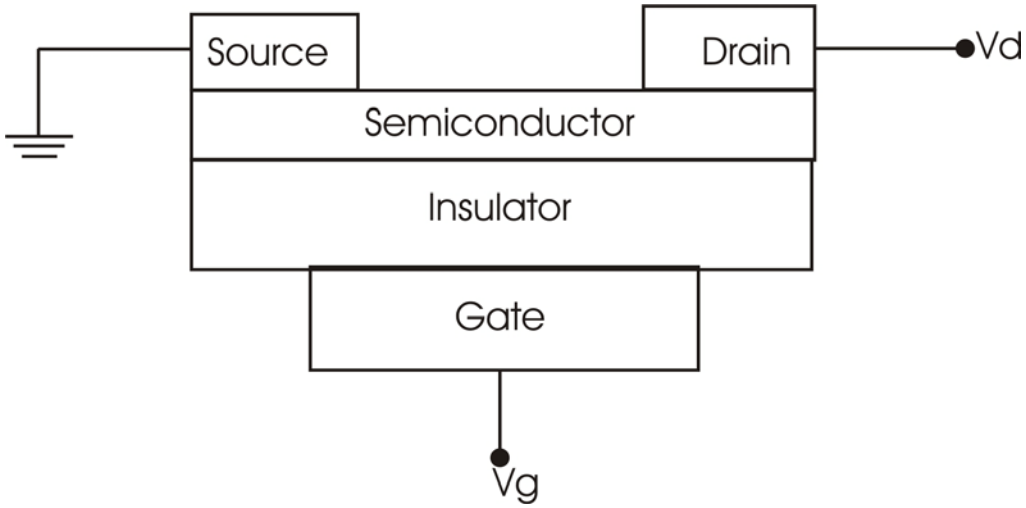

Figure 2.2: Schematic structure of a field-effect transistor and applied voltages. Vd: drain voltage; Vg: gate voltage [1].

3) Organic Photovoltaic Cells

Since organic photovoltaic cells may be manufactured easier and at lower-cost than inorganic semiconductor solar cells, scientific research is stimulated for efficient organic photovoltaic devices [16].

The general structure used for organic solar cells is similar to the OLEDs. The devices are fabricated in sandwich geometry. As substrates, transparent, conducting electrodes (e.g. glass or plastic covered with ITO) are used. The substrate electrode can be structured by a PEDOT:PSS layer, improving the surface quality of the ITO electrode (reducing the probability of shorts) as well as facilitating the hole injection. Furthermore, the work function of this electrode can be changed by chemical or electrochemical redox reactions of the PEDOT layer. The active layer is made from polymers or small molecules. Most polymer-based photovoltaic elements are solution processed at low temperatures, such as spin-coating, doctor blading, screen printing and inkjet printing. For small organic molecules, spin-coating, doctor blading, screen-printing methods and vacuum evaporation are applied. The top electrode is evaporated. In general, a lower work-function metal (as compared to ITO) such as aluminum is used with an ultrathin lithium fluoride underlayer. The schematic device structure is displayed in Figure 2.3 [17].

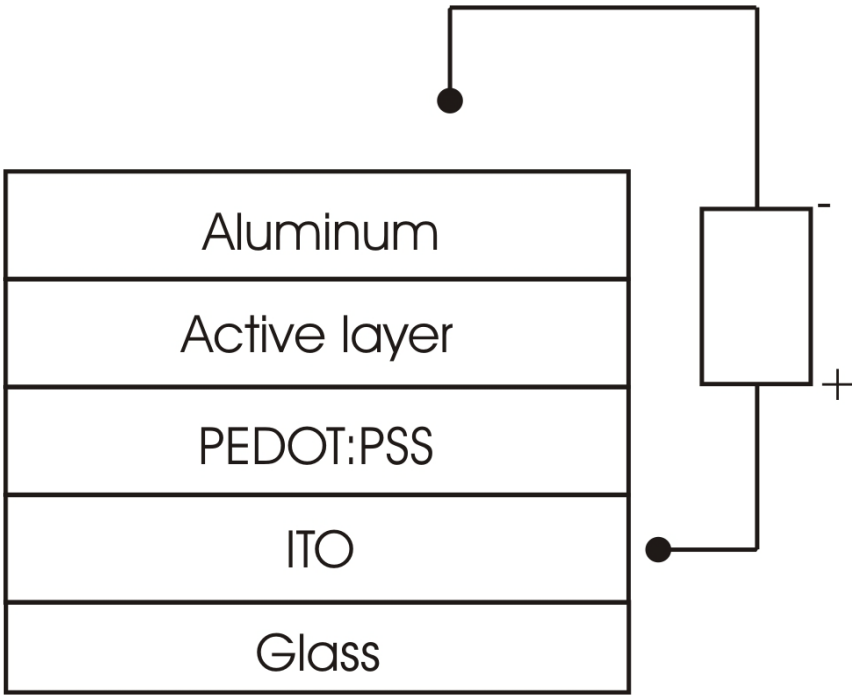

Figure 2.3: Schematic device structure of organic photovoltaic cells [17].

4) Organic Semiconductor Lasers

Organic semiconductors combine novel optoelectronic properties, with simple fabrication and the scope for tuning the chemical structure to give desired features, making them attractive candidates for laser materials. Organic materials for use in laser emission have been a subject of investigation since the first report of a dye laser [18].

A laser consists of a material capable of amplifying light in a cavity or resonator, which applies feedback. The amplification occurs by the process of stimulated emission, illustrated schematically in Figure 2.4. An incident photon stimulates a transition between the excited state and the ground state of the medium, generating further photons. The crucial point about stimulated emission is that the additional photons have the same phase as the incident photon, and this leads to the distinctive coherence of the emitted light, so laser beams can have extremely well-defined frequency and very small divergence.

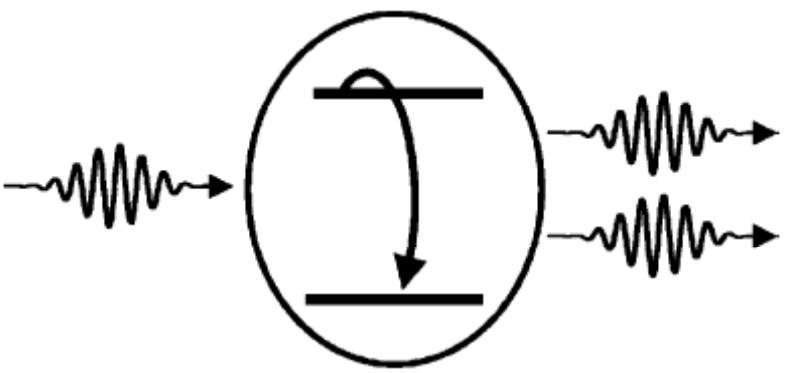

Figure 2.4: Schematic illustration of the stimulated emission process [19].

In certain applications, e.g. organic field electric transistors, batteries and solar cells, high charge mobility is necessary. The mobilities of various semiconducting materials are displayed in Figure 2.5. Charge mobility is intimately connected to the solid-state structure either via the width of conduction- or valence-band (coherent transport), or via the transfer integral and reorganization energy (hopping transport). The molecular organization within a solid has a strong influence on the magnitudes of the bandwidth and the transfer integral. Both quantities are enhanced by a regular, crystalline structure in which there are close intermolecular contacts. The close molecular contacts of conjugated molecules, such as pentacenes and thiophenes, in the solid state appear to fall into two classes: π-stacked and herringbone. Due to electrostatic interactions, π-stacks with adjacent molecules lying directly over one another are unstable with respect to stacks in which the molecules are "slipped" with respect to one another. The "slip" can be resolved into two components: a displacement in the direction of the long molecular axis ("pitch" displacement) and in the direction of the short molecular axis ("roll" displacement). Herringbone packing occurs under the roll displacement [20].

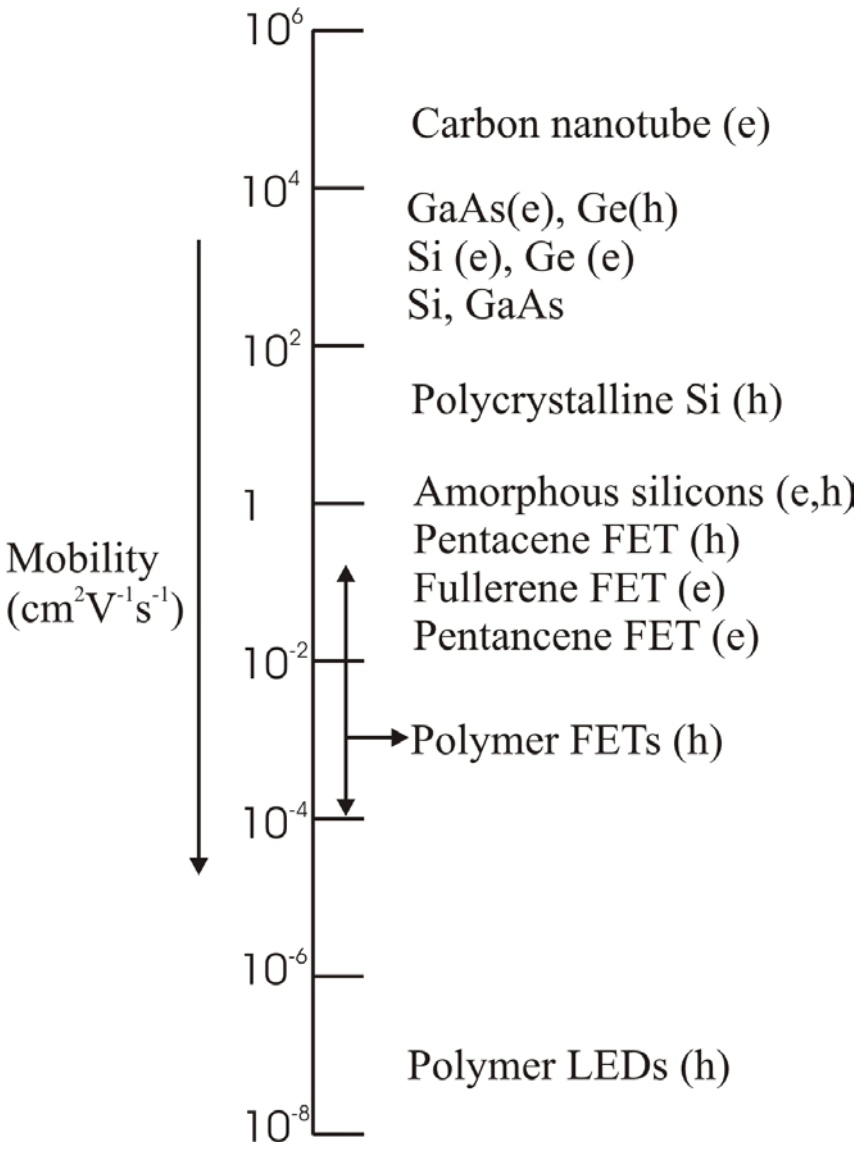

Figure 2.5: Mobility of semiconducting materials. Here “e” denotes electron mobility and “h” is hole mobility [21].

2.1.2 Molecular electronics

Molecular electronics has recently become a very active area of endeavours as an alternative approach to building circuits, i.e. an alternative paradigm to microelectronics device minmization. It is foreseen as a possible and reasonable way to assemble a large number of nanoscale objects (molecules, nanoparticles, nanotubes and nanowires) to from new devices and circuit architectures. The following works paved the foundation of this molecular scale electronics field. In 1971, Mann and Kuhn were the first to report tunneling transport through a monolayer of aliphatic chains [22]. In 1974, Aviram and Ratner theoretically proposed the concept of a molecular rectifying diode, where an acceptor-bridge-donor (A-b-D) molecule can play the same role as a semiconductor p-n junction [23]. Since then, many groups have

reported molecular–scale devices based on organic molecules with size ranging from a single molecule to a monolayer, as shown in Figure 2.6 [24]. The materials selected for study at the molecular scale can be designed with a specific functionality, such as switching function, employing electron donor or electron acceptor properties, and conjugated molecules.

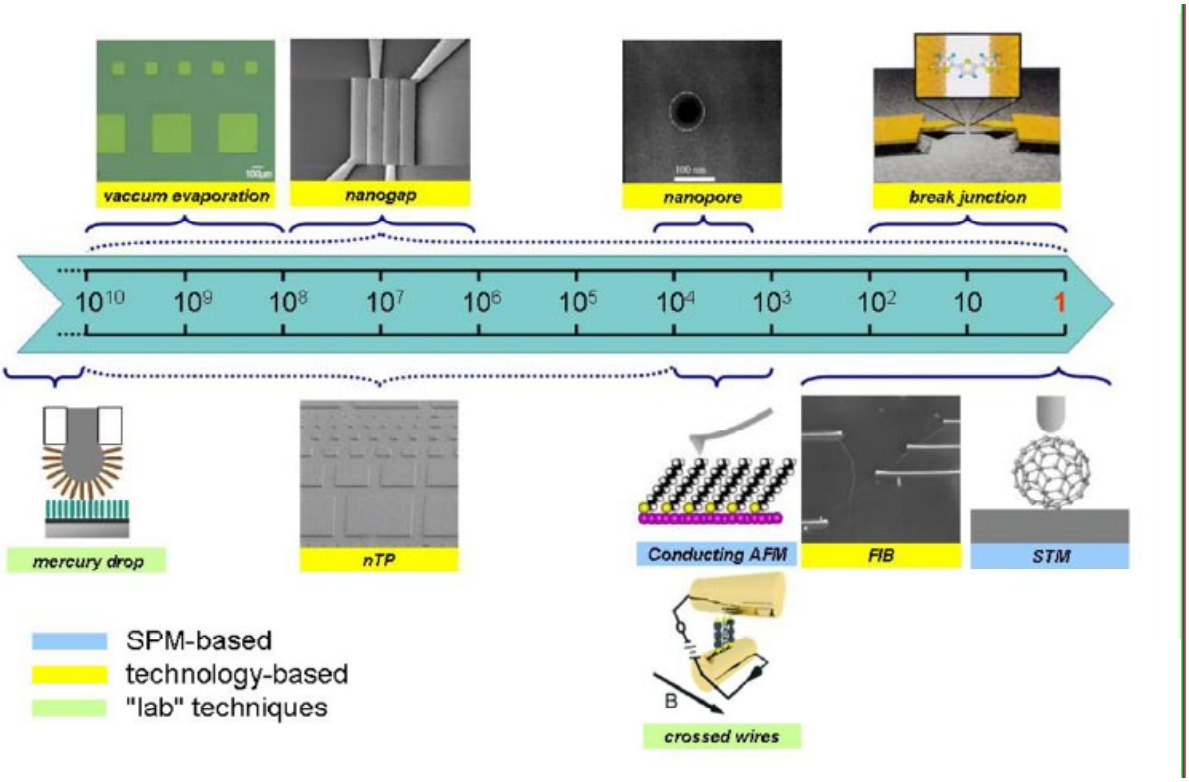

Figure 2.6: A schematic overview of the different test-beds used to electrically contact organic molecules. The scale is the approximate number of molecules contacted from monolayer to single molecule. The techniques are (from left to right): in the upper part micrometer-scale metal evaporation, nanogaps patterned by e-beam lithography, nanopores, break-junctions, and in the lower part mercury drop, nanotransfer printing, conducting SFM, crossed wires, metal deposition by FIB, STM [24].

2.2 Nanotemplates

Highly ordered two-dimentional functional nanostructures have the potential for a broad range of applications in molecule electronics [25], ultra-high density data storage [26], biosensors [27], single-electron [28], single-photon [29] and quantum computation devices [30]. Various surface nanotemplates that are naturally or artificially patterned at the nanometer scale have been used to guide the formation of well-defined periodic nanostructures. In contrast to typical top-down approaches such as a variety of lithography and micro-printing techniques [31], this bottom-up method aims to lead the assembly of atoms and molecules into nanostructures with desired properties, such as controlled shape, composition and high spatial density over macroscopic areas, via inherent processes (adsorption, surface diffusion, nucleation and so on) [32].

In recent years, nanotemplates formed as two-dimensional host-guest systems by non-covalent interactions have attracted much attention in molecular engineering and recognition [33]. The self-assembly of porous networks serve as the host on surfaces and guests accommodated within the cavities have been investigated by scanning tunneling microscopy (STM), which provides real-space structural information at the single molecular level. The main methods for nanotemplate fabrication include:

1) Hydrogen bonding: In ultrahigh vacuum (UHV) STM experiments, the host systems are assembled from two substances which interact with each other through hydrogen bonding. The nanoporous honeycomb network on Ag-passivated Si (111) substrate formed by triple hydrogen-bonds between perylene tetracarboxylic diimdie (PTCDI) and melamine molecules, as displayed in Figure 2.7 [34]. A variation of the post-annealing temperature after deposition of PTCDI and melamine on Au under vacuum lead to the formation of a supramolecular network with parallelogram cavities or hexagonal cavities. Subsequent deposition of C_{70} guest molecules onto these networks results in paired C_{70} in parallelogram voids and C_{70} heptamers in hexagonal voids [35]. At a solid-liquid interface, the porous network formed by trimesic acid self-assembled via hydrogen bonding on HOPG is a two-dimensional nanotemplate to trap coronene or C_{60} guest molecules [36].

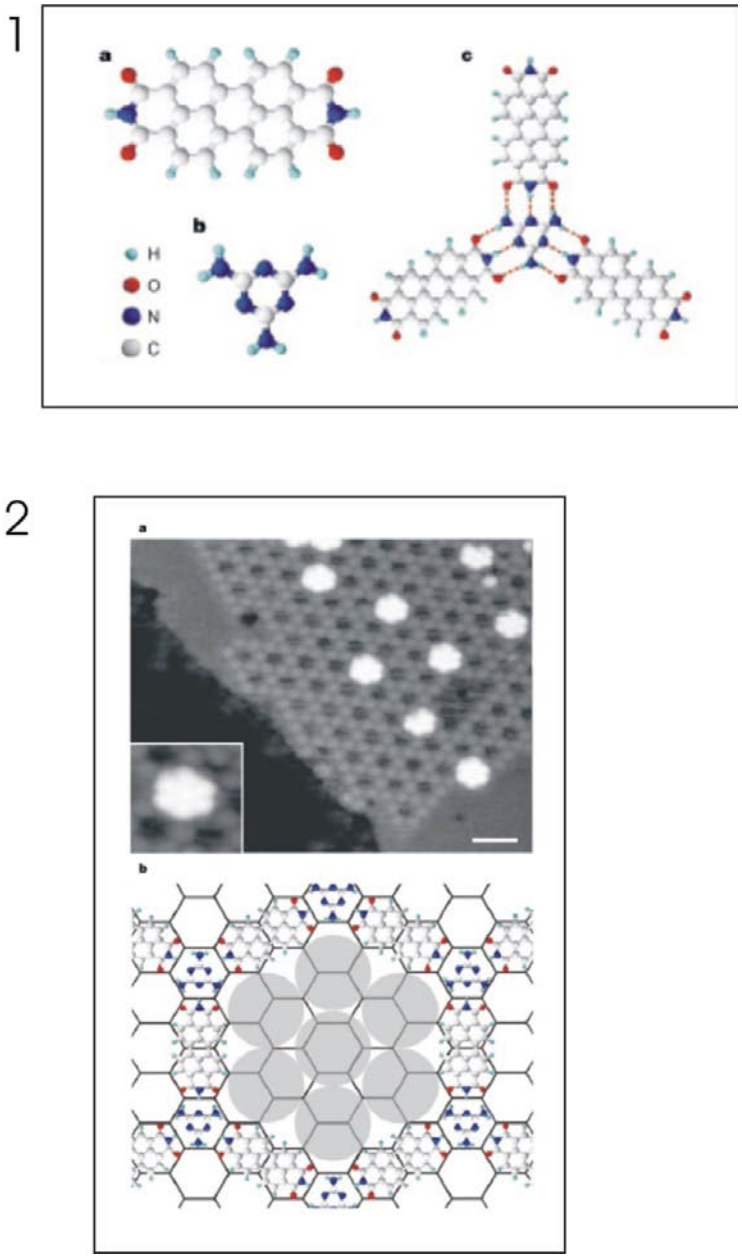

Figure 2.7: 1) a, b, Chemical structures of PTCDI (a) and melamine (b). c, Schematic diagram of a PTCDI-melamine junction. 2) a, STM image of C_{60} heptamers on a PTCDI-melamine network. The inset is a high-resolution view of an individual cluster. Scale bar, 5nm. b, Schematic diagram of a C_{60} heptamer [34].

2) Metal-organic coordination: Hybrid inorganic-organic framework compounds constitute an important class of materials that have been studied extensively over the last few years due to their potential applications in catalysis, gas separation and storage. Other properties which draw attention to these materials include magnetic, optical and electronic properties. It requires to understand how hybrid materials link. The network of polytopic organic carboxylate linker molecules and iron atoms on a Cu (100) surface by the metal-organic coordination has been demonstrated to have an ability to accommodate C_{60} guest molecules in

the pore of the network at the nanoscale [37]. An elegant example is depicted in Figure 2.8. A rectangle Mn-based coordination network on a Au(111) substrate with 4-4'-biphenyl dicarboxylic acid (BDA) as the linker molecule can capture a single C_{60} molecule or C_{60} dimer, aligned in the diagonal direction of the nanocavity rectangle [38].

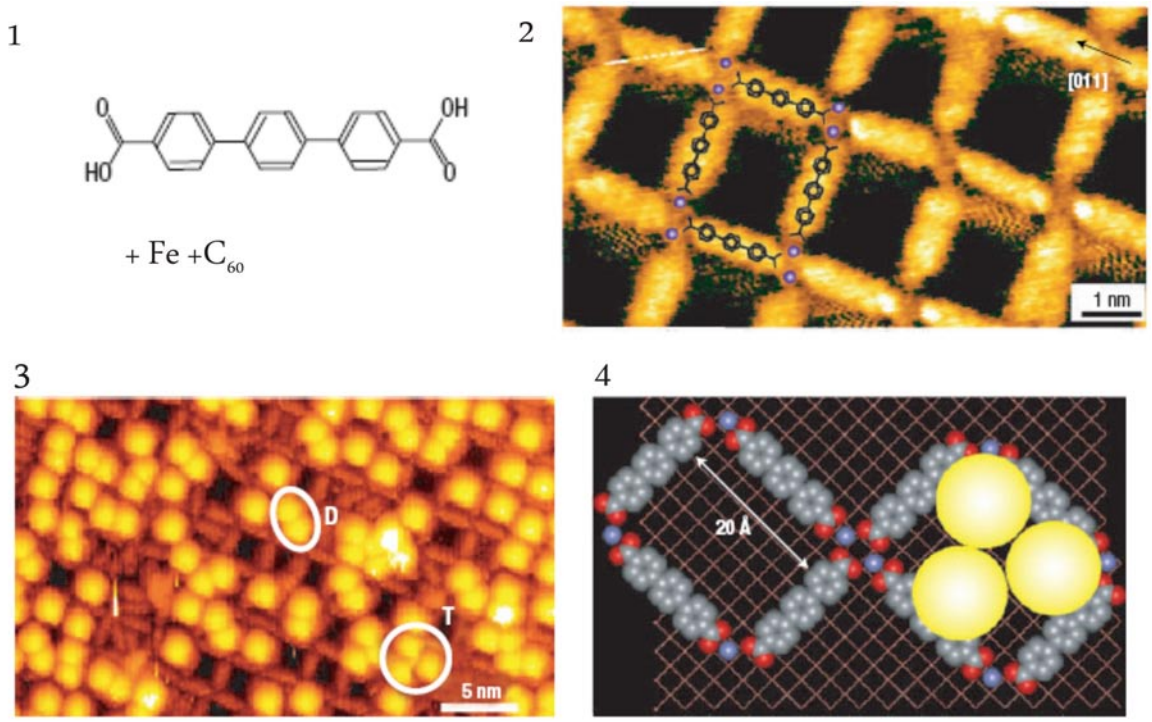

Figure 2.8: 1) Chemical structure of 4, 1', 4', 1"-terphenyl-1, 4"-dicarboxylic acid (TDA), iron atom and C_{60} (b). 2) STM image of Fe-TDA open network with rectangular nanocavities. Arrows on the images indicate the high-symmetry (011) direction of the Cu (100) substrate; positions of molecular backbone and ligands are marked; Fe atoms are shown as blue spheres. 3) The nanocavities in the Fe-TDA networks can host C_{60} monomers, dimers (D) or trimers (T). 4) Schematic diagram of rectangular cavity and accommodation of a C_{60} trimer [37].

3) Charge transfer: C_{60} nanomesh, made up by the binary molecular phases of C_{60} and pentancene on Ag (111) through charge transfer, can accommodate guest C_{60} into the nanocavities, forming ordered 2D C_{60} arrays with large intermolecular distance (2.1 nm) between the nearest neighbor C_{60} molecules, as shown in Figure 2.9 [38]. α-sexithiophene (6T) monolayer nanostripes on HOPG provide an effective surface nanotemplate for the assembly of an ordered "zigzag" C_{60} chain array by the delicate balance of the interactions between the homointermolecular (C_{60}-C_{60} and 6T-6T van der Waals force), heterointermolecualr (C60-6T charge transfer), and molecule-substrate (6T-HOPG, π-π interaction) [39].

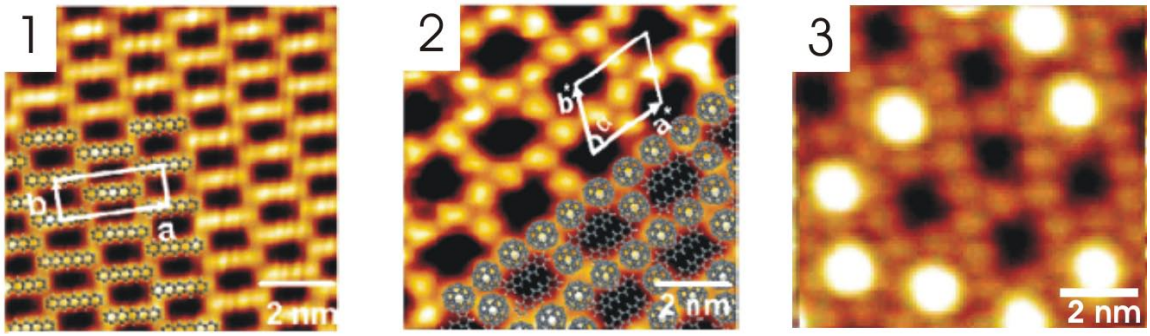

Figure 2.9: 1) STM image of ordered pentacene superstructures on Ag (111). 2) STM image of C_{60} self-assembled into a 2D nanomesh on pentacene; a proposed model is depicted on the image. 3) STM images of C_{60} molecules assembled on the C_{60} nanomesh [40].

4) Van der Waals interactions: A two-dimensional molecular network is self-organized with honeycomb cavities via van der Waals interactions of alkyl chain interdigitation of the 1,3,5-tris[(E)-2-(3,5-didecyloxyphenyl)-ethenyl]-benzene (TSB35) molecules at the interface between the basal plane of HOPG and a solution. The hosting capability of the honeycomb voids has been demonstrated by adding guest molecules, coronene or HBC molecules, depicted in Figure 2.10 [41]. The self-assembled network of the dehydrobenzoannulene (DBA) derivatives also provide appropriately sized cores formed through directional alkyl-chain interdigitation. The host matrix only recognizes and captures flat molecules containing large π-conjugated moieties, such as coronene, hexakis(phenylethynyl benzene), or phthalocyanine [42].

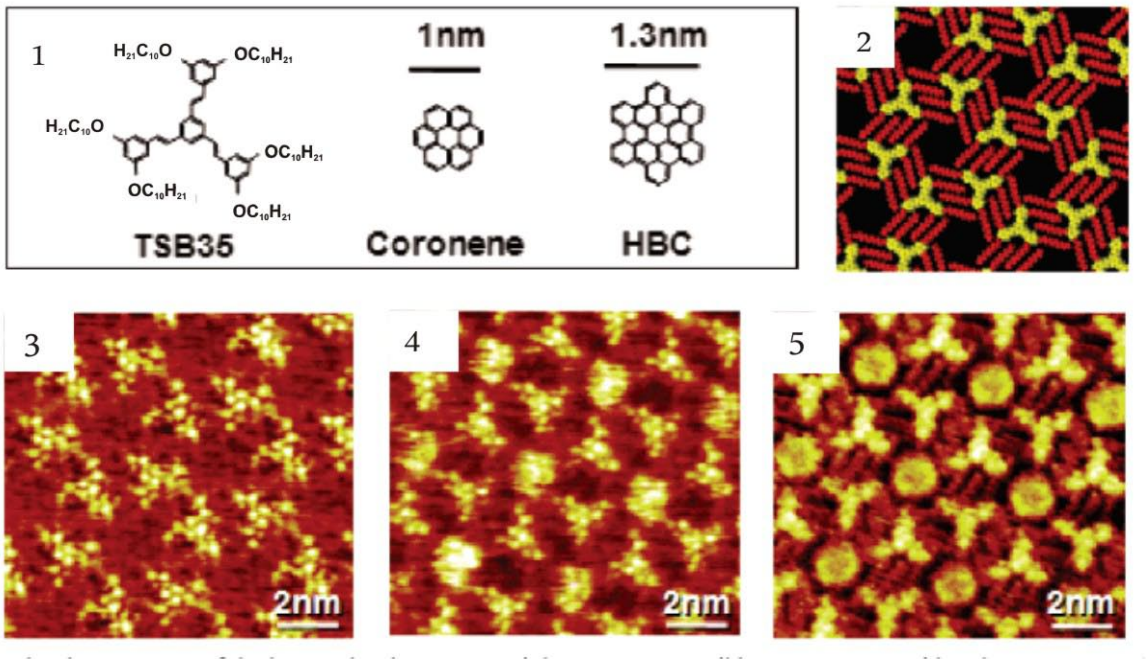

Figure 2.10: 1) Molecular structures of TSB35, coronene and hexabenzocoronene (HBC). 2) the proposed model for the assembly of TSB35 molecules at the HOPG-solution interface. The cavities are bound by barriers formed by the conjugated cores of TSB35 (yellow) and linked by channels constituted by epitaxially adsorbed alkyl moieties (red). 3) STM image of ordered monolayer of TSB35 on HOPG. 4) STM image of coronene hosted in the cavities of the TSB35 network. 5) STM images of HBC molecules assembled in the TSB35 honeycomb voids [41].

2.3 Nanographenes

Graphene is the two-dimensional (2D) building block for carbon allotropes also of other dimensionalities. It can be stacked into 3D graphite, rolled into 1D nanotubes, or wrapped into 0D fullerenes. Transport measurements [43,44] have shown that graphene is a conductor with remarkable electronic properties, which is supported by theory [45]. It makes the transport properties of this material highly interesting from the point of view of both fundamental physics and potential applications. It is widely believed that graphene-based devices may be of outstanding importance for future nanoelectronics. Nanographene is graphene on the nano scale in all three dimensions. It is made up of well-defined, nanosized polycyclic aromatic hydrocarbons (PAHs) possessing interesting electronic properties [46,47]. Self-assembly of PAHs at solid-liquid interfaces and on surfaces shows high structural order which provides the potential to be fabricated for applications, such as molecular wires [48], field effect transistors (FET) [49], photovoltaic devices [50]. Nanographene stand either "edge-on" (FET, molecule wires) or "face-on" (for photovoltaic devices) on the surfaces.

2.3.1 Electronic devices based on nanographenes

The mobility of charge carriers in solid-sate materials is one of the most important parameters determining electronic and optoelectronic performance. These electronic mobilities depend not only on the intrinsic electronic properties of the materials but also on the macroscopic order of the molecules. Structural defects or failure to form a preferred order will dramatically reduce charge carrier mobilities. Organic molecules offer the unique advantage that such mobilities can be increased by establishing supramolecular order within the charge transport channels. The highly ordered packing of HBC derivatives via π-stacking on top of each other offers the favorable overlap. The promising advantages of the columnar approach are obvious: i) defect-free molecular structures are available, ii) easier processing from the melt or from solutions, iii) self-healing ability after the formation of order structure. Due to these advantages, the value of charge carrier mobility is as high as 1.1 $cm^2V^{-1}s^{-1}$ for HBC materials [51,52]. Owing to their unique, highly organized columnar structures and the large π-orbital area of the cores, HBC based materials qualify as active semiconductors in OFETs and photovoltaic devices.

An important requirement for the implementation of discotics in FETs is in the uniaxial alignment of the columnns on the surface of the gate electrode to create a bridge between the source and the drain. By applying an adequate gate voltage, it is possible to accumulate charges at the first monolayers resulting in source-drain current flow. For the application in OFETs (Figure 2.11a), the "edge-on" nanostructure of HBC derivatives in the molecular columns is achieved by a "zone casting" technique [53], by the Field-Force effect [54,55], by the application of magnetic fields [56], expitaxial growth on pre-oriented and friction-deposited poly(tetrafluoroethylene) (PTFE) surfaces [49], by the Langmuir-Blodgett (LB) technique [57], or by thermal processing from the isotropic phase [58].

For the application in photovoltaic cell, the "face-on" orientation on the electrodes is required (Figure 2.11b). The HBC derivatives with large disk cores in columnar arrangements offer the route for charges carrier motion from the anode to the cathode, resulting in improved device performances. The "face-on" arrangement is obtained by rapid cooling rate from the isotropic phase [59], or by adsorption to a surface [60]. All photovoltaic cells based on discotics consist of a two layer system with an electron acceptor and electron donor. When a mixture of HBC-PhC12 (Figure 2.12) and perylene diimide was spin-coated from solution, a controlled phase separation was achieved. The mixture produced vertical layers of both compounds that were separated by a rough interface and therefore led to a large surface contact area between materials [61]. Due to this special morphology, a photovoltaic cell with very high efficiency and an external quantum efficiency as high as 34% at a wavelength of ~490 nm was demonstrated.

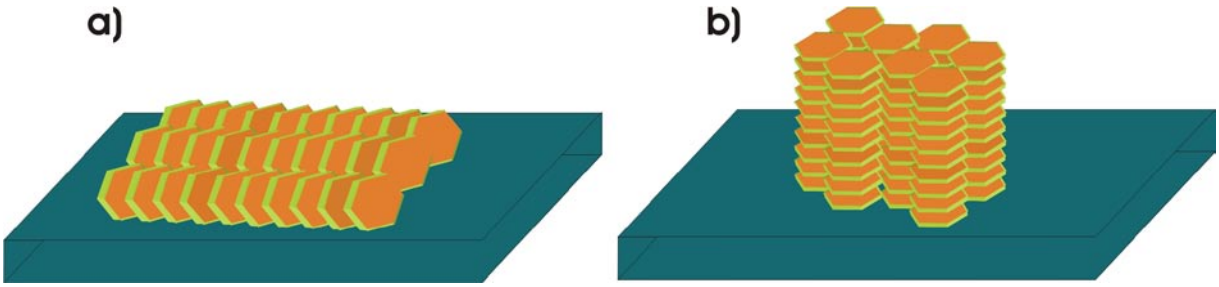

Figure 2.11: Schematic representation of the orientation of the molecules on a surface. a) edge-on arrangement, where the columnar axis is oriented parallel to the surface. b) face-on arrangement.

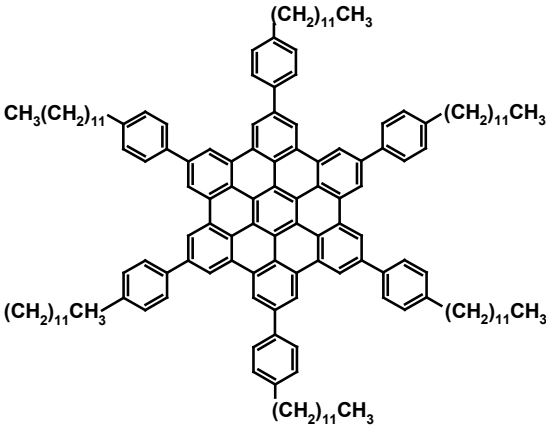

Figure 2.12: Chemical structure of the HBC-PhC_{12} molecules.

Since the development of functional structures is strongly synthesis driven, the synthesis of polycyclic aromatic hydrocarbon derivatives will be introduced in the section 2.3.2.

2.3.2 Synthesis of polycyclic aromatic hydrocarbon derivatives

The properties of variously substituted polycyclic aromatic hydrocarbon will be discussed in charpter 4. They have been synthesized by Dr. Jishan Wu, Xinliang Feng and Xi Dou in the group of Prof. Dr. Klaus Müllen in the Max Planck Institute for Polymer Research in Mainz within a collaborative project.

a) General synthesis concept for hexa-*peri*-hexabenzocoronene (HBC) derivatives

The first synthesis of the parent HBC was carried out by Clar and co-workers [62]. Later Halleux, Scholl, and Müllen *et al.* are the main contributors to the synthensis and structural characterization of various HBCs using different methods [63,64,65,66]. Müllen‘s group has developed an efficient way to prepare HBC and related PAH structures by oxidative cyclodehydrogenation of branched oligophenylenes with Cu (II) salts such as $CuCl_2$ and Cu $(OSO_2CF_3)_2$ catalyzed by $AlCl_3$ [67], and the weaker Lewis acid $FeCl_3$ possessing an oxidation potential sufficient for the C-C bond formation. The synthetic protocol is displayed in Figure 2.13. The hexaphenylbenzenes (**b**) [68] were first synthesized by $Co_2(CO)_8$-catalyzed cyclotrimerization of substituted diphenylacetylene (**a**), and then oxidative cyclodehydrogenation of **b** gave HBC molecules **c** in high yields, such as sixfold symmetric alkyl- [69], alkylphenyl- [70], and alkylester-substituted HBCs [71].

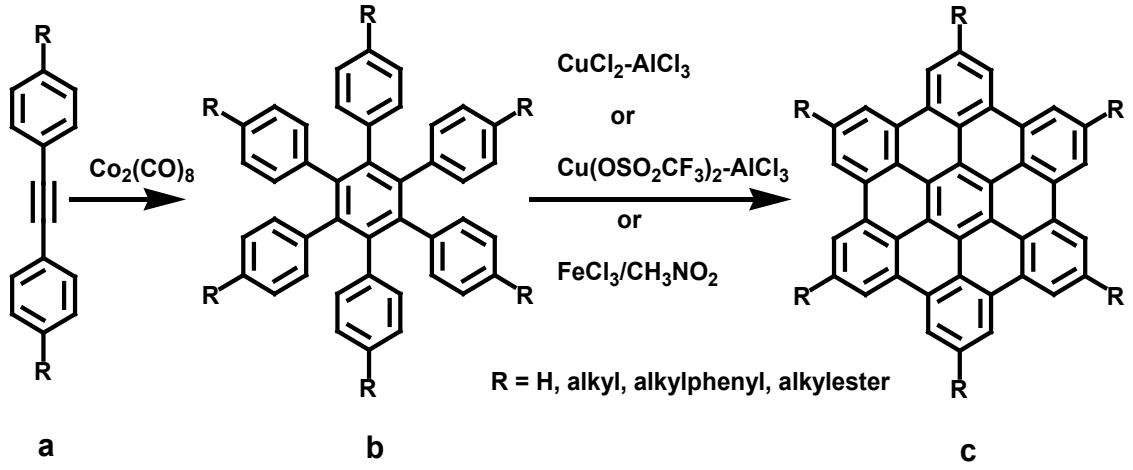

Figure 2.13: General synthetic route to HBC derivatives.

b) Synthesis of an "HBC-star"

The precursor hexa(4-iodophenyl) hexaphenylbenzene (**b**) (Fig. 2.14) was prepared by reaction of excess iodine monochloride with hexa(4-trimethylsilyphenyl)hexaphenylbenzene (**a**), which was synthesized by two different routes. The first so-called convergent route (Route 1) involves a Stille coupling [72] and a cobalt-catalyzed cyclotrimerization [73]. To avoid the toxic organotin chemistry, as well as to simplify the synthesis, an alternate divergent route (Route 2) requiring one sixfold bromination and one sixfold Suzuki coupling reaction [74] was developed. Final cyclodehydrogenation of **b** with iron(III)chloride gave the desired compound **c**. Despite the virtual insolubility of compound **c**, palladium-catalyzed Hagihara-Sonagashira coupling reactions [75] with solubilizing acetylene groups work smoothly, thus obtaining the "HBC-star".

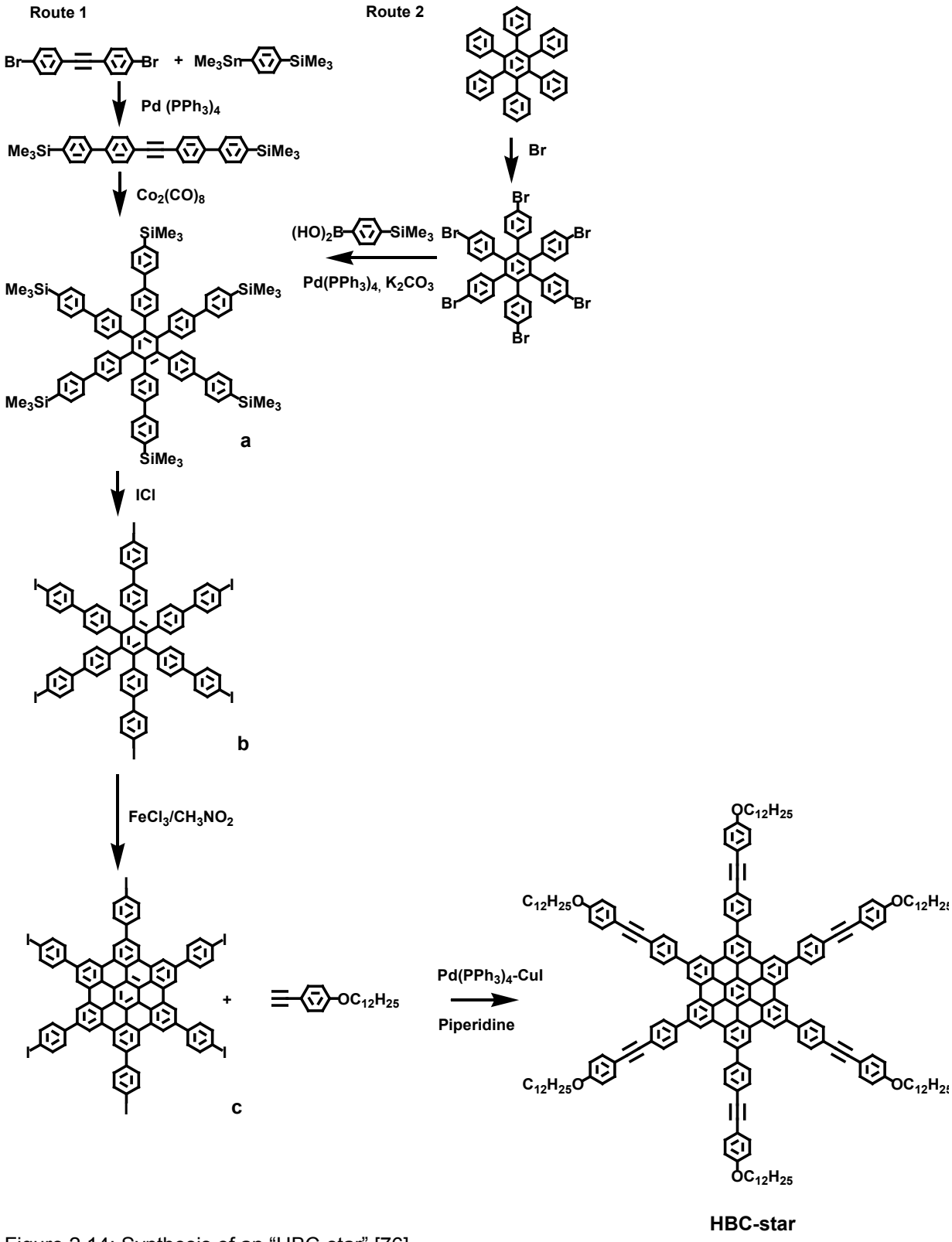

Figure 2.14: Synthesis of an “HBC-star” [76].

c) HBC-amines

The synthesis of a HBC derivative linking the electroactive triaryl amine moieties is unknot successfully accomplished using the standard oxidative cyclodehydrogenation of the related

hexaphenylbenzene precursors due to the preferential localization of charge on the nitrogen as radical cations [77,78]. An alternative way is by the palladium catalyzed Buchwald-Hartwig coupling reaction [79,80], starting from HBC building blocks carrying two bromo functionalites. Bis-arylamine substituted HBCs ("HBC-amine") were synthesized as shown in Figure 2.15 [81].

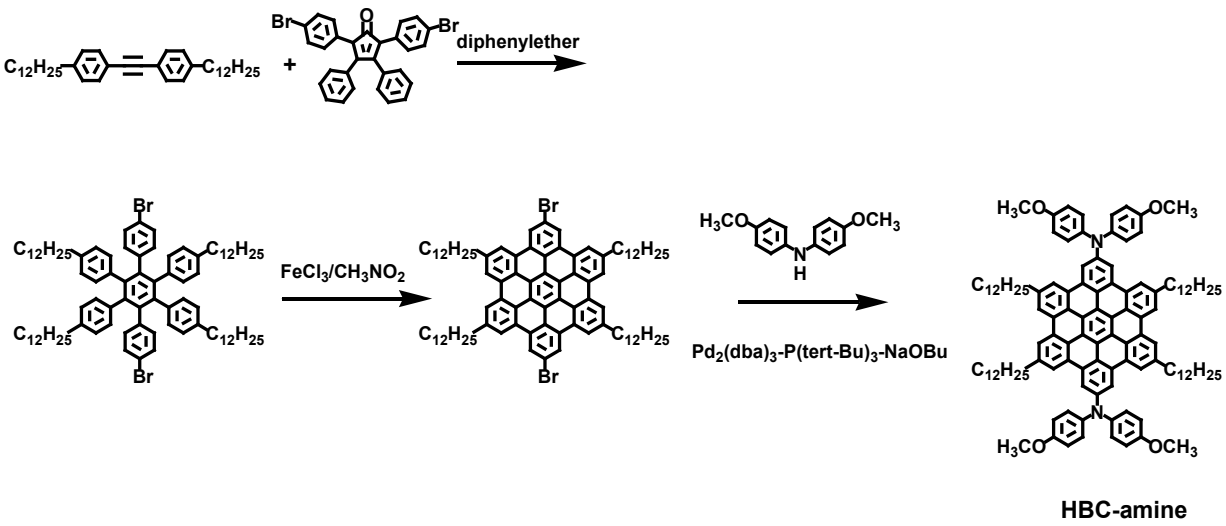

Figure 2.15: Synthesis of HBC-amine by Buchwald-Hartwig coupling reactions [81].

d) Symmetrically but not six-fold substituted HBCs

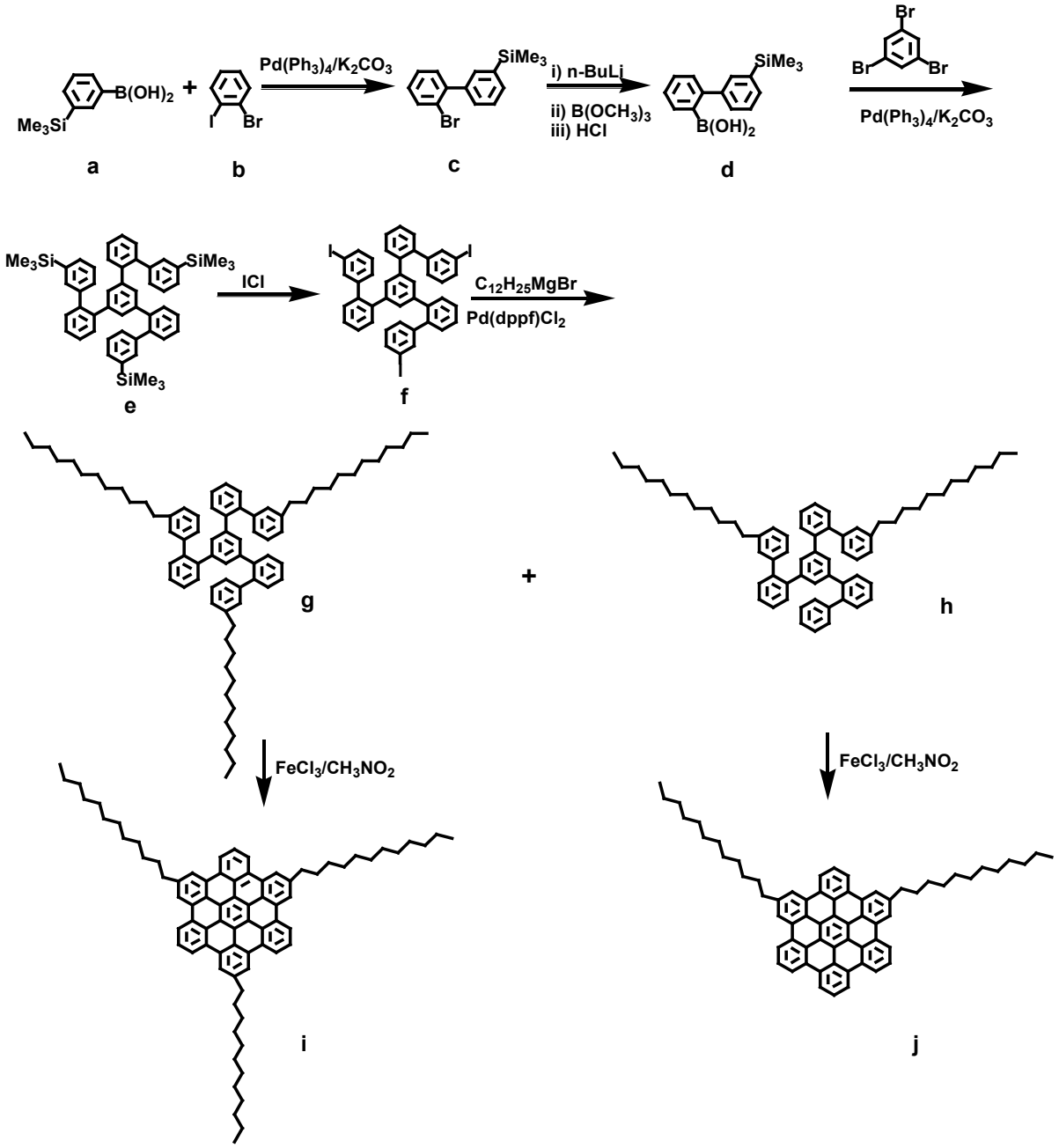

Figure 2.16: Synthesis of 1,7,13-trisdodecyl-hexa-*peri*-hexabenzocoronene (**i**) or 1,7-bisdodecyl-hexa-*peri*-hexabenzocoronene (**j**) [82].

The synthesis started from the selective Suzuki coupling reaction between 4-(trimethylsilyl)benzene-3-boronic acid (**a**) and 1-bromo-2-iodobenzene (**b**) (Figure 2.16). The selective reaction with the iodide sites *vs.* bromide gave 1-bromo-3 [trimethylsilyl]phenyl]benzene (**c**). The compound **c** was then converted into the related boronic acid derivative **d** by lithium-bromide exchange followed by the reaction with trimethoxyborane and acidic work-up. A three-fold Suzuki coupling reaction between **d** and 1,3,5-tribromobenzene provided the C_3-symmetric compound **e**. The trimethylsilyl groups in

compound **e** were then transformed into iodides with iodine monochloride, affording the desired precursor **f** [82].

1,3,5-tris-2'-(3''-I)biphenylbenzene (**f**) and Gringard reagent catalyzed by Pd(dppf)Cl_2 in THF were converted to 1,3,5-tris-2'-(3''-dodecyl)biphenylbenzene (**g**) and 1,3-bis-2'-(3''-dodecyl)biphenyl-5-2'-biphenyl-benzene (**h**). A mixture of **g** and **h** separated by column chromatography (Silica gel, PE:DCM = 6:1), afforded **g** and **h** as colorless oil, respectively. 1,7,13-trisdodecyl-hexa-*peri*-hexabenzocoronene (**i**) or 1,7-bisdodecyl-hexa-*peri*-hexabenzocoronene (**j**) was obtained by an intramolecular oxidative cyclodehydrogenation of the precursor **g** or **h** with iron(III) chloride/nitromethane [83,84].

e) Tri-zigzag polycyclic aromatic hydrocarbons

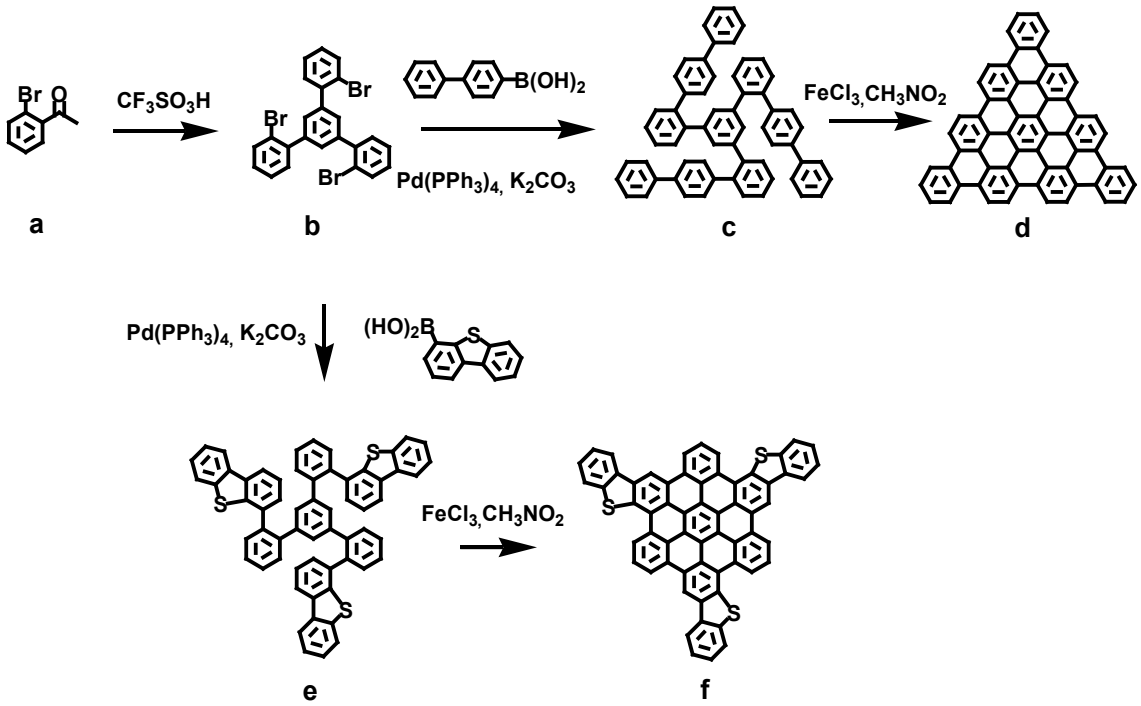

Figure 2.17: Synthesis of triangle PAH (**d**) and trisdibenzothiopheneHBC (**f**).

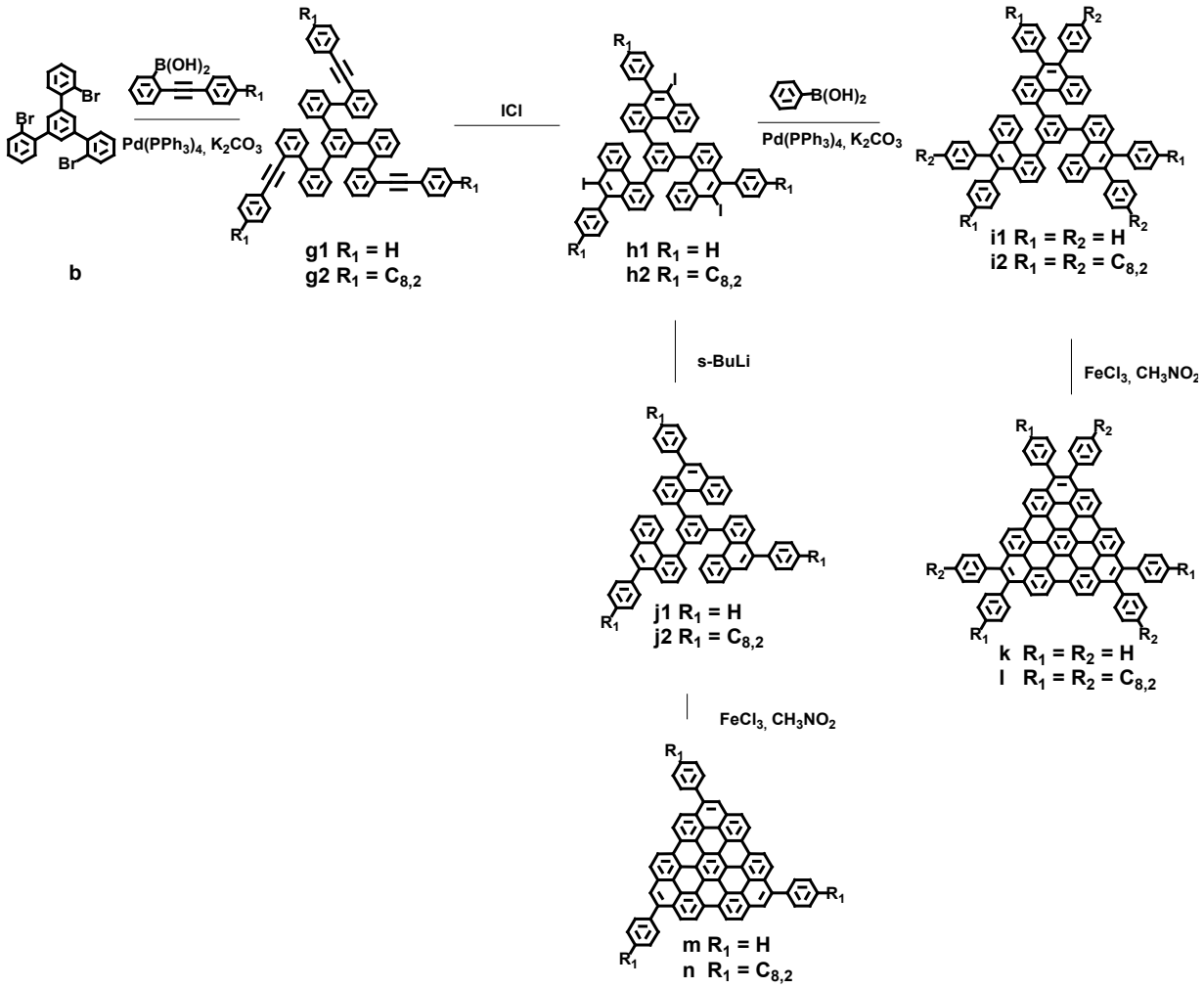

Figure 2.18: Synthesis of triangle PAHs (**k,l,m,n**).

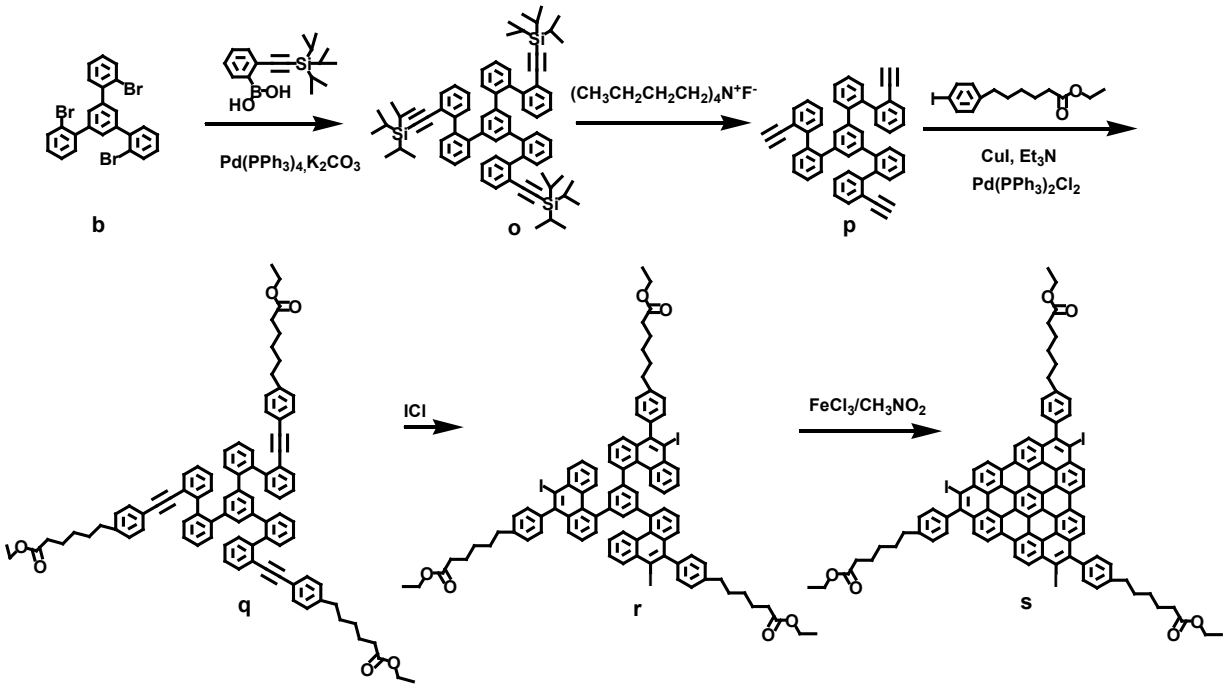

Figure 2.19: Synthesis of triangle PAHs with ether end group (**s**).

The synthesis of all triangle molecules **d**,**f**,**k**,**l**,**m**,**n** (Figure 2.17 and 2.18) was based on the same precursor, 1,3,5-tris-(2'-bromophenyl)benzene (**b**), which was synthesized by trifluoromethanesulfonic-acid-mediated trimerization of 2-bromoacetophenone (**a**) [85]. The further synthetic protocol comprised the following steps: a) Suzuki coupling of 1,3,5-tris-(2'-bromophenyl)benzene (**b**), b) ICl induced low-temperature ring cyclization, and c) protonhalogen exchange or further Suzuki coupling to afford the precursors with 1,3,5-tris (2'-biaryl)benzene (**c** and **e**) or 1,3,5-tris(2'-phenanthrenyl)benzene (**i** and **j**). Intramolecular oxidative cyclodehydrogenation reactions were then performed for the precursors by using $FeCl_3$ as oxidant, affording triangle discs **d**,**f**,**k**,**l**,**m**,**n** (Figure 2.17 and 2.18). For the synthesis of compound **s**, besides the above 3 steps, there are two more steps between step a and step b. The first step was to use tetra-n-butylammonium fluoride removing silyl ether protecting groups, affording **p**. In the second step compound **q** was synthesized by palladium-catalyzed Hagihara-Sonagashira coupling reactions, as shown in Figure 2.19.

2.4 Self-assembly of molecules at surfaces

The fabrication methods of today's microelectronic industry have been refined to produce smaller and smaller devices, which will soon reach fundamental limits. A promising alternative route to attain much smaller and thinner devices at the nanoscale is the self-assembly of atoms and molecules on atomically well-defined surfaces. The mechanisms

controlling the self-assembly phenomena are indispensably understood, in order to precisely control the self-assembly processes to create a broad range of surface nanostructures from diverse materials. The self-assembly involves non-equilibrium including kinetically and thermodynamically controlled processes for both “physisorption” and “chemisorptions” of molecules on surfaces in order to control the molecular assembly.

2.4.1 Physisorption

Physisorption (physical adsorption) is a type of adsorption in which the adsorbate adheres to a surface by relatively weak interactions, such as van der Waals interaction. The enthalpy is typically smaller than 20 kJ/mol [86] (various energy terms are 100 kJ/mol, corresponding to about 24 kcal/mol and to 1 eV.) The small enthalpy change is insufficient to lead to bond breaking, thereby the adsorbate retains its identity, although it may be distorted by the substrate. The self-assembly of molecules is influenced by several interactions and their respective balance.

1. Interfacial interaction (adsorbate-substrate interaction): adsorption. The adsorption energy is the strongest of all interactions and presumably the primary driving force for the self-organization process.
2. Interfacial interaction: corrugation. The substrate corrugation leads to different energies between different adsorption sites (HOPG A-B).
3. Intermolecular interaction: At higher coverages, the intermolecular interaction will become more and more important and, ultimately, play a crucial role in the crystal packing.
4. Intermolecular interaction: endgroup-endgroup interaction. Different endgroups will lead to different molecular patterns. For methyl-terminated molecules the endgroup-endgroup interaction is not strong, but for other terminations, such as carboxyl acid and amine, it can play a significant role.
5. Intermolecular interaction: admolecule energetics. Once a monolayer is obtained, the additional impinging molecules will experience the interaction with the molecules of the existing layer. Initially, these molecules will form a partial second layer on top of those molecules in the monolayer, before they are potentially included in the growing layer. The strength of the admolecule interaction is expected to be between the bulk interaction and the physisorption interaction with the surface. For example, for decanethiol, the admolecule energy would be between 66 kJ/mol (0.68 eV) and about 104 kJ/mol (1.08 eV).
6. Intramolecular interaction: conformational energies. The energy cost of a *gauche* defect in an isolated hydrocarbon chain is ~ 0.022 eV, which can be thermally activated at room temperature. This gives the molecule a certain flexibility, which might support the structure formation process[87].

2.4.2 Dynamics from physisorption

The formation of a self-assembled molecular monolayer from a solution on a substrate via physisorption mostly comprises of two steps.

The first step is molecular adsorption onto the surface when it is in thermodynamic equilibrium. The difference of the thermodynamic potential at constant pressure and temperature, the total free energy ΔG, describes the change during the adsorption of the molecules, which at a solid-liquid interface implies the replacement of solvent molecules by the desired adsorbate. ΔG is related to differences in enthalpy and entropy: $\Delta G = \Delta H - T\Delta S$.

When the system is in thermodynamic equilibrium, the modulus of ΔG has its maximum, associated with a large (negative) ΔH, and a large (positive) ΔS.

1. The physisorption causes a maximum coverage of molecules on the surface, thereby maximizing the modulus of ΔH;
2. The entropy S increases when a large adsorbate molecule replaces many solvent molecules at the surface. This effect is counteracted by a decrease of conformational entropy, but less so for rather rigid adsorbates. Therefore, large and rigid molecules are favoured to be adsorbed at solid-liquid interfaces to maximize ΔS.

The next step is the molecular rearrangement or reorganization on the surface [88,89,90,91,92]. For instance, Ostwald ripening in two dimensions implies that larger domains in two dimensional polycrystals grow at the expense of smaller domains at the solid-liquid interface, which has been visualized by STM. The driving force is the reduction of the circumference-to-area ratio and thereby the lowering of the interfacial or line energy [73].

2.4.3 Chemisorption

Chemisorption (chemical adsorption) is the adsorption whereby the adsorbate adheres to a substrate by forming a chemical bond. The enthalpy of chemisorption is much greater than that of physisorption, and typical values are in the region of 200 kJ/mol [86]. The chemisorption of molecules on substrates occurs via “wet chemical” or UHV methods. In the “wet chemical” method the modified surface is formed by the immersion of an appreciate substrate into a solution of an active surfactant in an organic solvent. The wet chemical reactions requires a metastable surface to successfully carry out the surface chemistry: The

precursor surface must be stable enough to be handled at atmospheric pressure in the presence of solvent vapors, inert gas impurities, and other contaminants, and yet it must be reactive enough to undergo chemistry. Here, only some examples of modified surfaces via the "wet chemical" method are referred to.

1) Au: To date, monolayers of alkanethiolates on gold are probably the most studied self-assembled monolayers. Kinetic studies of alkanethiol adsorption onto Au (111) surfaces have shown that at relatively dilute solution (10^{-3} M), two distinct adsorption kinetics can be observed: a very fast step, which takes a few minutes, by the end of which the contact angles are close to their limiting values and the thickness at about 80%-90% of its maximum, and then a slow step, which lasts several hours, at the end of which the thickness and contact angles reach their final values. At 1 mM solution the first step was over after ~ 1 min, while it requires over 100 min at 1 mM concentration. The second step can be described as a surface crystallization process, where alkyl chains get out of the disordered state and into unit cells, thus forming a two-dimensional crystal. Therefore, the kinetics of the first step is governed by the surface-head group reaction, and the activation energy may depend on the electron density of the adsorbing sulphur. The second step is related to chain disorder, the different components of chain-chain interaction (van der Waals, dipole-dipole, etc.), and the surface mobility of chains. Increasing the van der Waals interaction by increasing the length of alkyl chains, the kinetics becomes faster [93,94].

2) Si or Ge: Silicon or germanium surfaces have been terminated with hydrides by immersion of a native oxide terminated Si or Ge wafer in 10% aqueous HF for 10 min, which results in hydride termination with a surface roughness on the order of 3-4 nm. Further, alkyne or alkylene hydrosilylation on Si-H-terminated surfaces yield alkenyl or alkyl termination, repectively. For example, monolayers prepared from octadecene, resulting in octadecyl groups on the surface, are densely packed and titled approximately 30° from the surface normal. As a result of the good coverage provided by the film, silicon surfaces exhibit excellent stability and withstands extended boiling in aerated boiling chloroform, water, acid (2.5 M H_2SO_4 in 90% dioxane) and base (10% aqueous 1 M NH_4OH) and are resistant to fluoride (immersion in 48% aqueous HF). Under ambient conditions in air, little oxidation of the silicon surface is observed, indicating the usefulness of this approach for technological applications [95]. A schematic of the interaction potential is displayed in Figure 2.20.

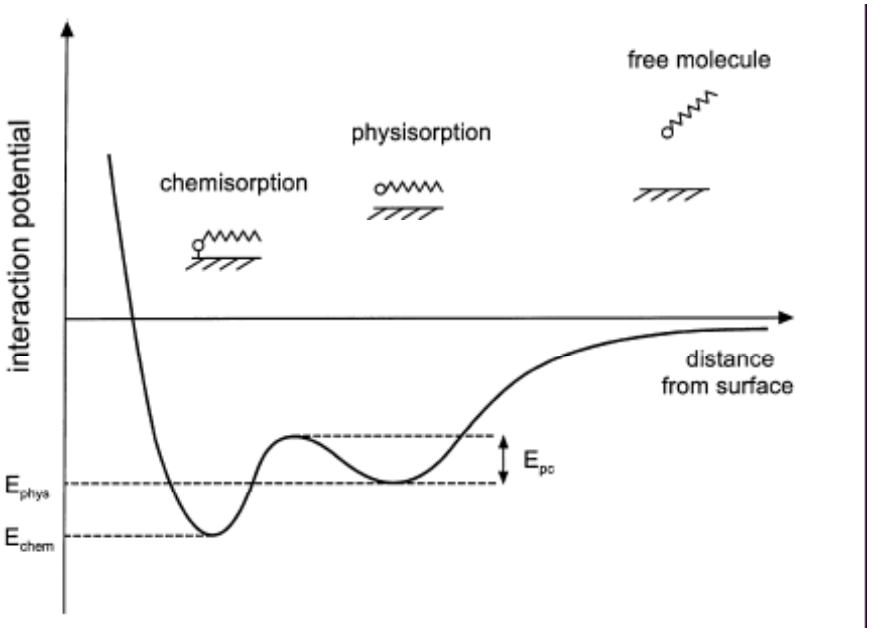

Figure 2.20: Schematic diagram of interaction potential between molecules and surfaces as function of distance [96].

3) TiO_2: Single-crystalline TiO_2 surfaces have a wide range of applications, for instance, in heterogeneous catalysis as photocatalysts, in solar cells for the production of hydrogen and electric energy, as gas sensors, as white pigments, as corrosion-protective coatings, for optical coatings, in ceramics, and in electric devices. They are important in earth sciences, play a role in the biocompatibility of bone implants, as spacer materials in magnetic spin-valve systems, and find applications in nanostructured form in Li-based batteries and electrochromic devices. Therefore, the surface chemistry of TiO_2 attracts worldwide interest. Formic acid and other carboxylic acids have become the most investigated organic molecules on single-crystalline TiO_2 surfaces [97].

2.5 Scanning probe microscopy

2.5.1 Scanning tunneling microscopy

The invention of scanning tunneling microscopy (STM) by Binnig and Rohrer was a milestone in the development of experimental physics. STM provides the ability to study surfaces, to modify them, to move individual atoms and molecules, to dissociate individual molecules and to form new structures on the atomic length scale. In this section, the basic

experimental principle of STM will be explained and the general configuration and operating mode of the instrument will be described.

2.5.1.1 Basic principle of scanning tunneling microscopy

The phenomenon behind scanning tunneling microscopy is quantum tunneling of electrons between two electrodes separated by a thin potential barrier (Figure 2.21). A very sharp tip (usually of platinum/iridium or tungsten) is mounted on a three-dimensional piezoelectric drive. The tip is scanned in the x-y plane above the sample using the X and Y actuators, while its height is controlled using the Z actuator. The sharp tip is approached to within a few atomic diameters of the surface under investigation without actual physical contact, so that there is a very small overlap of the wavefunctions of the surface with the apex atom of the tip. When a small bias voltage (10mV-4V) is applied between the sample and tip, electrons tunnel across this gap with a certain probability, resulting in a measurable tunneling current. An electronic feedback loop is used to maintain this current constant by permanently adjusting the tip height [98].

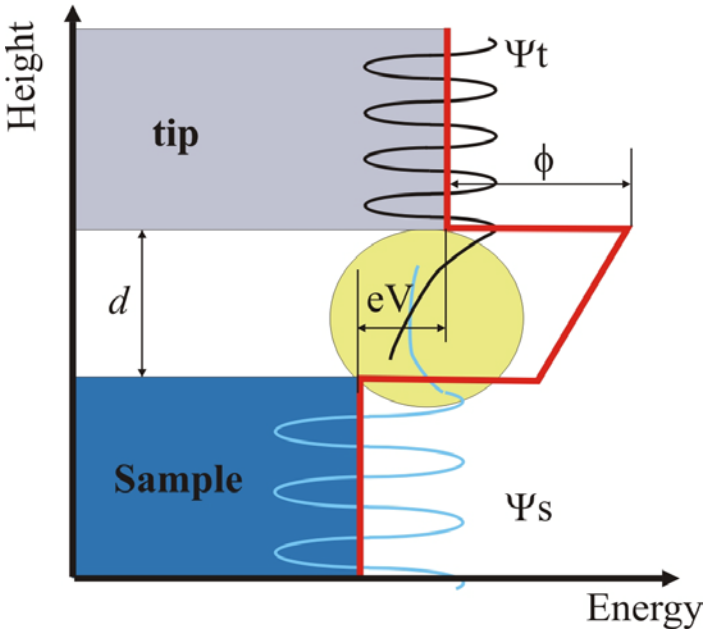

Figure 2.21: Tunneling process between the STM tip and the sample across a gap of width d and potential height (for simplicity, the tip and sample are assumed to have the same work function). The electron wave functions decay exponentially with a small overlap, allowing electrons to tunnel from one electrode to the other. With a positive bias voltage *V* applied to the sample, electrons tunnel preferentially from the tip into unoccupied sample states (after[99]).

The most striking feature of this instrument is the remarkable spatial resolution it can achieve. The key for reaching a vertical resolution of a few hundredths of an angstrom is the exponential dependence of the tunneling current on the sample-tip separation *d*:

$$I \sim e^{-2\kappa d}, \quad \kappa = \sqrt{\frac{2m\phi}{\hbar^2}} \approx 0.5\sqrt{\phi\ (\mathrm{eV})}\ \text{Å}^{-1}.$$

with ϕ: average work function between the two electrodes.

For a typical metal (ϕ ~5 eV) the current will decrease by about one order of magnitude for every Angstrom increase in the electrode spacing. The lateral resolution mainly depends on the apex geometry and electronic orbitals of the scanning tip, which confine the unique opportunity to perform real-space imaging down to atomic length scales.

2.5.1.2 Operating modes

A scanning tunneling microscope offers the possibility to collect topographic and spectroscopic data on a local scale. In the topographic mode, the surface is mapped via the dependence of the tunneling current upon the tip-to-sample distance. In spectroscopy, the LDOS of the material is extracted through measurements of the tunneling conductance.

1. Topographic mode

a. Constant current mode

In this mode, the tunneling current *I* is kept constant by continuously feedback-adjusting the tip vertical position during the scan (Figure 2.22a). Because the tip follows the corrugations of the surface at a constant spacing, the scan speed is limited by the feedback loop bandwidth.

b. Constant height mode

In this mode the tip is scanned over the sample surface while maintaining the tip at a constant absolute height (Figure 2.22b). For the ideal tip and sample, modulations of the tunneling current $I(x, y)$ are due only to variations in the tip-to-sample spacing, and recording the current as a function of position will reflect the surface topography. This mode allows fast

scanning, but is restricted to surface areas where corrugations do not exceed a few angstroms, to avoid tip collisions with large surface protrusions.

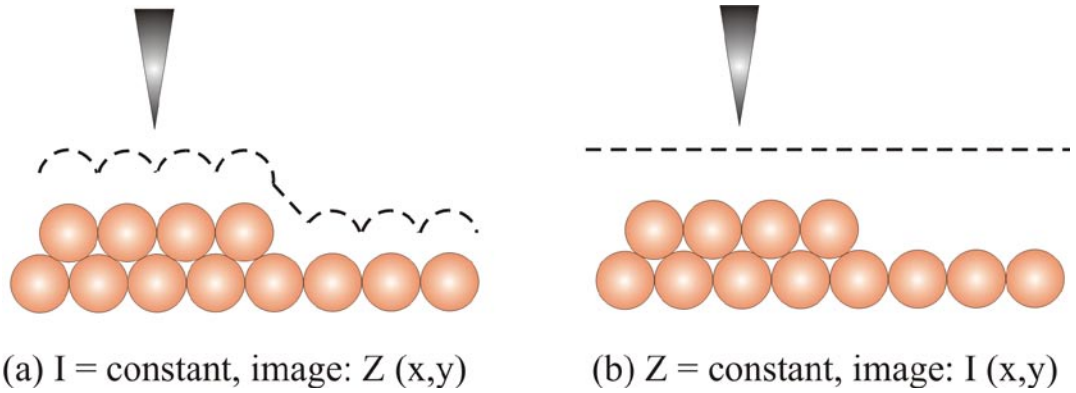

Figure 2.22: STM operating modes: (a) constant current and (b) constant height imaging.

2. Local tunneling spectroscopy

Locally resolved electron spectroscopy is probably the most sophisticated application of STM. The electronic density of states can be accessed by recording the tunneling current while the bias voltage is swept with the tip held at a fixed vertical position. If a positive bias voltage V is applied to the sample, electrons will tunnel into unoccupied sample states, whereas at negative bias they will tunnel out of occupied sample states. Although the interpretation of spectra can be quite complex, it can be shown that in ideal conditions the tunneling conductance $dI/dV(V)$ provides a valid measurement of the sample LDOS. This straightforward way to interpret the experiments is used in most STM and STS studies. dI/dV spectra can be obtained either by numerical differentiation of $I(V)$ curves or by a lock-in amplifier technique. In the latter case, a small ac-voltage modulation $V_{ac}(\cos\omega t)$ is superimposed on the sample bias V, and the corresponding modulation in the tunneling current is measured. Expanding the tunneling current into a Taylor series

$$I = I(V) + (dI/dV)Vac * \cos(\varpi t) + O(Vac^2) \quad ,$$

one finds that the component at frequency ω is proportional to $dI/dV(V)$. This statement is valid only if $V_{ac} << V$ and if $I(V)$ is sufficiently smooth. For optimal energy resolution V_{ac} should not exceed k_BT, and typical values are in the few hundred μV range. The advantage offered by the lock-in technique is that the sampling frequency ω can be selected outside the typical frequency domains of mechanical vibrations or electronic noise, considerably enhancing the measurement sensitivity [100].

2.5.1.3 Theory of scanning tunneling microscopy

The theory is indispensable to understand the relationship between the STM image and the geometric and electronic properties of the surface. In increasing order of theoretical difficulty, the four main approaches are 1) the Tersoff-Hamann approach, in which constant current contours are modeled from the electronic structure of the surface alone; 2) the transfer Hamiltonian or Bardeen approach, in which the tip electronic structure is explicitly included in the calculation; 3) the scattering or Landauer-Bütticker approach, which includes multiple pathways of tunneling electrons from their initial to their final crystal states; 4) the Keldysh or nonequilibrium Green's-function approach, which also considers inelastic effects like electron-electron or electron-phonon scattering [101].

The probably most widely used theoretical model of the STM was proposed by Tersoff and Hamann, applying the transfer Hamiltonian approach of Bardeen, who expressed the tunnel current by the density of states of the sample at the position of the STM tip, modelling the tip using s-type wave functions:

$$I = \frac{2\pi|e|}{\hbar}\sum_{\mu,\nu}[f(E_\nu) - f(E_\mu)]|M_{\mu\nu}|^2\delta(E_\nu + |e|V - E_\mu)$$

In this equation, we have

$f(E)$: the Fermi function (the first factor in the summation reflects the fact that electrons must tunnel from an occupied electronic state to an unoccupied electronic state)

$M_{\mu\nu}$: the tunneling matrix element between state μ on the sample and state ν on the tip

δ-function term: energy conservation during the tunneling process

E_ν and E_μ: the corresponding energies of the states ν and μ in the absence of tunneling

V: the applied bias [98].

2.5.1.4 Scanning tunneling microscopy of molecules on surfaces

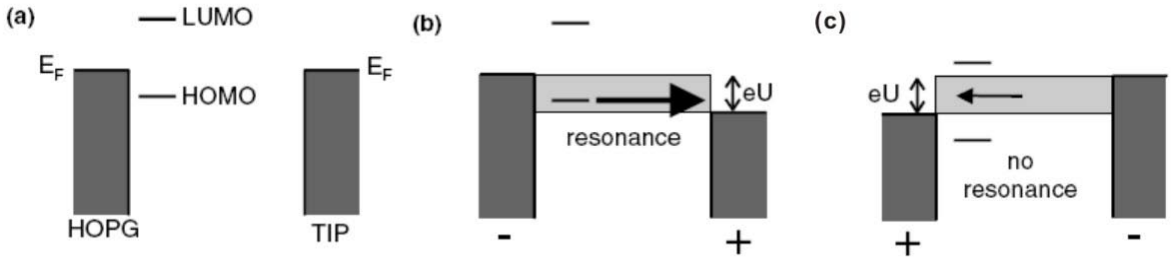

Figure 2.23: Schematic representation of resonance tunneling of a physisorbed molecule aligned between HOPG and a STM tip. a) A molecule is placed asymmetrically in the tunneling junction (closer to the substrate than to the STM tip and with its HOMO closer to the substrate Fermi level than with its LUMO). b) With negative bias on HOPG, more electrons tunnel from HOPG to the STM tip via filled HOMO of the molecule, than if they had to directly tunnel from HOPG to the STM tip. c) With positive bias on HOPG, the electrons tunnel directly from the STM tip to HOPG without resonance tunneling [47].

Different molecules on various solid surfaces have been observed with STM, however, the mechanism which renders the adsorbates visible in the STM images are not complete understandood. The adsorption onto solid surfaces is simply classed into “physisorption” and “chemisorption”, as decribed in the section 2.4. In physisorption, the adsorbate preserves essentially its electronic structure despite the interaction between the adsorbate and the surface [47,102]. When the interaction is much stronger, however, the molecular orbitals of adsorbate may be hybridized with the wave function of the substrate [103,104]. In chemisorptions, it results in modified electronic levels of the adsorbate due to the formation of chemical bonds with the surface, such as ionic or covalent bonds.

The simple model of resonance tunneling may be used to explain the STM visualization of the adsorbates, which is physisorbed on HOPG [47,102], as illustrated in Figure 2.23. The adsorbated molecules have orbitals with electrons. If the tunneling electrons are energetically close to a molecular orbital, the probability for electrons to tunnel from occupied states in the substrate into empty states of the tip (or vice versa) strongly increases.

2.5.2 Scanning force microscopy

Scanning force microscopy (SFM) invented by Binnig, Quate and Gerber in 1986 as a tool for studying non-conducting and conducting surfaces on the atomic level, provides nowadays images with true atomic resolution. Force-distance measurements performed locally aim to provide an understanding of tip-sample interactions of different physical origins and of the imaging mechanisms in SFM.

2.5.2.1 Fundamental principles of Scanning force microscopy

The operation of the SFM can be illustrated with regard to Figure 2.24 if the tip is attached to a cantilever, which is used to detect the tip-sample interaction. The cantilever is mechanically oscillated near its resonant frequency (usually 10~500 kHz). At relatively small sample-tip separations (usually 0.5~100 nm), the van der Waals interaction between the sample and the tip causes a force that alters the oscillation. The force is measured by detecting the motion of the cantilever with a laser reflected into a position-sensitive photodiode. The topographic structure of the surface can be mapped by scanning across the surface while using a feedback signal to maintain a constant force between the tip and the surface.

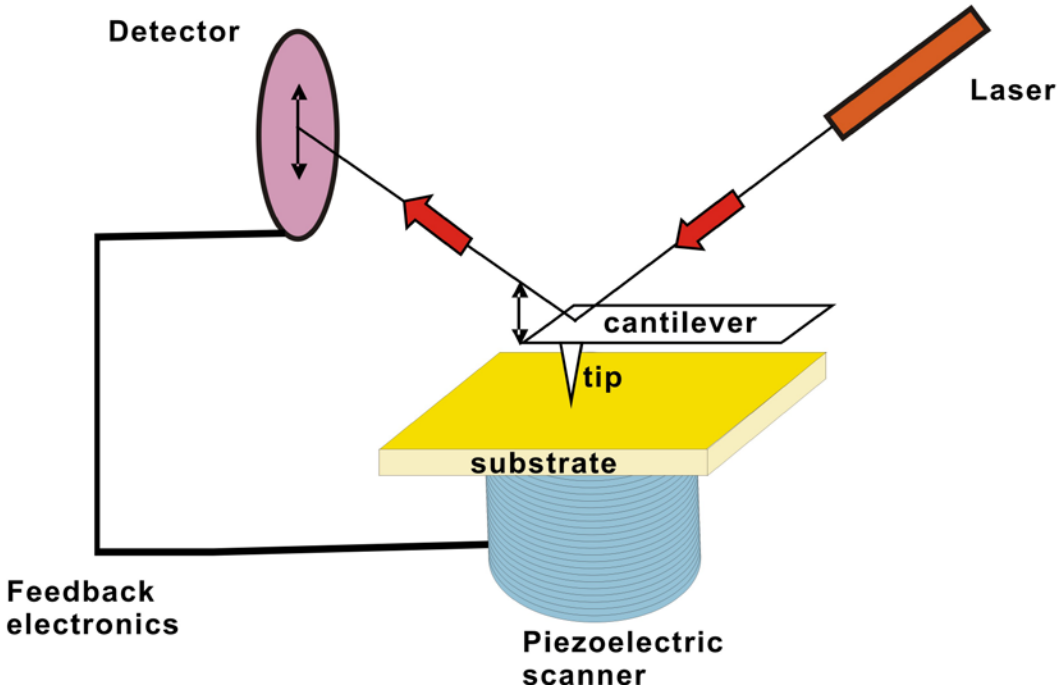

Figure 2.24: Schematic of scanning force microscopy (SFM).

2.5.2.2 Interacting forces

The interacting forces between the atoms at the tip and the sample in SFM can be classified into attractive and repulsive forces. Towards attractive forces, van der Waals interaction, electrostatic forces, chemical forces and capillary forces may contribute. For the repulsive forces hard sphere repulsion, or Pauli-exclusion interaction and electron-electron Coulomb interaction may be considered. In general, the repulsive forces are very short-range forces and have an exponential decay or an inverse power law dependence on distance.

1. van der Waals interactions: based on the Coulomb interaction between electrically neutral atoms which are locally charged by thermal or zero-point quantum fluctuations. It is well known that the van der Waals potential between two atoms has a distance dependence of ~d^{-6}. In the case of SFM measurement, however, there are several hundred atoms at a tip and sample, and the resultant force should be calculated from a vector sum of the van der Waals forces between them.
   Hamaker's approach:
   For a spherical tip and a flat sample, the van der Waals potential V_{vdw} and force F_{vdw} are defined by
   $V_{vdw} = -\frac{HR}{6d}$ and $F_{vdw} = -\frac{HR}{6d^2}$,
   where H is the Hamaker constant, related to the properties of the materials such as atomic polarizability and the density of the tip and the sample. R is the radius of a spheical tip. d is the closest distance between the tip and the sample [105].
2. Electrostatic force: generated between a charged or conductive tip and sample. Its definition is given by [106]
   $F_{el} = -\frac{\pi\varepsilon_0 R U^2}{d}$,
   where π_0 is the dielectric constant, *R* is the tip radius, *U* is potential difference between a charged or conductive tip and the sample, and *d* is the tip-sample distance.
3. Chemical force: bonding between atoms to form a molecule. The chemical bonding energy is described by the Morse potential [107]:
   $V_{morse} = -E_{bond}(2e^{-\kappa(d-z)} - e^{-2\kappa(d-z)})$,
   where E_{bond} is the bonding energy, *z* the equilibrium distance, and $1/\kappa$ the decay length.
4. Capillary force: caused by a meniscus formed between the tip and the sample with a water layer. The basis of the capillary force is the van der Waals forces among the water molecules and atoms at the tip and the samples [108] .
5. Repulsive force: referred to either as Coulomb force or Pauli exclusion. When two atoms are close, the electronic wave function will be overlapped and a very strong repulsion will be generated [109].
6. As an approximation for the forces contributing to the deflection of an SFM cantilever a superposition of the van der Waals and the repulsive force can be considered, which is defined by the Lennard-Jones potential:
   $\varepsilon(r) = -4\varepsilon_0\left[\left(\frac{\sigma}{d}\right)^6 - \left(\frac{\sigma}{d}\right)^{12}\right]$,

where, ε_0 is potential energy at the minimum, σ is the distance at which the force is zero, and *d* is the distance between two atoms. The d^{-6} distance dependence comes from the van der Waals attractive interaction and d^{-12} is given by the repulsive force between two atoms [109].

3 Experimental section

Scanning probe methods have developed into ubiquitous tools in surface science. These techniques are used to study surface topography, electronic and vibrational properties, and film growth; they have been used to measure adhesion, the strength of individual chemical bonds, and friction, and they have been employed to investigate lubrication, dielectric and magnetic properties, contact charging, and molecular manipulation. The family of scanning probe microscope techniques is very diverse, with different approaches specializing in different surface properties. In this work, the focus is on the two most commonly used techniques: scanning tunneling microscopy and scanning force microscopy.

3.1 Scanning tunneling microscopy

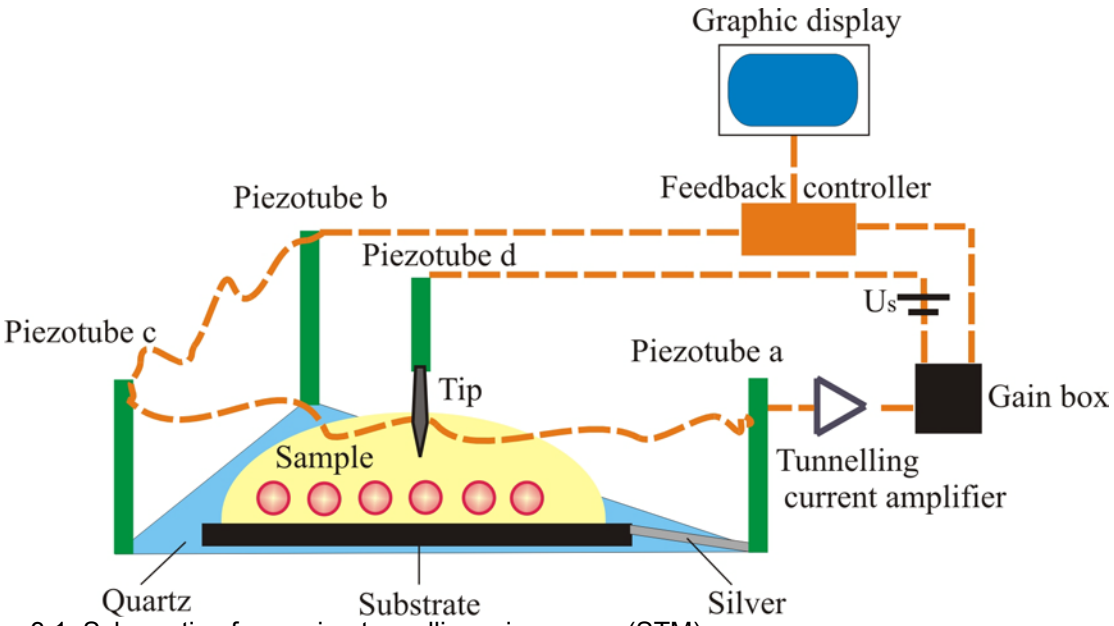

Figure 3.1: Schematic of scanning tunnelling microscopy (STM).

At the liquid/solid interface experiments under ambient conditions are performed with a home-made STM. The STM was used with Omicron electronics (Omicron Vakuumphysik GmbH, Taunusstein, Germany). Figure 3.1 presents the setup of the home-built STM. Its main components are a sample holder, i.e. a triangle quartz, on which the substrate is mounted with sample solution; three piezotubes, which hold the sample holder and move in lateral and vertical directions when deformed by applied electric fields; a tip; an electronic feedback loop; and a computer to monitor and record the operation. When the tip is approaching to the sample, and upon applying a small bias voltage, a tunnelling current occurs, which is

converted into a voltage by the current amplifier. A gain box amplifies the voltage, which is compared with a set point value, and set by the controller. Via an electronic feedback loop, the position of sample is adjusted according to the tunnelling current through the motion of three piezotubes, when the controller records the actual tunnelling current and transfers the error signal to the corresponding piezo drive voltage.

3.1.1 Sample preparation

STM at the solid-liquid interface: The sample solutions are prepared by dissolving the investigated molecules in 1,2,4-trichlorobenzene. Since the boiling point of 1,2,4-trichlorobenzene is 213.5 ºC , which is very high, it offers the opportunity to carry out STM experiment for several hours before the solvent is completely evaporated.

STM on dry film:

a) Dry films are prepared by drop casting a solution at room temperature onto freshly cleaved HOPG overnight.

b) Dry films are made by drop casting a solution on HOPG, while an electrical field in the range of 4-5x10^5 V/m is applied parallel to the surface, as displayed in Figure 3.2. The experiments are performed in a small glass box to control the evaporation rate of the solvent.

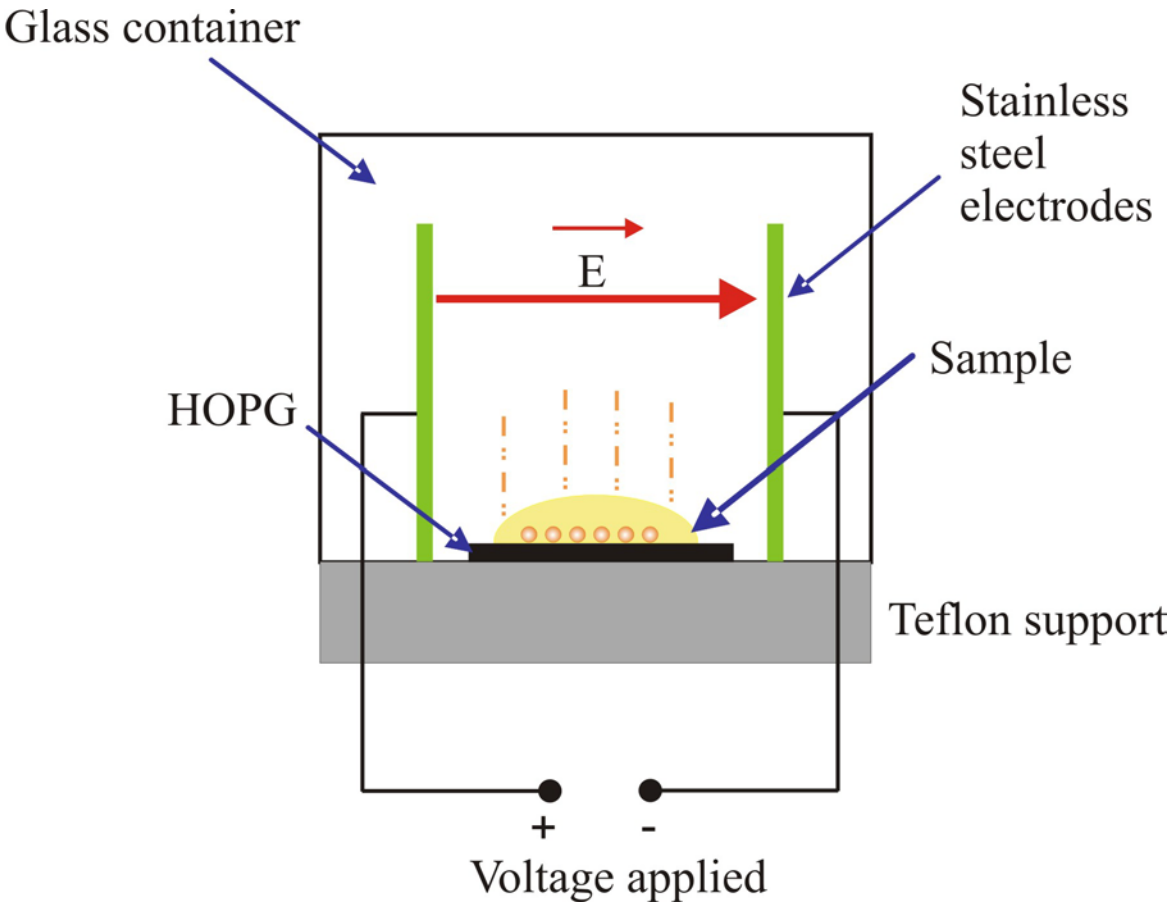

Figure 3.2: Setup of apparatus for dry film preparation under applied electric field.

The tips are prepared by mechanically cutting platinum/iridium (Pt/Ir 80:20) wires. Platinum is preferred for use in air because it does not easily oxidize. The small fraction of Iridium in the alloy makes the tips much harder.

The substrate is highly oriented pyrolytic graphite (HOPG) (grade ZYH, Advanced Ceramics, Cleveland, Ohio, U.S.A). Since HOPG is a layered compound exhibiting weak interlayer bonding strength via van der Waals interaction, preparation of a flat, clean, inert surface is simple by peeling upper layers off with adhesive tape. The unit cell of HOPG layer is well-known, thereby it is also used for calibration of the lateral scale of the piezoelectric elements.

Small amount of almost saturated solution is dropped between the fresh cleanly HOPG and a tip with a syringe. The tip is immersed in the solution observed with the optical microscopy.

3.2 Scanning force microscopy

SFM experiments were carried out with a Nanoscope III (Digital Instruments, Inc., Santa Barbara) in the tapping mode with an E-type scanner (12 x 12 μm^2) in air at room temperature. Commercial silicon tips (Digital instruments) on cantilevers with spring constants between 17 and 64 Nm^{-1}, were used at typical resonance frequencies in the range between 280 and 320 kHz.

3.3 Image processing

Most of the important information obtained from STM is related to distance. It is therefore important to ensure that the scale of the image is accurately obtained. Due to the piezo drift in the STM instrument, the molecular images have to be corrected. Using HOPG as a substrate, which has a known regular lattice structure, allows accurate measurements of distances on the image. The dimension of the unit cell of every image is determined according to the underlaying HOPG using Scanning Probe Image Processor (SPIP), version 3.2.11.0, developed by J. F. Jorgensen.

4 Results and Discussion

4.1 Self-assembled 2D monolayer from one substance

Self-assembled monolayers are widely used to modify and tune the physical properties of surfaces. A powerful method to investigate the 2D organization of functionalized organic molecules on surfaces is STM at a solid-liquid interface, which provides access to molecular and supramolecular structure and dynamics on the single molecule level [89]. In the following the two-dimensional structures of monolayers of differently substituted HBCs and various C_3 symmetric PAH derivatives are introduced.

4.1.1 HBC self-assembly influenced by the position of $C_{12}H_{25}$-substituents

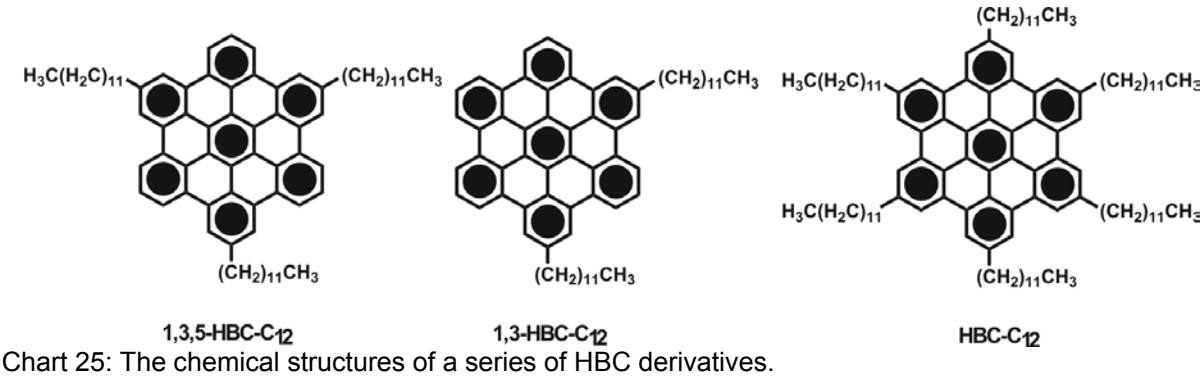

Chart 25: The chemical structures of a series of HBC derivatives.

Substituted triphenylenes can self-assemble into highly ordered columnar mesophase, inducing a high charge carrier mobility [110,111]. To further increase charge carrier mobility by enlarging the size of the conjugated aromatic core, the properties of HBC derivatives influenced by diverse substituents have been exploited in recent years [81]. For potential applications in molecular and organic electronics, the self-assembly of monolayers on solid substrates is of considerable interest, as it can be investigated in detail by STM. In previous work various substituents, such as alkyl chains with different lengths and substitution symmetries, have been considered for different monolayer arrangements, self-assembled at the interface between the atomically flat basal plane of highly oriented pyrolytic graphite (HOPG) and organic solutions. For instance, hexaalkyl HBC and pentaalkyl HBC exhibit the same two typical motives, namely a rhombic and a dimer structure [81]. Here, the self-assembly of HBC derivatives with much less substituents, maintaining a high substitution symmetry is studied at the solid-liquid interface.

The organization of **1,3,5-HBC-C$_{12}$** and **1,3-HBC-C$_{12}$** (Chart 4.1) in a quasi-2D system has been investigated by STM at the solution-HOPG interface. Here, for D_3 symmetric **1,3,5-HBC-C$_{12}$**, a significantly different packing besides dimer patterns (Figure 4.1b) is obtained, namely a zigzag pattern, as shown in Figure 4.1a. The STM current image of **1,3,5-HBC-C$_{12}$** in the large scale reveals many domains (Figure 4.1c). The zigzag pattern comprises six bright features (corresponding to high tunneling probability) in a unit cell, which are ascribed to the π-conjugated HBC discs; the substituents, however, cannot be resolved. At low bias the resonant tunneling through some density of states within the HOMO-LUMO gap of the conjugated core is small, but it increases at higher bias, when the energy gap between molecular orbitals and the Fermi energy of the substrate vanishes. However, the tunneling current through the alkyl substituents remains very small because of the larger energy separation between the molecular LUMO and the HOMO on the one side and the Fermi energy of the HOPG on the other side [112]. Furthermore, no high resolution images of the substituents can be obtained, possibly due to their high conformational mobility on a time scale faster than the STM imaging.

C_2 symmetric **1,3-HBC-C$_{12}$** also self-assembles into two different coexisting crystallographic phases (Figure 4.2c). In addition to a zigzag structure (Figure 4.2a), which is similar to **1,3,5-HBC-C$_{12}$**, a flower-like pattern is found (Figure 4.2b). The flower-like pattern consists of six triangle-shaped objects, i.e. **1,3-HBC-C$_{12}$** trimers. Noteworthy, the centers of the flowers are sometimes empty, but in few cases accommodate an object inside, marked by white and red hexagons; correspondingly; in Figure 4.2b. Fewer alkyl substituents and thus lower symmetry of **1,3,5-HBC-C$_{12}$** and **1,3-HBC-C$_{12}$** result in significantly distinguishable packings, i.e. the zigzag and flower-like nanostructures, in comparison with the D_{6h} symmetric HBC derivatives.

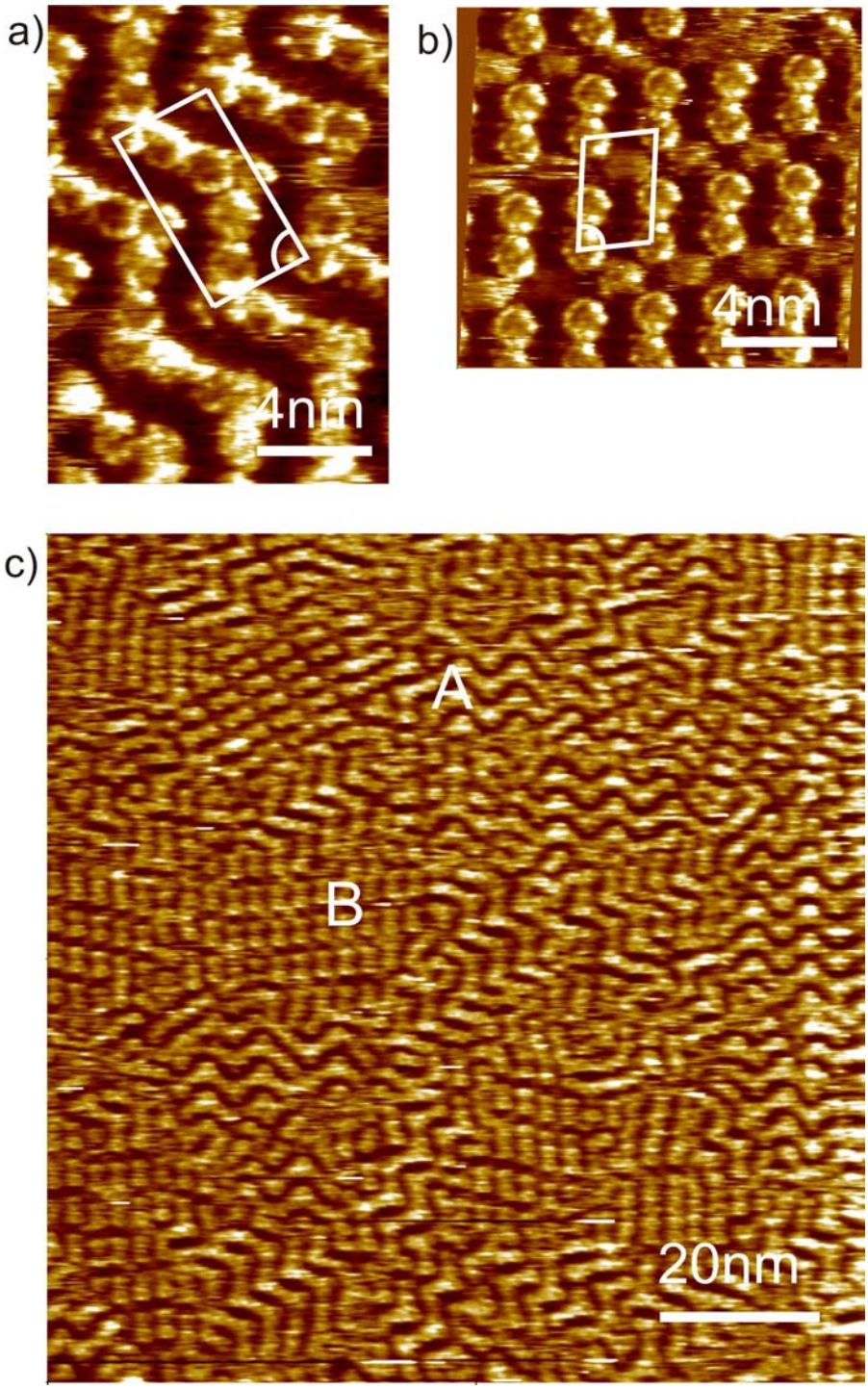

Figure 4.1: STM current images of **1,3,5-HBC-C_{12}** monolayer. a) zigzag structure; b) dimer pattern; c) polycrystals in the large scan image.

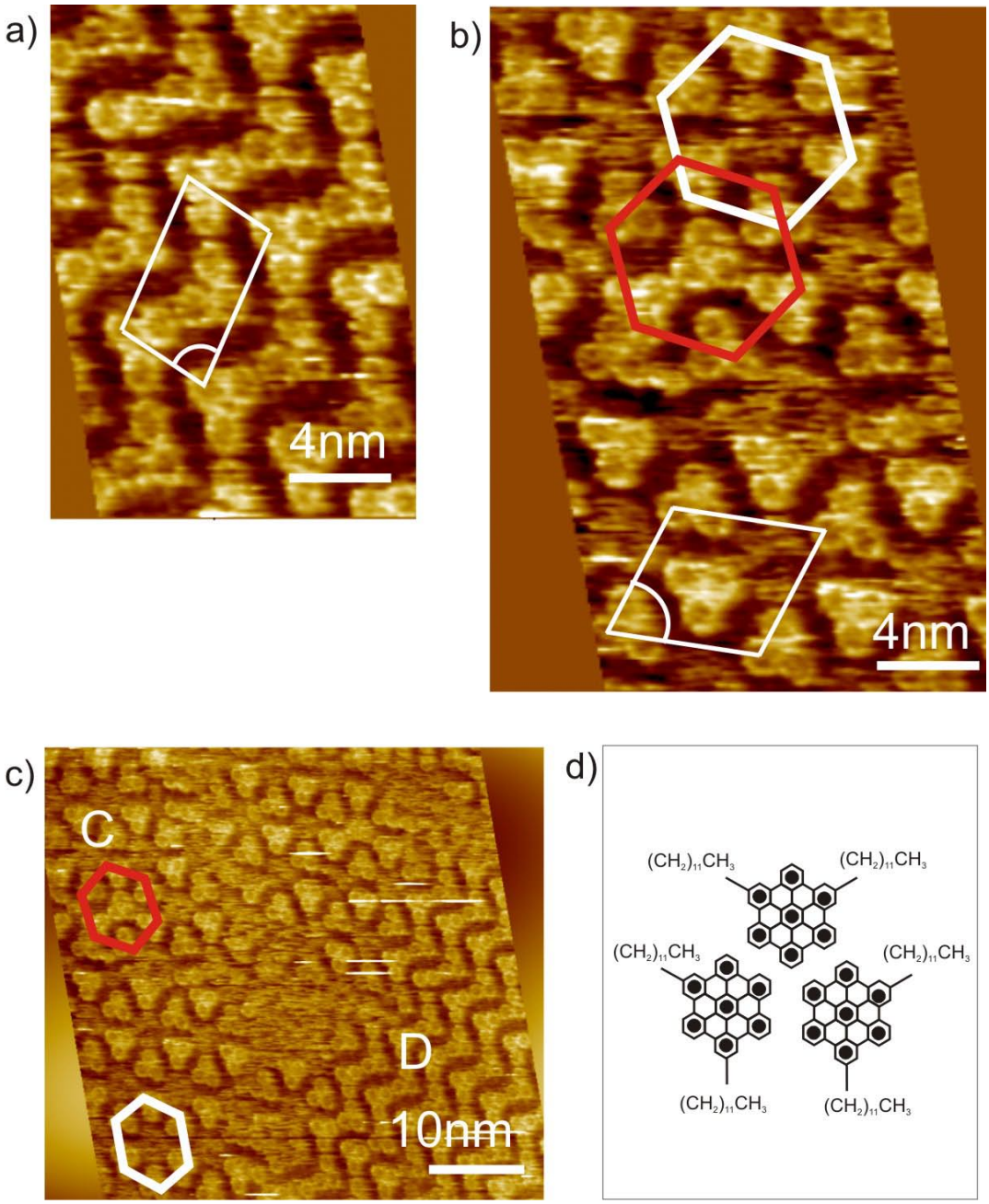

Figure 4.2: STM current images of **1,3-HBC-C_{12}** monolayer. a) zigzag structure; b) flower-like pattern; c) polycrystals in the large scan image. d) Schematic diagram of a **1,3-HBC-C_{12}** trimer.

The smaller number of substituents on HBC not only increases the solubility of HBC derivatives, but also causes differently ordered packings at the solid-liquid interface. For example, the C_2 symmetric **1,3-HBC-C_{12}** molecules form trimers, because the parts of HBC without alkyl chains nanophase-separate to form head-to-head structures, as shown in Figure 4.2d. This is in agreement with the formation of dense packings by HBC molecules in the first layer [91]. The alkyl chains on the **1,3-HBC-C_{12}** molecules prevent the HBC cores to get closer, which is supported by the loose pattern formed by HBC-C_{12} molecules [81]. In summary, a strong influence of the symmetry of the substitution is revealed on the self-

assembly of HBC derivatives at the solid-liquid interface. STM images exhibit novel zigzag and flower-like patterns with a lower symmetry than the D_{6h} symmetric analogue.

4.1.2 Triangle-shaped nanographene derivatives

C_3 symmetric polycyclic aromatic hydrocarbons such as triphenylene and truxene derivatives have been studied as active materials in field effect transistors and light-emitting diodes, as well as for the construction of bowl-shaped subunits of fullerenes [113,114]. To date the largest C_3 symmetrical discs investigated are derivatized triphenylenes [110]. The increasing size of the conjugated PAH cores dramatically influences the bulk charge carrier mobilities due to the large overlaps of conjugated part [115].

Recently, considerable progress has been made in synthesizing a new class of triangle-shaped PAH derivatives, which have been attractive substances owing to their improved and novel properties in comparison with HBCs [84]. Introducing various peripheries into a molecule is an approach to tune diverse properties. Various attractive substituents can be synthetically introduced to the trizagzagHBC scaffold. Particular substitutions are taken into account such as various lengths and numbers of alkyl chains, which might produce different patterns on HOPG [116]. The intermolecular interactions are also considered, like, e.g., hydrogen bonding, which has been used in some compounds before, where it was found to have a great impact on the self-assembly [117,118,119]. Given that the trizigzagHBC core is electron-rich, the “double cable” including two electron donors linked by alkyl chains or donor-acceptor links are attractive for potential organic and molecular electronic devices. For a donor-donor dyads two kinds of electron donors with different electronic properties are attached to each other, which implies that an electron acceptor might have dissimilar impact on these two donor species via charge transfer. Donor-acceptor dyads have been of interest since decades as a molecular rectifier [23]. The more and more complex donor-acceptor molecules aiming at the generation of new electronic devices prompted great activity in the synthesis and characterization. For instance, the self-assembly of donor-acceptor dyads based on HBC derivatives has been investigated in nanophase-separated structures at the solid-liquid interface [120], and a single-molecule chemical-field-effect transistor at a solid-liquid interface was conceived, using charge transfer complexes from electron acceptors covalently bound to the molecule and electron donors coming from the fluid [47] .

Here, we report on a novel series of large triangle-shaped PAH molecules **1-12** (Chart 4.2) with different substituents and peripheral structures. We expected that these discs might be exploited to form new 2D superstructures at interfaces. The compounds are grouped as follows: a) PAH cores combined with phenyl groups, such as **1** and **2**; b) alkylated phenylene groups on the PAH cores, for instance **3**, **4**, **5**; c) side groups of PAH molecules containing carboxyl groups, donor moieties or acceptor moieties, **6**, **7**, **8**, **9**, **10**, **11**; d) PAH fused with electron-rich thiophene rings, **12**.

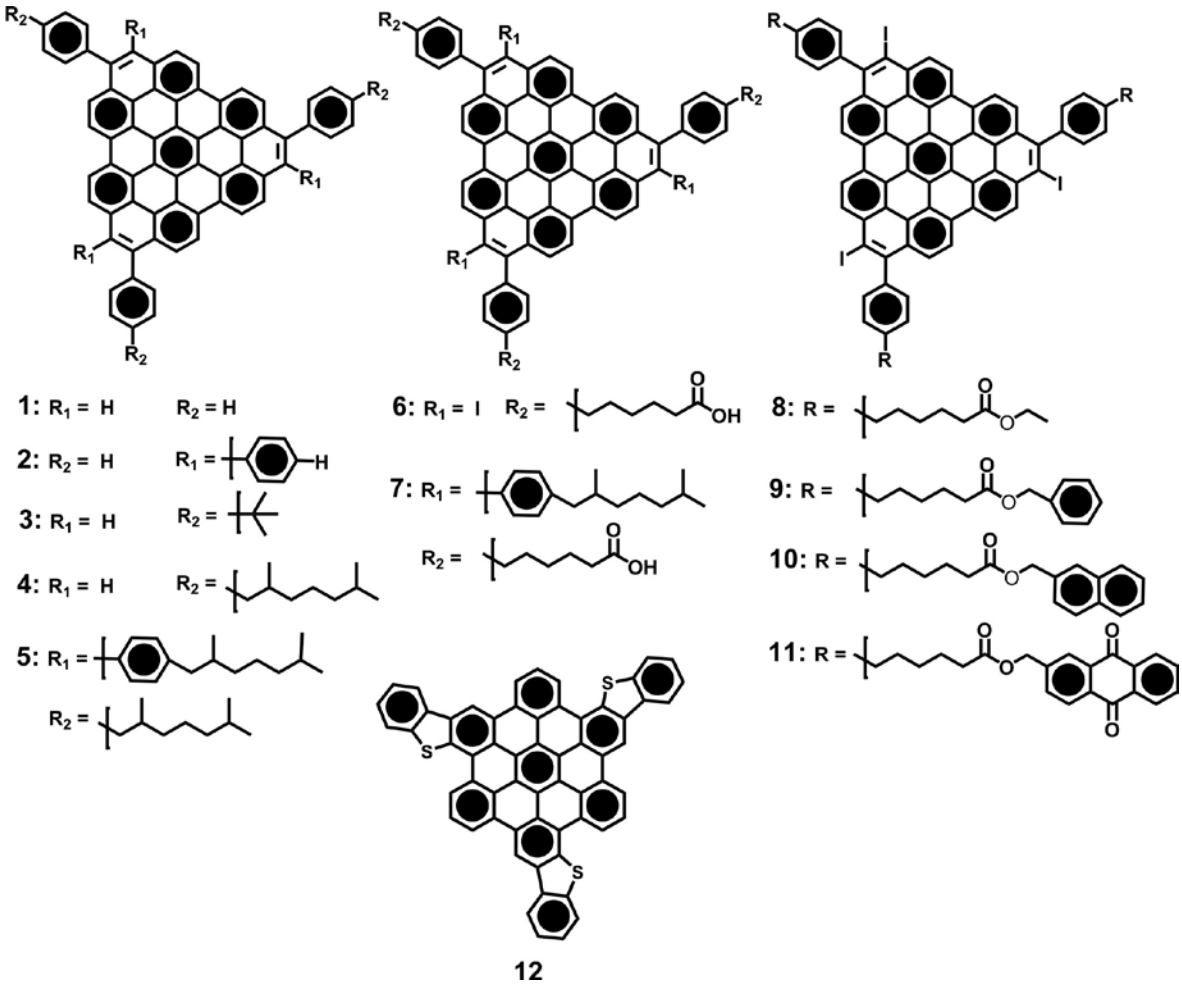

Figure 4.2: The chemical structures of a series of derivatives of diphenanthro[3',4'5,'6'-efghi:3,4,5,6-uvabc]ovalene trizigzagHBC, **1-11** and tribenzothiophene HBC, **12**.

a) PAH cores combined with phenyl groups

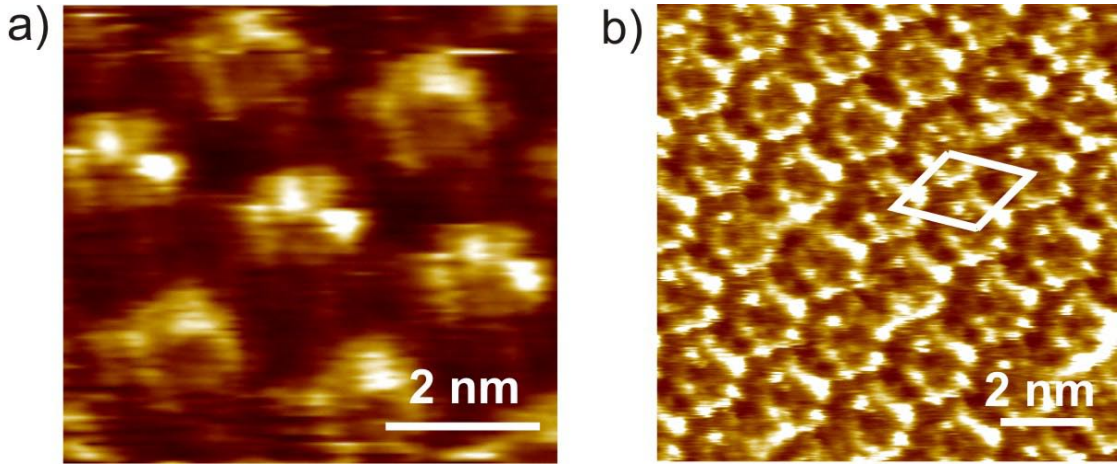

Figure 4.3: Constant-height STM images of regular nanostructures of compound **1** (a) and **2** (b) at the interface with a solution in 1,2,4-trichlorobenzen and HOPG.

Figure 4.3a,b shows STM current images of the 2D self-assembled monolayers of compound **1** and **2** at the interface between a concentrated solution in 1,2,4-trichlorobezene and the basal plane of HOPG, respectively. Both of the images demonstrate highly organized nanostructures. Each bright spot in the images (corresponding to high tunneling probability) can be assigned to a π-conjugated disc core [121]. The dark areas corresponding to low tunneling probability might be occupied by solvent molecules.

The arrangement of the compound **1** (Figure 4.3a) at the interface exhibits a hexagonal structure with one molecule per unit cell and the lattice constants of a = (2.24 ± 0.08) nm, b = (2.42 ± 0.13) nm, and an angle of α = (62 ± 2)º between the unit cell vectors. The orientation between the short unit cell vector of the nanostructure and the underlying HOPG hexagonal lattice is (23 ± 2)º. The area of the unit cell occupied by one molecule physisorbed on HOPG is (4.76 ± 0.20) nm^2, which is larger than the area within the van der Waals contour of a single molecular lying flat on the surface, i.e. its footprint is ~ 3.27 nm^2. It indicates the self-assembled molecules lie completely flat on the substrate with the interstitials filled by solvent molecules.

The introduction of one more phenyl ring in all of the three peripheral positions leads to a small change in the supramolecular structure on the HOPG surface. Figure 4.3b displays the STM image of the two-dimensional crystal of compound **2** physisorbed on the solid surface. Similar to the case of **1**, the lattice of the highly ordered monolayer is hexagonal within experimental error. However, the area of a unit cell of the monolayer of compound **2** containing one molecule amounts to (2.84 ± 0.10) nm^2, which is smaller than its footprint (~

4.01 nm^2). The lattice is characterized by a unit cell with parameters a = (1.76 ± 0.06) nm, b = (1.86 ± 0.05) nm, and α = (60 ± 2)º. The orientation of the lattice with respect to the underlying HOPG hexagonal lattice is (5 ± 2)º. It indicates the partial phenyl substituents dissolve in the supernatant solution.

Tabelle 4.1: Lattice constants of the two-dimensional crystal structures of compounds 1, and 2

	a (nm)	b (nm)	α (º)	Area (nm^2)	Footprint /molecule (nm^2)
1	2.24± 0.08	2.42 ± 0.13	62 ± 2	4.76 ± 0.20	3.27
2	1.76± 0.06	1.86 ± 0.05	60 ± 2	2.84 ± 0.10	4.01

Compound **1** can be self-assembled flat on HOPG, however, compound **2** with three more phenyl groups in comparison to compound **1** lifts partially its substituents into the solution and packs densely on the solid surface. The neighboring phenyl groups directly attached to the molecular core in compound **2** play a role in the organization of the molecules when physisorbed into a monolayer at the HOPG-solutions interface. To minimize the steric interaction of the ortho phenyl groups, the sustituents are likely to arrange in a nonplanar conformation with respect to the molecule disc core. Some are possibly suspended in the solution, rather than packed on HOPG, inducing the smaller area of the lattice of the monolayer than the footprint of the single molecule.

b) Alkylated phenylene groups on the trizigzagHBC cores

In previous work, D_{6h} symmetric HBC-(t-butyl)$_6$ or HBC-(chiral $C_{8,2}$)$_6$ with bulky side chains have been investigated [122]. HBC-(t-butyl)$_6$ cannot be visualized at the solution-graphite interface by STM because the steric interaction of the bulky substituents induce the loss of the planarity of the HBC aromatic cores on the surface. HBC-(chiral $C_{8,2}$)$_6$ has been found densely packed in hexagonal crystals in monolayers with all conjugated cores lying equally flat on the basal plane of the HOPG with partial side chains. In the latter case, it is suggested that the steric hindrance forces the part of alkyl chains from the methyl branches in the γ–positions to be solubilized in the supernatant solution [122]. Moreover, the compound of HBC-(Ph-chiral $C_{8,2}$)$_6$ comprising phenylene between the aromatic cores HBC and bulky alkyl side chains have been studied to exhibit hexagonal structure with different contrasts within a monolayer [123].

With the purpose of expanding the database on molecular nanostructures from molecules with bulky side chains in monolayers for molecular electronics and organic electronics, compounds

have been synthesized by combining bulky substituents and C_3 symmetric large aromatic cores of PAHs. t-butyl or $C_{8,2}$ alkyl chains were introduced in the *para* positions of phenylene rings of the C_3 symmetric molecular cores **3** or **4** or **5**, shown in Chart 4.2. The introduction of alkyl groups on phenylene rings provokes a dramatic change in the macromolecular arrangement in comparison to compounds **1** and **2**, which leads to the change from hexagonal molecular patterns of compounds **1** or **2** to extremely regular honeycomb nanostructures of compounds **3**, **4** or **5**.

Figure 4.4a, c, e displays large-scale STM images of the highly ordered monolayers of **3, 4** and **5** at the interface HOPG-solution in 1,2,4-trichlorobenzene, respectively. Figure 4.4b, d, f displays correspondingly high-resolution STM images of monolayers of **3, 4** and **5** on HOPG. The bright spots in each image are PAH cores (corresponding to high tunneling probability), while the substituents could not be resolved.

Figure 4.4a shows STM images of nanopatterns from compound **3** physisorbed at the interface between its solution and HOPG. It reveals a 2D supramolecular network with some defects. The highly ordered honeycomb nanostructure is shown in the high resolution STM image (Figure 4.2b). The unit cell is comprised of two molecules with parameters a = (2.57 ± 0.12) nm, b = (2.76 ± 0.15) nm, and α = (62 ± 3)º. The corresponding area of one molecule is 3.10 nm^2, which is smaller than to be expected for a single molecule that lies completely flat on the surface (~ 4.2 nm^2). Therefore, the alkylated phenylene groups are believed to either be dissolved in the supernatant solution or dynamically moving in the voids shown in the images. High resolution images such as the one displayed in Figure 4.4b reveal triangle-like features, corresponding to the π-conjugated PAH cores. Since the larger the PAH cores, the stronger the affinity with HOPG will be, the large C_3 symmetry PAH cores may be visualized at the HOPG-liquid interface by STM, while the more mobile substituents attached on the aromatic disks of PAHs are not resolved.

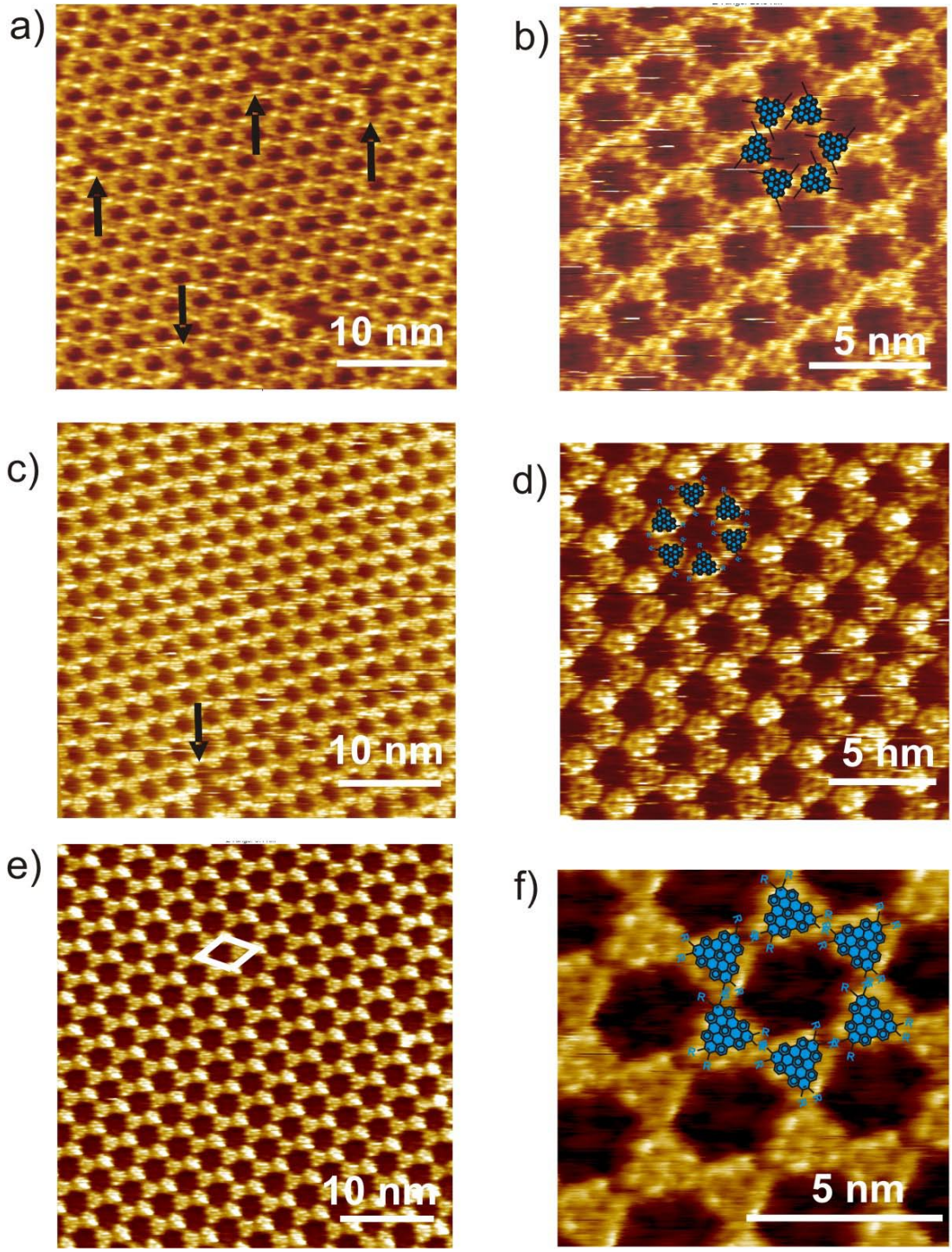

Figure 4.4: Large-scale (a) and high-resolution (b) STM current images of **3**. In the image a, the missing molecules in the network are marked by the black arrows. (c) and (d) STM current images of **4**. In the zoom-out (c) images, the missing molecule is pointed out by the black arrows. (e) and (f) STM images of **5**. Molecular structures of the conjugated parts of the molecules are superimposed for illustration.

The molecular arrangement observed in the STM experiment for compound **4** is depicted in Figure 4.4c and d. The lattice is characterized by the parameters of a = (2.57 ± 0.19) nm, b = (2.86 ± 0.09) nm, and α = (65 ± 3)º. The area of the unit cell with two molecules is

6.69 ± 0.40 nm^2. The deduced occupied space by one molecule is about 3.35 nm^2, smaller than the area within the van der Waals contour of a single molecule lying flat on the surface (~ 5.58 nm^2). In the image scale of 50 x 50 nm^2 (Figure 4.4a), defect are exhibited, as marked by the black arrows. The number of defects for compound **4** is less than that for compound **3**. It can be explained by enhancing the interaction between molecules and HOPG due to the increased affinity of longer alkyl chain to HOPG.

Figure 4.4e, f displays the self-assembled monolayer of compound **5** at the interface of the solution and the basal plane of HOPG. Compound **5** packs highly regular within a honeycomb lattice, with the determined unit cell parameters of a = (3.34 ± 0.14) nm, b = (3.49 ± 0.16) nm, and α = (62 ± 2)º. The corresponding area (~5.12) nm^2 is smaller than required for two molecules lying totally flat on the graphite surface (8.67 nm^2 per molecule), indicating that the alkyl chains dissolve partially in the supernatant organic solution. In the zoom-out image Figure 4.4e, the perfect network is shown. It may be employed for the design of nanotemplates based on PAHs as a host and a second molecular species as a guest.

Table 4.2: Lattice constants of the two-dimensional crystal structures of compounds 3, 4, and 5

	a (nm)	b (nm)	α (º)	Area (nm^2)	Area /molecule (nm^2)	Footprint /molecule (nm^2)
3	2.57± 0.12	2.76 ± 0.15	62 ± 3	6.20 ± 0.30	3.10	4.20
4	2.57± 0.19	2.86 ± 0.09	65 ± 3	6.69 ± 0.40	3.35	5.58
5	3.34± 0.14	3.49 ± 0.16	62 ± 2	10.25 ± 0.80	5.12	8.67

The number of defects for compound **3** is four times larger than that for compound **4** on the images on the scale of 50 x 50 nm^2, while compound **5** has no defect on the same imaging area. This is possibly due to the increased length and the number of alkyl chains, which enhance the interaction between molecules and HOPG due to the considerable affinity of alkyl chains to HOPG.

A possible explanation for honeycomb nanostructures is on the one hand that the alkyl chains in phenylene trizigzagHBCs (**3**, **4**, **5**) increase the distance between each molecule, and on the other hand, that because of the C_3 symmetry of the PAH cores the formation of the chicken-wire pattern is natural for structure stabilization.

In summary, with a molecular scale visualization of monolayers of a series of large C_3 symmetric PAHs with bulky alkylated phenylene side chains, it has been demonstrated that

they self-assemble into highly regular honeycomb nanostructures at the interface between the basal plane of HOPG and its solution in 1,2,4-trichlorobenzene. The honeycomb pattern may be attributed to nanophase separation between the side chains and the PAH core. The incompatibility of the side chains and the PAH core play an important role for the stability of the honeycombs. For example, the longer an alkyl chain is the smaller the number of packing defects. This kind of substituted trizigzagHBCs gives rise to a new superstructure, which may be employed for the design of molecular electronic devices based on PAHs as a host and a second molecular species as a guest.

c) Side groups of trizigzagHBC molecules containing carboxyl groups, electron donors or acceptor moieties

Functionalization of the triangle-shaped PAHs is attractive for molecular engineering, e.g., employing molecular self-assembly controlled by hydrogen bonds [92,117,124] and via charge transfer [47,120]. The carboxyl groups are introduced in the PAH derivatives. On the other hand, given that the PAHs have been studied to be electron-rich, the "dyads" are designed with electron donor or electron acceptor moieties at the end of alkyl chains.

Molecules **6** and **7** (Chart 4.2) connected with carboxyl groups were studied by STM at the solution-HOPG interface. However, no stable structure could be observed, probably due to the strong hydrogen interaction, which enhances the attractive interactions between discotic mesogens in the columnar phase due to π-π stacks in the supernatant solution, rather than allowing their break-up and the physisorption on HOPG [125].

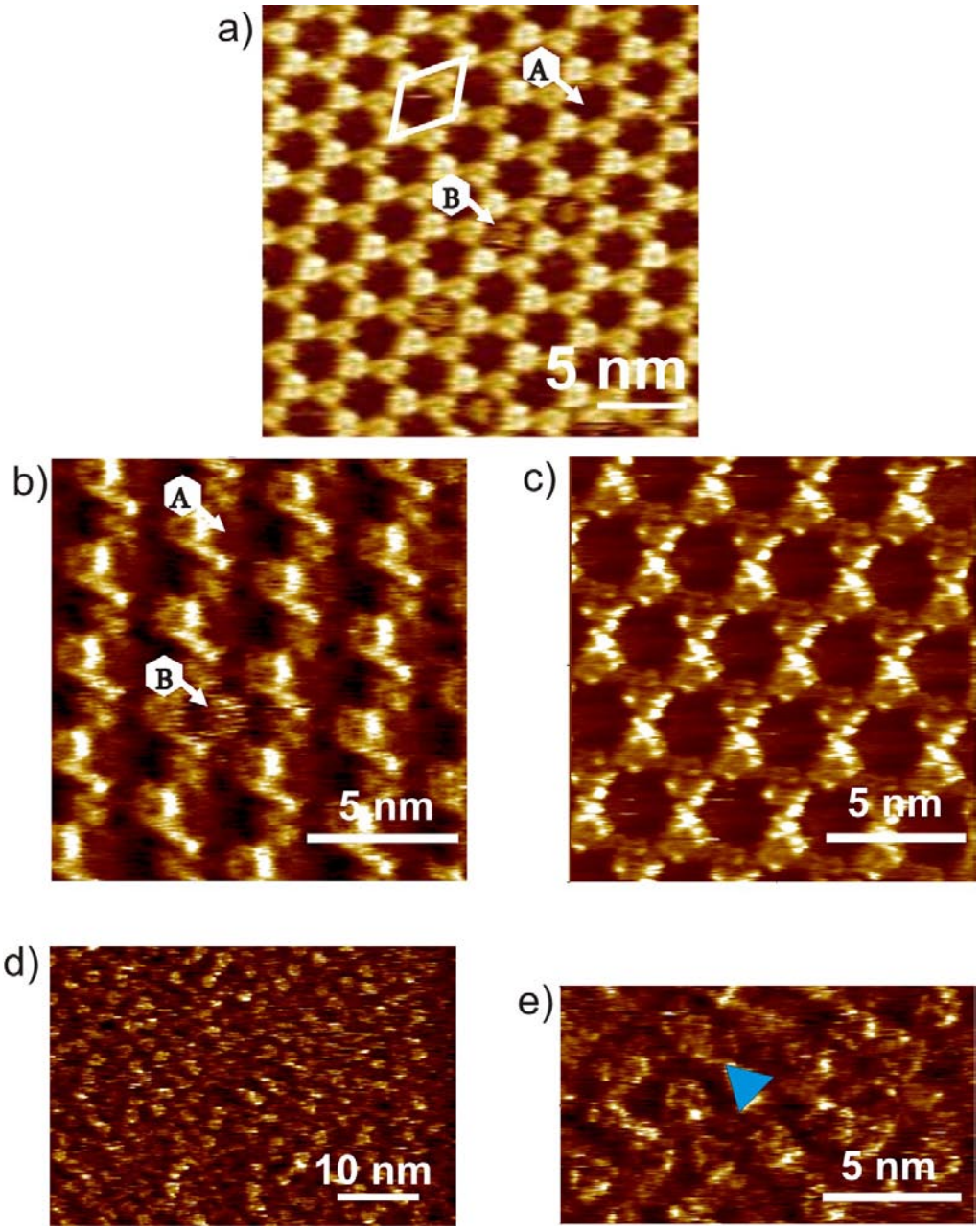

Figure 4.5: (a) High-resolution STM current image of **8**. The nanocavities are marked by A, the filled nanocavities marked by B. (b) STM current image of **9**. Empty nanocavity marked by A, occupied nanocavity marked by B. (c) Highly ordered chicken-wire structures of **10**. Large-scale (d) and zoom-in (e) STM current images of **11**. In the images, **11** formed disordered structures, and the triangle-shaped cores are obviously visualized, marked by the blue triangle.

Within the "dyads" investigated here, we have three kinds of donor moieties, ethyl (**8**), phenyl (**9**) and naphthyl (**10**). The STM image of compound **8** in Figure 4.5a demonstrates that a honeycomb pattern is formed from alkylated phenyl trizigzagHBCs, with some cavities occupied by non-solvent molecules. The objects in the voids have not been identified, because they are dynamically in motion. The template provides the high possibility to accommodate guest molecules into the voids, or replace the dynamically occupied features. The

macromolecular arrangement is described by a unit cell with parameters of a = (3.31± 0.14) nm, b = (3.41 ± 0.12) nm, and $\alpha = (63 \pm 3)^{o}$. The related area of one molecule in the lattice (~5.03 nm^2) is smaller that the footprint of a single molecule lying flat on the surface (~ 5.74 nm^2). Obviously, partially the side chains attached to the trizigzagHBC aromatic cores are solubilized by the supernatant solution. Within experimental errors, the monolayer nanostructure of compound **8** is indistinguishable from that of compound **5**. Therefore, both compounds are used in the investigation of nanotemplates in the section 4.2.2.

Figure 4.5b displays an STM image of a highly ordered monolayer of compound **9**. The 2D crystal is indistinguishable from that of compound **8**, except for less occupied voids in the honeycomb network. The nanostructure is characterized by the unit cell of a = (3.33± 0.22) nm, b = (3.68 ± 0.09) nm, and $\alpha = (62 \pm 4)^{o}$, the corresponding area of one molecule is (~ 5.40 nm^2). The calculated van der Waals contour of a single molecule (~7.06 nm^2) is larger than the experimental value, indicating that a part of the side chain is in the solution.

Figure 4.5c shows an STM image of a regular arrangement of compound **10** at the solid-liquid interface, exhibiting a honeycomb network. The lattice constants of the 2D assembly are determined to be a = (3.30± 0.16) nm and b = (3.40 ± 0.26) nm, with $\alpha = (64 \pm 3)^{o}$. The occupied size of one molecule in the lattice, containing two molecules, is about 5.1 nm^2, smaller than the footprint of a molecule flat lying on the surface (~7.62 nm^2). The subsituents are partially suspended in the solution.

The molecular arrangements of compounds **8**, **9**, and **10** at the interface between the basal plane of HOPG and a solution in 1,2,4-trichlorobenzene is indistinguishable with respect to the lattice constants, displayed in Table 4.3. This finding indicates that when the end moieties of the alkyl chain at the *para*-position of phenylene in trizigzagHBC disks has electron-rich properties such as the conjugated trizigzagHBC cores with ethyl, phenyl, naphthyl, the end groups will be suspended in the supernatant solution.

Table 4.3: Lattice constants of the two-dimensional crystal structures of compounds 8**,** 9**, and** 10

	a (nm)	b (nm)	α (º)	Area (nm^2)	Area /molecule (nm^2)	Footprint /molecule (nm^2)
8	3.31± 0.14	3.41 ± 0.12	62 ± 4	10.06 ± 0.61	5.02	5.74
9	3.33± 0.22	3.68 ± 0.09	62 ± 4	10.79 ± 1.09	5.40	7.06
10	3.30± 0.16	3.40 ± 0.26	64 ± 3	10.20 ± 0.77	5.10	7.62

The STM images of **11** with the electron acceptor moiety (anthraquinone) are shown in Figure 4.5d and e. In the large scale image (Figure 4.5d), the randomly ordered structure is exhibited. The triangle-shaped PAH cores are displayed in the high resolution STM image (Figure 4.5e), and marked by blue triangle. The disordered packing can be possibly ascribed to inter- or intramolecular stacks formed by the interaction between acceptor moieties and their PAH cores with their electron pushing properties, or be partially solvated in the supernatant solution, which induces the disordered molecular packing on HOPG.

In summary, the modified end groups of side chains influence the self-assembly of C_3 symmetric trizigzagHBC derivatives. The strong hydrogen bonding interaction between carboxyl groups to cause networks in the solution prevents the monolayer formation of compounds **6** and **7** on HOPG. Electron donor moieties at the end of side chains within compounds **8**, **9** or **10**, lead to the formation of honeycombs in self-assembled monolayers. The electron donor moieties are found to be suspended in the solution, rather than adsorbed to the basal plane of HOPG. A disordered nanostructure is found for compound **11** with electron acceptors combined. The electron acceptors in the side chain may cause charge transfer complexes with PAH core, which counteract the formation of honeycombs.

d) PAH fused with electron-rich thiophene rings

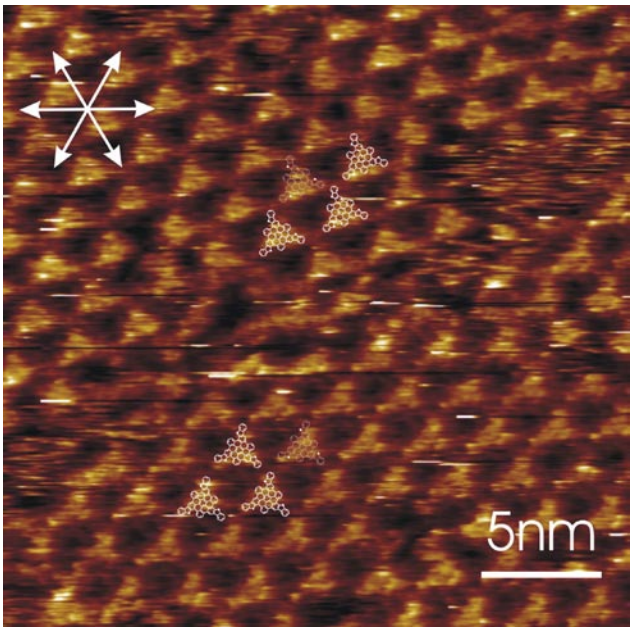

Figure 4.6: STM current image of polycrystalline monolayer with domains of compound **12** at the HOPG-solution interface.

Thiophenes are relatively electron rich, p-dopable, and primarily p-type semiconductors. Polycrystalline films of unsubstituted linear oligothiophenes are one of the first organic molecular films to be investigated for use in thin film transistors. A problem associated with the use of electron rich oligo/polythiophenes is their easy oxidation (doping) in air because of their high HOMO energies, which can be lowered by replacing some thiophenes with phenyl rings [126,127,128]. Compound **12** represents the first example of large PAHs fused with electron-rich thiophene rings.

The 2D self-assembly of **12** was investigated at the interface between a concentrated solution of 1,2,4-trichlorobenzene and the basal plane of HOPG. Figure 4.6 displays a two-dimensional polycrystalline structure, where the single crystallites were oriented epitaxially along one of the three graphite axes. In each grain, the two dimensional crystal exhibits a hexagonal unit cell with one triangular molecule. The unit cell is described by lattice constants a = (2.42± 0.10) nm, b = (2.55 ± 0.13) nm, and $\alpha = (61 \pm 4)^{o}$. The corresponding unit cell area of (5.40 ± 0.28) nm^2 is about twice as large as a footprint of a single molecule (~ 2.85 nm^2), indicating that the self-assembled molecules completely flat on the substrate, all oriented in the same direction with the interstitials filled by solvent molecules.
In summary, large PAHs fused with electron-rich thiophene rings pack loosely into monolayers, which provides a new road to obtain soluble and large conjugated molecules without alkylated substituents.

4.2 Self-assembled 2D monolayers from two substances

4.2.1 Non-covalent electron donor/ electron acceptor coadsorption

Two-dimensional molecular nanostructures of non-covalently interacting electron donors and acceptors, coadsorbed within the same layer, are investigated because of their potential to fabricate prototypical organic electronic devices by growing donor and acceptor molecules alternately in three-dimensions [129]. In a physisorbed monolayer the nature of the individual molecules is maintained during the molecular self-assembly, which can be scrutinized with the aid of STM [47,73,89,118,120].

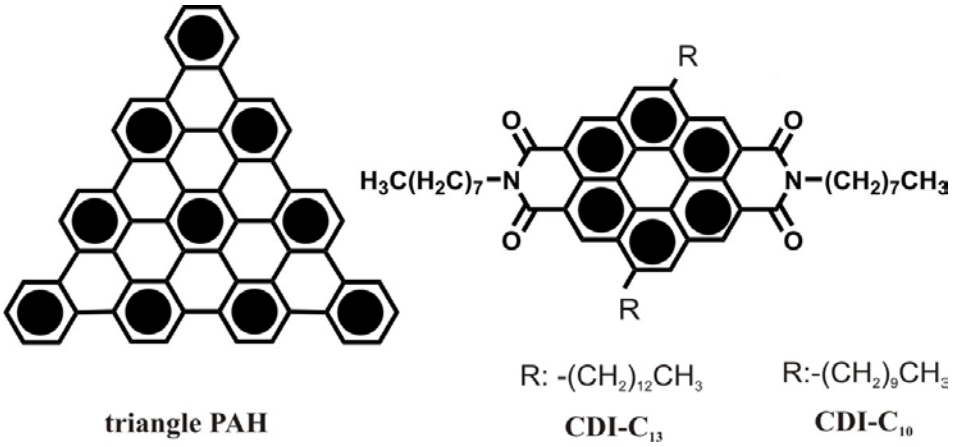

Chart 4.3: Chemical structures of molecules: **triangle PAH**, and alkylated coronene bis(dicarboxyimide) molecules (**CDI-C_{13}** and **CDI- C_{10}**).

The electron donor **triangle PAH**, an unsubstituted PAH, forms π–π stacked 1D aggregates in solution [130]. However, such a property prevents **triangle PAH** from forming flat layers on solid substrates, which are important for scaling up an electronic device by bottom-up processes. Taking advantage of its electron donor property, the electron acceptor **CDI-C_{13}** was introduced into the solution leading to the breakage of the donor aggregation due to stronger donor-acceptor interaction.

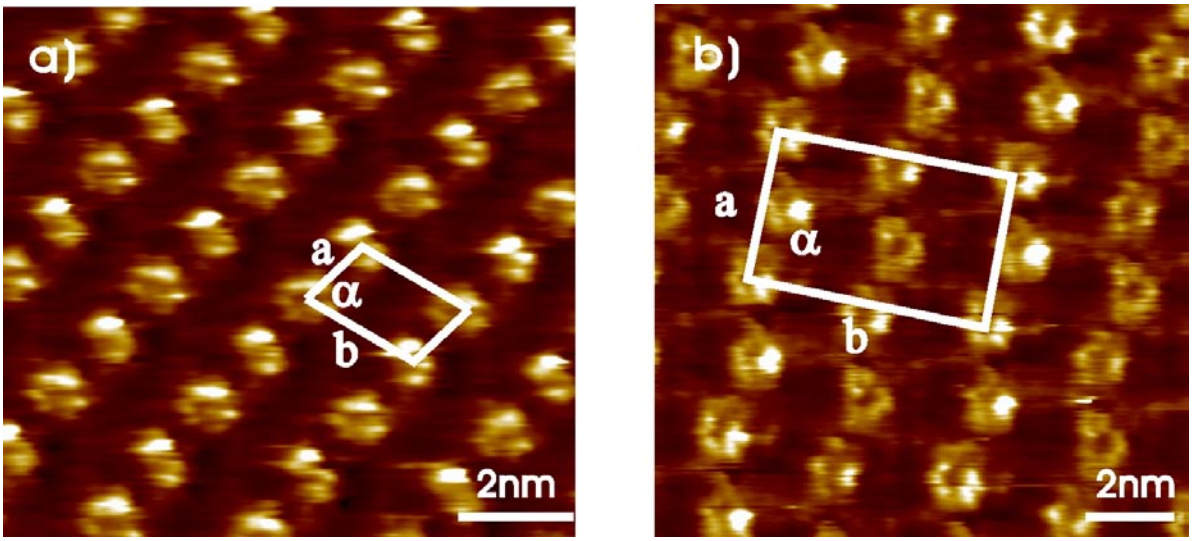

Figure 4.7: STM current images of **CDI-C_{13}**. a) oblique structure; b) zigzag structure.

Figures 4.7a and 4.7b display STM current images of two coexisting crystal structures"Oblique" and "Zigzag" of electron acceptors **CDI-C_{13},** physisorbed at the interface between HOPG and a solution in 1,2,4-trichlorobenzene. The contrast of adsorbates is similar to unsubstituted coronene deposited on HOPG in UHV-STM which has a hole at its center [131]. The lattice constant (Table 4.4) of the oblique crystal in Figure 4.7a is smaller (~2.6 nm^2) than a footprint of the molecule (~3.67 nm^2) based on van der Waals contours, indicating

that parts of the alkyl chains are in the organic solvent to provide enough space for the core of molecules on HOPG. However, the zigzag crystal in Figure 4.7b contains four molecules in a unit cell, where each molecule is larger than the footprint of the molecule, and the void part is filled with solvent molecules. We assume that the molecules are lying completely flat on the substrate. Based on the image features of the two structures, packing models are proposed (Figure 4.8), which are consistent with the experiment. They are constructed such that the conjugated cores of **2** are packed on HOPG as an A-B packing. The alkyl chains in the packing models are packed along one axis of HOPG, even though they will not be as ordered as indicated in the sketch.

Table 4.4: Lattice constants of the two-dimensional crystal structures of triangle PAH and CDI-C_{13}.

System	Lattice type	Lattice parameter	A (Area) in nm^2
Acceptor(CDI-C_{13})	Oblique	a = 1.26 ± 0.03 nm b = 2.17 ± 0.07 nm α^* = 71 ± 2 º β^* = 20 ± 1 º	2.60 ± 0.2
	Zigzag	a = 3.25 ± 0.21 nm b = 5.35 ± 0.21 nm α = 86 ± 3 º β = 25 ± 5 º	17.30 ± 0.80
Acceptor(CDI-C_{13}) /Donor(triangle PAH)	2A/2D	a = 2.87 ± 0.05 nm b = 3.55± 0.13 nm α =74 ± 2 º β =4 ± 2 º	9.81 ± 0.36
	2A/4D	a = 3.82 ± 0.06 nm b = 4.19 ± 0.19 nm α = 87 ± 2 º β = 26 ± 2 º	15.98 ± 0.73

*α: the angle between a and b; β: the angle between one of axis of HOPG and the lattices of molecules.

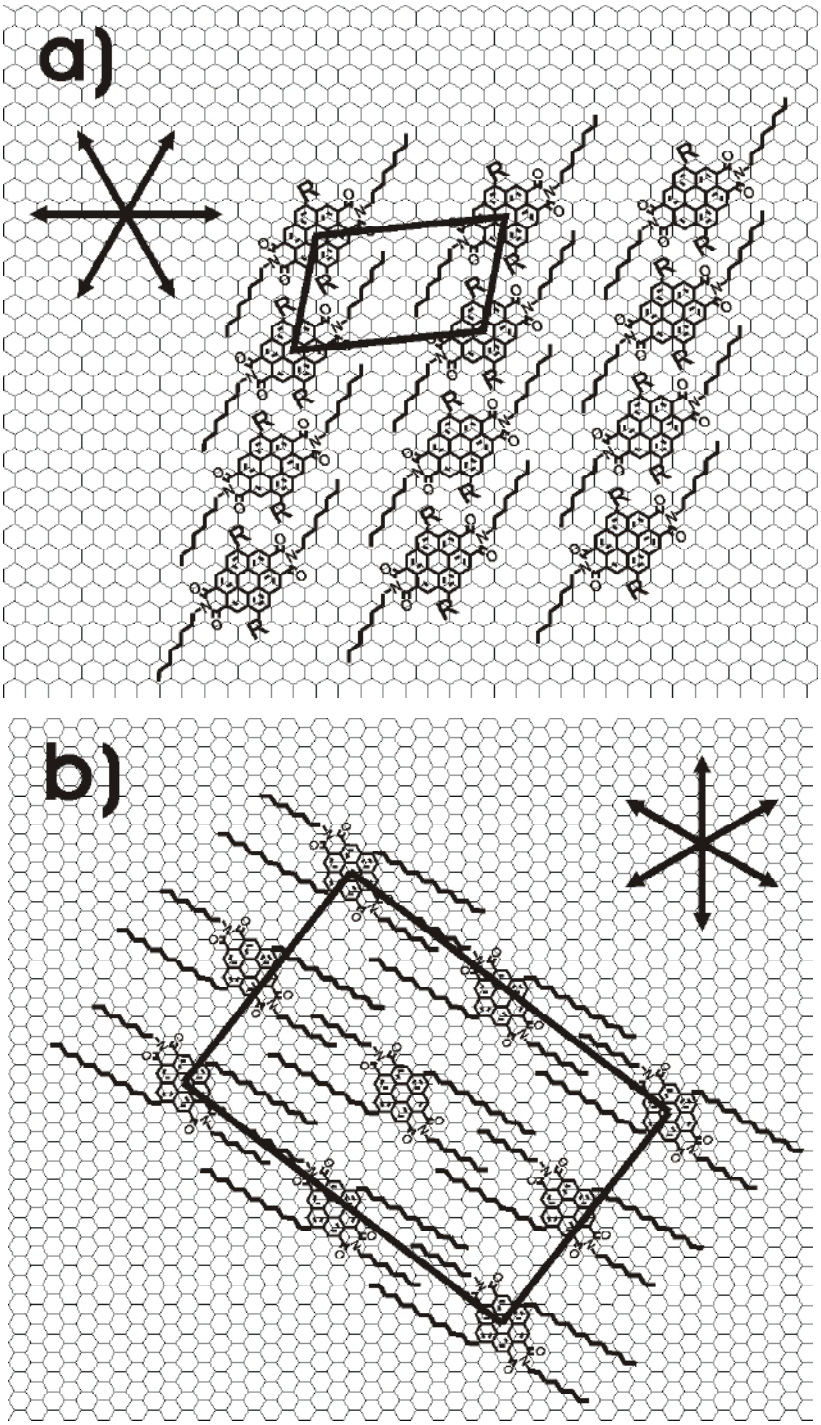

Figure 4.8: Proposed molecular packing model for the acceptor **2.** a) Oblique structure, R replaces the alkyl chain-CH_2 $(CH_2)_{11}CH_3$, which may dissolve in the solvent and not lie flat on HOPG. a = 1.29 nm, b = 2.10 nm, α = 73 °; b) Zigzag structure. a = 3.45 nm, b = 5.22, α = 89 °.

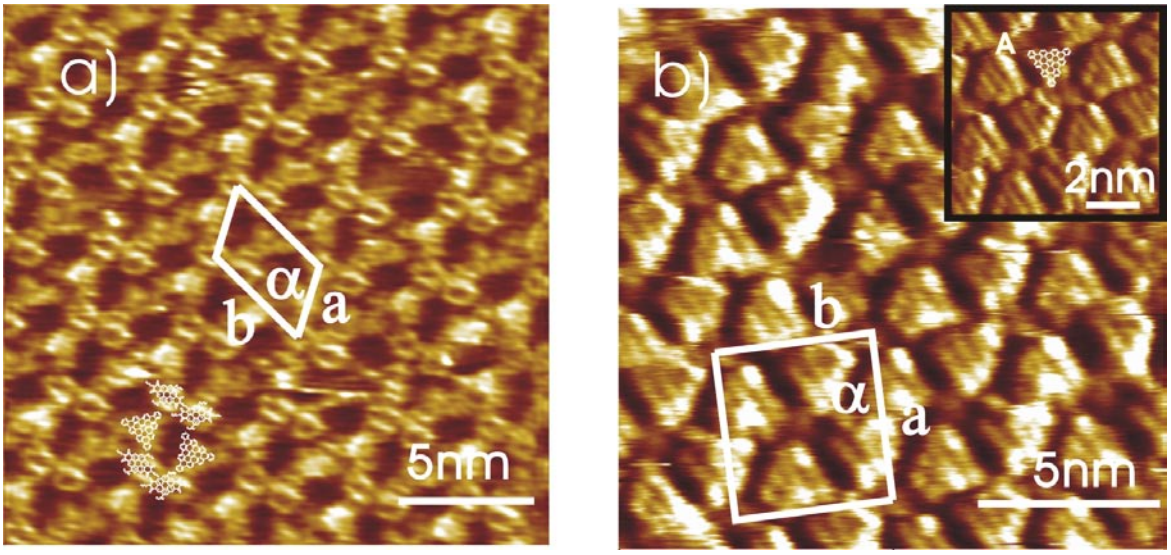

Figure 4.9: STM current images of mixtures of **triangle PAH** and **CDI-C_{13}**. a) two acceptors and two donors (2A/2D) , sample bias U_s=- 1 V; average tunneling current I_t = 0.1 nA. The unit cell comprises two molecules of **triangle PAH** and two of **CDI-C_{13}**; b) two acceptors and four donors (2A/4D).

From the mixture of electron donor **triangle PAH** and electron acceptor **CDI-C_{13}** in the solution, nanostructures from donor/acceptor codeposition are clearly discerned. In Figure 4.9a, a feature exhibits a hole at the center, which can be attributed to molecule **CDI-C_{13}** as in the neat **2** system. The triangle-shaped configurations are ascribed to **triangle PAH**, where the neighboring triangles are opposite so as to fit in the crystalline structure. The corresponding area (~9.81 nm^2) of the lattice, occupied by two acceptors and two donors (2A/2D), is smaller than the theoretical van der Waals contours of the four molecules (~12.78 nm^2). There is another structure (Figure 4.9b) with a unit cell of two acceptors and four donors (2A/4D) similarly as in the mixture system of **HBC** and **CDI-C_{10}** [132,133]. On the basis of Figure 4.9, a model is proposed (Figure 4.10). The conjugated cores of the acceptors and donors both pack on HOPG corresponding to the typical A-B packing in graphite. The alkyl chains connected with the conjugated cores of the acceptors are not indicated in the models since the void between the aromatic cores is not large enough to accommodate them, which agrees with the experimental results, i.e. the alkyl chains are dissolved in the supernatant solution.

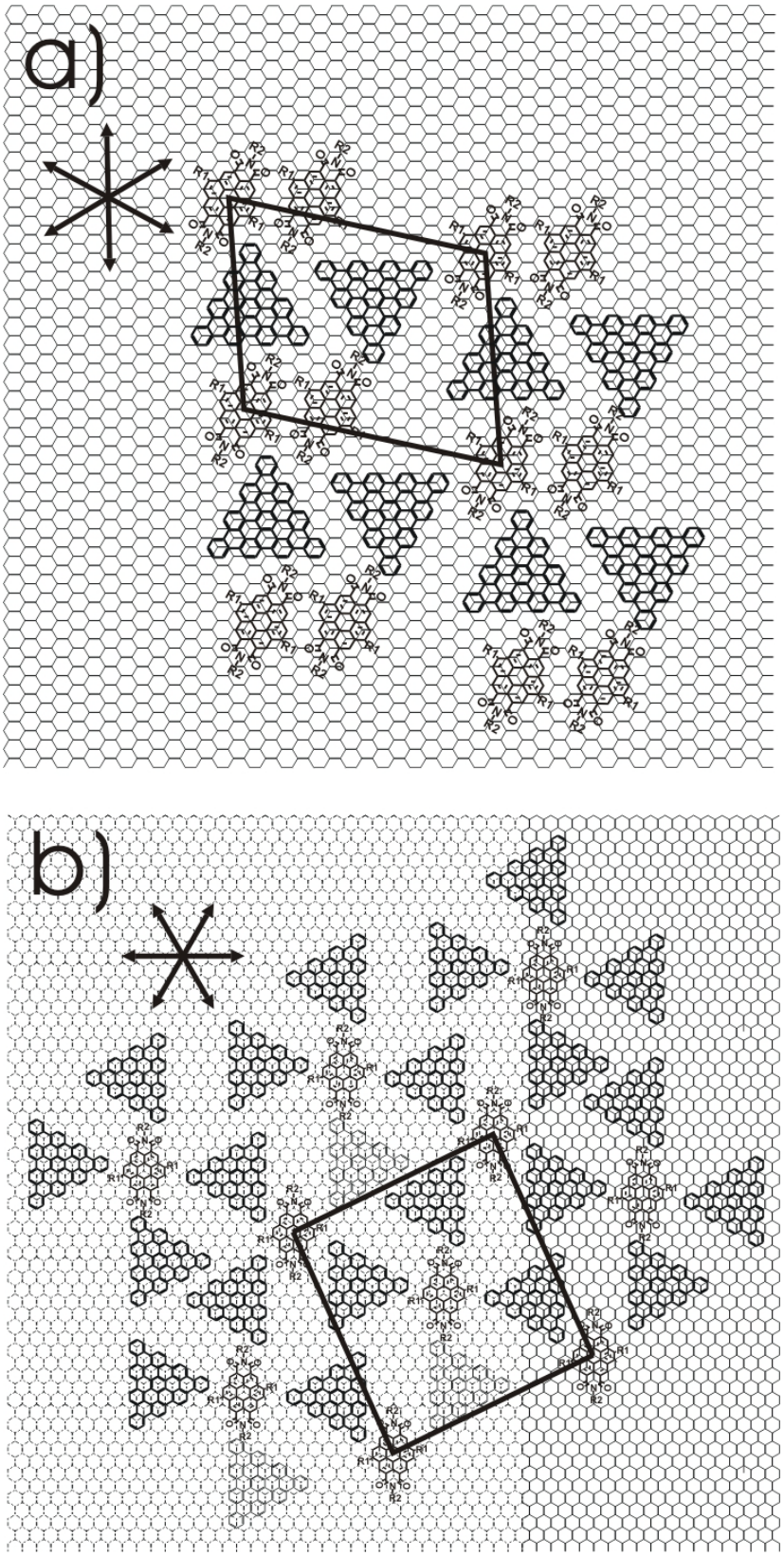

Figure 4.10: Proposed molecular packing model for the mixture of **triangle PAH** and **CDI-C_{13}**. R replaces the side chain. a) 2A/ 2D: a = 2.84 nm, b = 3.49 nm, α = 74°. b) 2A/4D: a = 3.85 nm, b = 4.22 nm, α = 88°.

In the neat system **triangle PAH**, no single molecules are observed at the HOPG-solution interface. Since the formation of crystalline structures on the surface depends on the competition between adsorption and desorption, it may be concluded that the electron donor **triangle PAH** may prefer to form molecular stacks in the solvent, rather than crystallize on HOPG. On the contrary, the electron acceptor **CDI-C_{13}** can form ordered structures on HOPG. The long alkyl chains on **CDI-C_{13}** increase the affinity to HOPG and might also disturb π-π stacking of the molecules in solution thereby increasing the solubility. The chain length dependence is supported by the comparison to the experiment with the **CDI-C_{10}** which exhibits shorter alkyl chains on the imides and is more difficult to crystallize on HOPG.

In a mixed solution of both electron donor **triangle PAH** and acceptor **CDI-C_{13}**, molecules **triangle PAH** are surprisingly coadsorbed with **CDI-C_{13}** to form a new crystal structure. Based on this observation we suggest that the donor-acceptor interaction breaks the donor/donor stacks in the mixed solution [129]. However the possibly formed 1D donor/acceptor stacks are also not energetically favorable on the HOPG surface due to the irregular shapes of the donor and acceptor. Consequently packing into 2D systems resulted on the one hand due to strong coupling between **triangle PAH** or **CDI-C_{13}** molecules and the HOPG surface, and on the other hand due to the donor-acceptor interaction within the same layer on HOPG ("parallel interaction"). Although the latter interaction is relatively weak, nevertheless it is not negligible, since the experiments of other electron donors of the substituted HBCs mixed with **2** have only shown phase separation, which indicates that the substituents increase the distance between donors and acceptors within the same layer, thereby the parallel donor-acceptor interaction is much weakened (Figure 4.11). Therefore, the driving force for the formation of the coadsorbed nanostructures in this experiment is not the donor-acceptor stack interaction but the "parallel interaction".

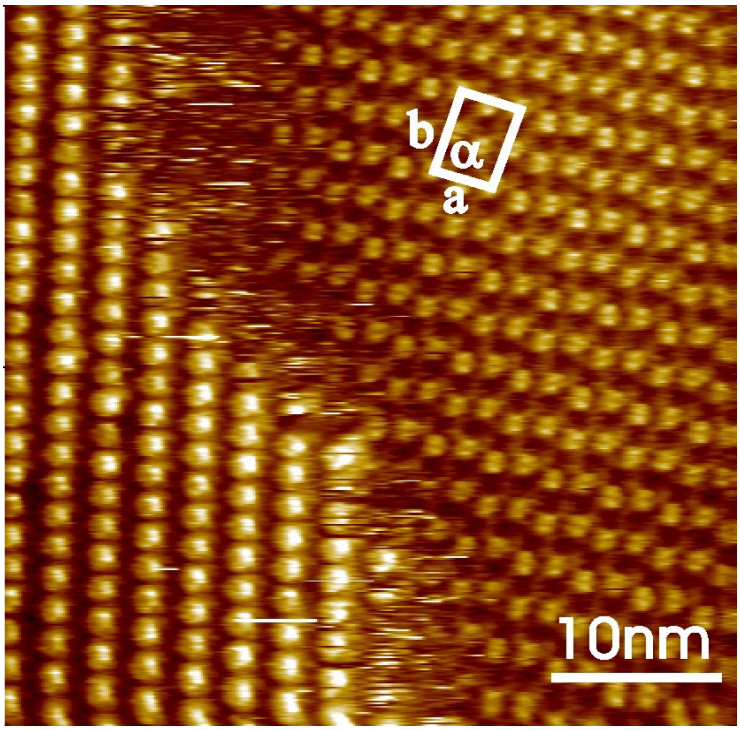

Figure 4.11: STM height images of the mixture of 2,5,8,11,14,17-hexa-(n-dodecyl)-HBC (HBC-C12) and **CDI-C_{13}** at the HOPG- solution in 1,2,4-trichlorobenzene. The left domain of the image is ascribed to HBC-C12 with an oblique unit cell, and the right part of the image is attributed to **CDI-C_{13}** with a zigzag cell (a = 3.27 ± 0.20 nm, b = 5.13 ± 0.16 nm, α = 87° ± 2°, β =26° ± 4°, A = 16.74 ± 1.2 nm^2).

In summary, a mixture system of novel D_{3h} symmetric electron donors and alkylated acceptors is investigated at the HOPG-solution interface by STM. The analysis of the results reveals that the donors, which cannot be adsorbed as a neat system, are coadsorbed with acceptors to form a monolayer on HOPG. The results indicate that the nanostructures can be formed from the mixture via weak non-covalent "parallel interaction". This work casts light on a 2D monolayer design consisting of electron donors and acceptors directly on the conducting solid substrate. Moreover, the system constitutes an intriguing model for further explorations of the many facets of the self-assembly of the molecular electron donor/acceptor complexes.

4.2.2 Chicken-wire nanostructures selection for guest molecules

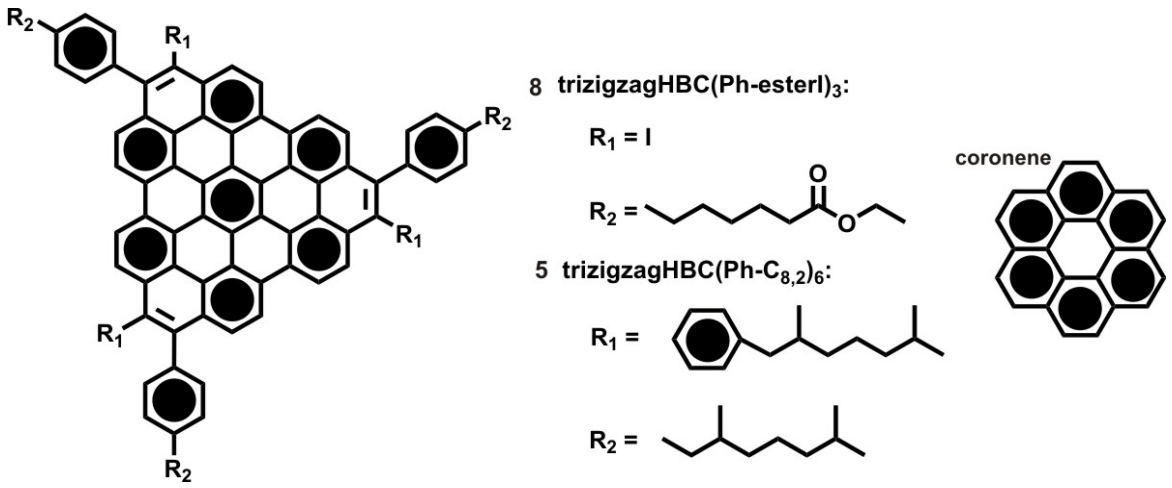

Chart 4.4: Chemical formulae of **8**, trizigzagHBC(Ph-esterI)$_3$, **5**, trizigzagHBC(Ph-$C_{8,2}$)$_6$, and **coronene**.

Porous molecular monolayers are potential two-dimensional hosts for molecular guests, which may be employed for molecular selection or the isolation of single molecules. They have been obtained from macrocycles at the interface between an organic solution and the basal plane of graphite, providing pores in the range of 1.2 to 2.7 nm [123,134,135,136,137]. Alternatively, supramolecular two-dimensional structures have been self-assembled at such solid-liquid interfaces, stabilized by van der Waals interactions between pending alkyl chains [41,42,81,84,116]. Thereby, cavities in the range of 3.1 to 3.7 nm may be obtained from identical molecular cores just by varying their side chains [116]. However, due to the weakness of the interactions stabilizing the networks the filling of the pores may be accompanied by structural transformations of the host [116]. More stable hosts were assembled from two molecular species interacting with each other by hydrogen bonding [34,138] or metal coordination [37]; however, the nanosize of cavity cannot be tuned due to the specific molecule interactions.

Here robust honeycomb structures are reported at the interface between an organic solution and the basal plane of HOPG. The hosts are formed by C_3 symmetric polycyclic aromatic hydrocarbons, stabilized by the weak interactions of alkyl side chains, and thereby providing nanometer-sized cavities. Honeycomb networks from alkylated PAHs with ester end groups **8** have been filled with single **coronene** molecules as guest molecules without changing their lattice parameters, indicating both their robustness and their potential to isolate nanometer-sized single molecules.

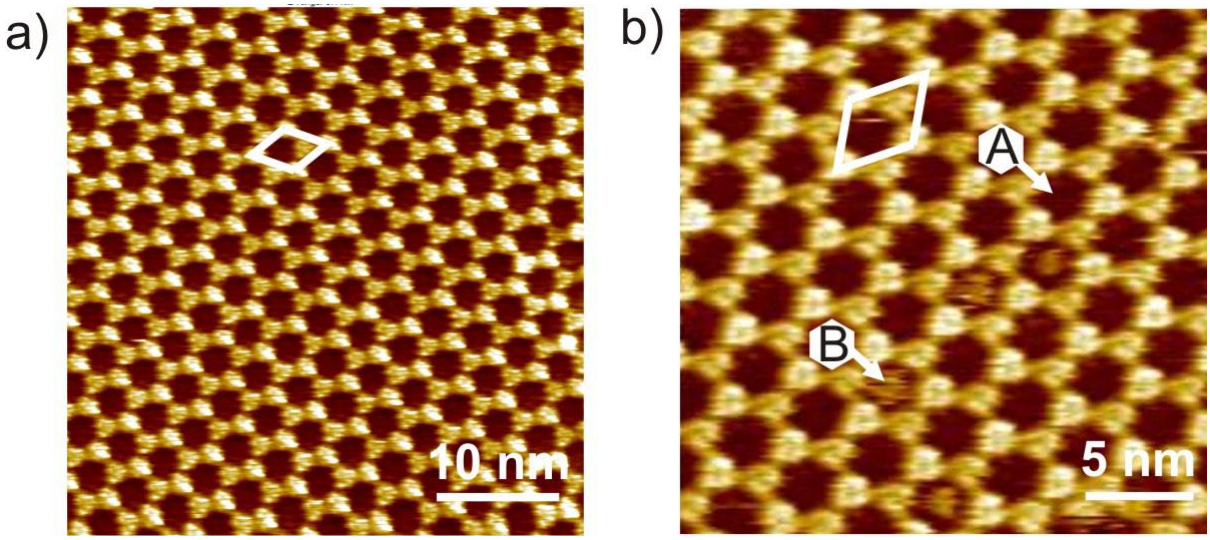

Figure 4.12: STM current images of molecular monolayers self-assembled at the interface between organic solutions of (a) **5** and (b) **8** and the basal plane of graphite. Both exhibit honey-comb structures consisting of two molecules in a unit cell as marked by parallelograms. In (b) most nanocavities appear empty (marked "A"), while some are filled (marked "B"). Sample bias U_s = -1V; average tunnelling current I_t = 0.1 nA.

The C_3 symmetric derivatives of diphenanthro[3',4',5'6'-efghi:3,4,5,6-uvabc] ovalene with three zigzag-peripheries ("trizigzagHBC") **8** and **5** have been shown to form self-assembled monolayers at the graphite-solution interface, exhibiting a honeycomb pattern with cavities on the nanometer scale in the section 4.1.2.

Scanning tunneling microscopy images obtained *in-situ* at the solid-liquid interface (Figure 4.12a) reveal defect-free honeycomb-lattices of **5** on scales larger than 50 x 50 nm^2. The bright features (corresponding to high tunneling probability) are attributed to the □ -conjugated aromatic rings, while the dark parts are attributed to the aliphatic side chains, which could not be resolved. The image is characterized by hexagonal cavities, whose symmetry and orientation reflect the underlying HOPG lattice.

Molecules **8** exhibiting alkyl side chains with ester end groups form similarly very uniform 2D honeycomb monolayers (Figure 4.12b). From the STM images, the unit cell can be determined with high accuracy (Table 4.5). Most cavities appear empty, indicating that they are filled with solvent molecules exhibiting a large HOMO-LUMO gap and therefore contributing much less to the tunneling current than the PAH cores. However, some cavities appear filled by single molecules of **8**, indicating that they may be also filled with different molecular guests.

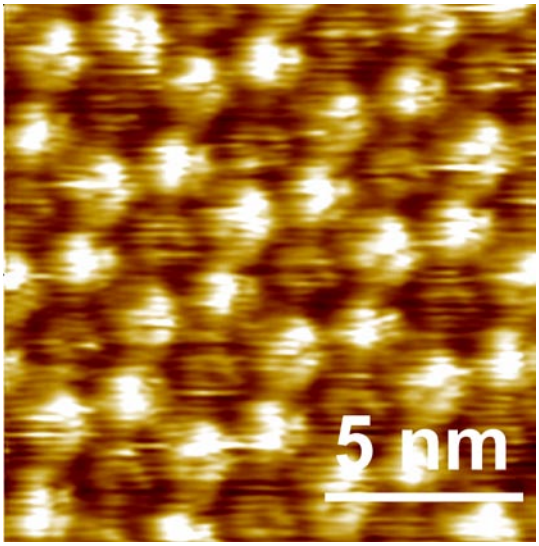

Figure 4.13: STM current image at the interface between an organic solution and the basal plane of graphite, displaying the filling of the nanocavities of the honey-comb monolayer of **8** with single **coronene** molecules. Sample bias U_s = -1V; average tunnelling current I_t = 0.1 nA.

Table 4.5: Lattice constants of the two-dimensional crystal structures of HBC derivatives

System	Lattice parameter	A (Area) in nm^2
8	a = 3.34 ± 0.14 nm b = 3.49 ± 0.16 nm α^* = 62 ± 2 º	10.25 ± 0.80
5	a = 3.31 ± 0.14 nm b = 3.41 ± 0.12 nm α = 63 ± 3 º	10.06 ± 0.61
8 + **coronene**	a = 3.34 ± 0.07 nm b = 3.44 ± 0.02 nm α = 60 ± 0.3 º	9.92 ± 0.24

$^*\alpha$: the angle between a and b.
(The footprints of single **8**, **5** and **coronene** are 5.74 nm^2 , 8.67 nm^2, and 2.8 nm^2 respectively.)

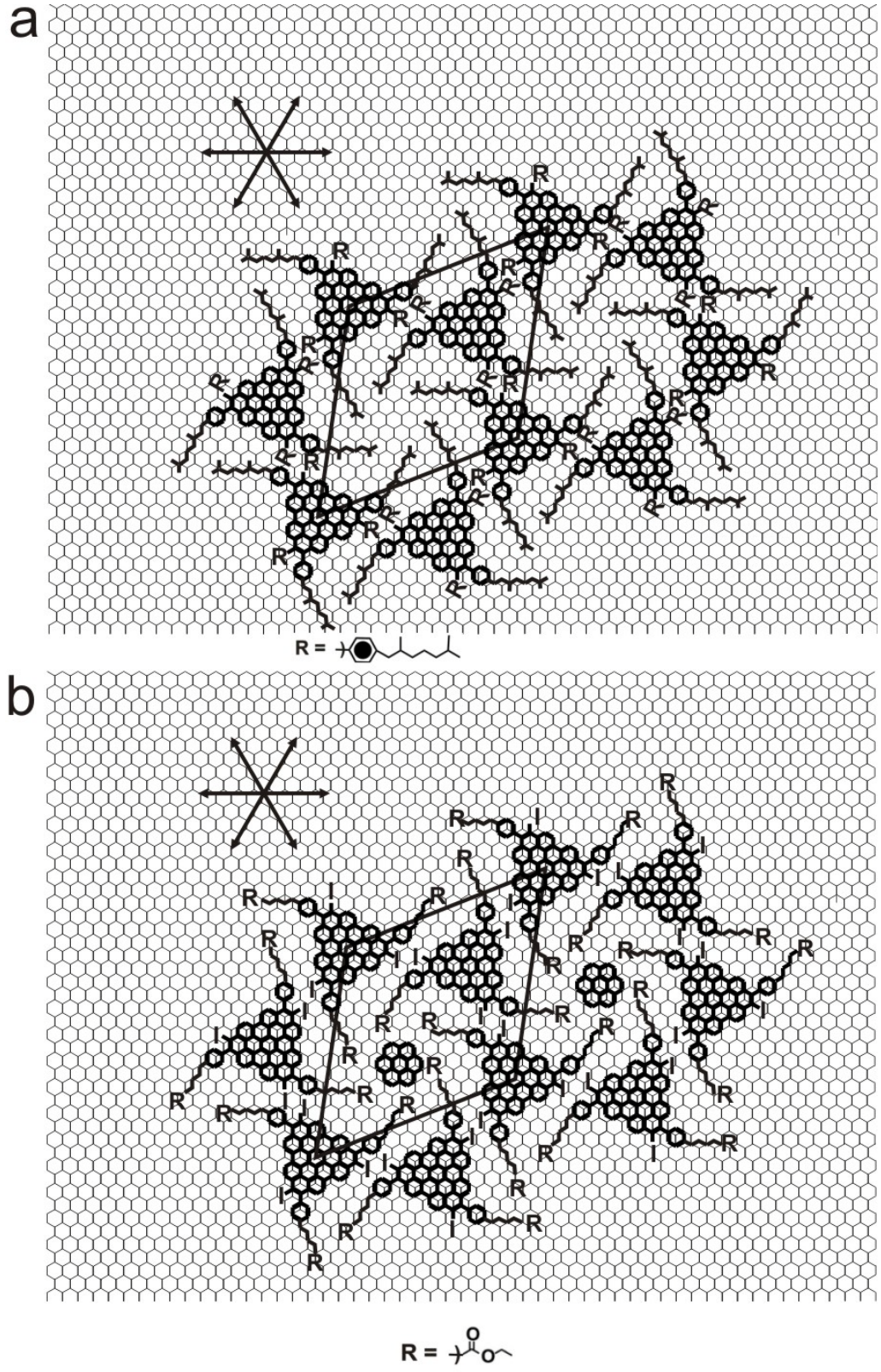

Figure 4.14: Proposed molecular packing models for (a) neat **5**, and (b) **8** coadsorbed with **coronene**. a = 3.46 nm, b = 3.46 nm, α = 60 ^{o}.

For that purpose, **coronene** was added to the solution because due to its relatively small HOMO-LUMO gap it can potentially be recognized in the STM, while as a neat system it

does not form a crystalline monolayer of flat lying molecules. Upon depositing a drop of the solution containing both **5** and **coronene**, only the same structure as in the neat system **5** has been visualized, indicating no pore filling. However, **8** mixed with **coronene** provides a hexagonal lattice, which has the same lattice constant as that from the pure monolayer of **8** (Figure 4.13, Table 4.3), but exhibits a different contrast with monodisperse, less bright objects in the nanocavities, instead of the mostly dark and occasionally occupied voids within the monolayers of neat **8**. It indicates that the **coronene** molecules are entrapped in the molecular template provided by the unaltered honeycomb lattice of **8**. In the STM image, the entrapped molecules are less bright than **8**, and dark at their centre. It has been reported previously that on HOPG the center of **coronene** exhibits less tunneling current than the outer parts of the molecule [131], supporting further that single **coronene** molecules are entrapped within the cavities.

The successful capture of **coronene** molecules in the nanocavities may be attributed to the ester function at the end of the alkyl chains pending from the PAH cores. In the section 4.1.2 the lattice constants of the monolayer arrangement of ethyl, or phenyl, or naphyl subsituted trizigzag HBC esters are indistinguishable in Table 4.1, also indicating the ester end groups are dissolved in the supernatant solutions.

In Figure 4.14 packing models are proposed, which are consistent with the experiment. The model for the packing of **5** (Figure 4.14a) is constructed such that the conjugated PAH cores are oriented on HOPG as the nano-graphene layers in graphite. One of every two neighboring side chains is not drawn since there is not enough space for them on the surface. It appears that the size of cavity in the network is not large enough to accommodate a **coronene** molecule. Thereby, in the mixture of **5** and **coronene**, the pattern is the same as in the neat system **5**. Figure 4.14b displays the model for **8** filled with **coronene**. The conjugated core of **8** is packed as **5**. However, only the part of the substituents until the fifth carbon from the PAH core are packed on HOPG, while the end groups of ester moieties have less affinity to HOPG, and suspend in the solution, similarly to HBC with branched alkyl chains [122]. Therefore the formed cavity becomes larger to host a single **coronene** molecule. Consequently, in the corresponding model the ester end groups of **8** provides the ability to host the guest molecules.

In summary, by functionalizing the end groups of its alkyl side chains we have controlled the capability of a honeycomb forming PAH to host a nanometer-sized guest molecule at the

interface between an organic solution and HOPG. This method may be used to trap single molecules for applications in molecular electronics or in sensors by appropriate chemical modification in the peripheries of suitable PAHs.

4.3 Investigation of molecular multilayers

4.3.1 HBC-amine bilayer

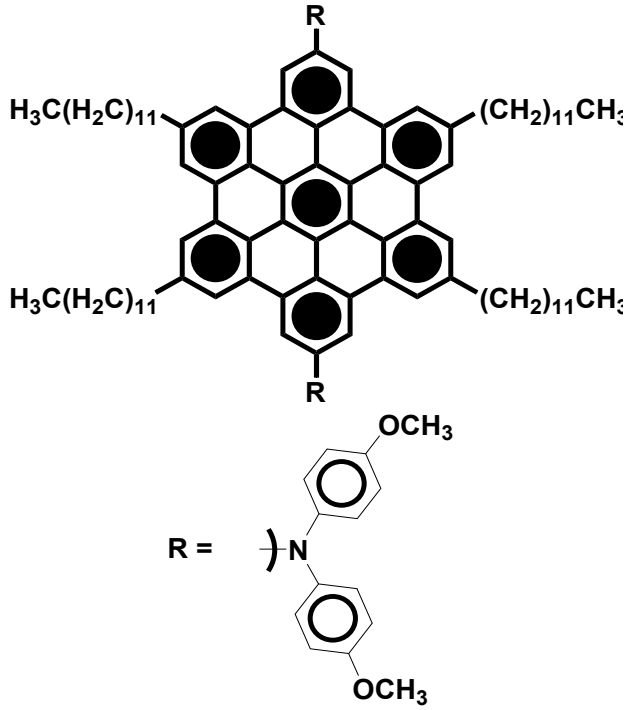

Chart 4.5: Chemical structures of HBC-diamine molecules.

Organic light-emitting diodes led to a practical display technology due to the distinctive attractions such as low materials costs, self-emission, efficient and broad color tenability, compatibility with complementary metal-oxide-semiconductor technology, and amenability to large-scale production. The principle of emission in OLEDs involves injection of electrons and holes from the cathode and anode, respectively, under application of an electric field. Some fraction of the electron-hole pairs recombine to form excitons, which in turn radiatively decay to the ground state and emit light. The scheme of a typical multilayer OLED is depicted in Schematic 4.1. The hole transport layer (HTL), the emissive layer (EML), and the electron transport layer (ETL) are all incorporated between the two electrodes. Recently much effort has been devoted to developing new HTL materials to fulfill criteria such as substantial hole mobility, good energy level matching with anodes and EMLs, i.e. low hole injection barriers from the anode to HTL and from HTL to EML, large electron injection barrier from EML to HTL, and good thermal properties (stability; Tg), low optical absorption in the visible region,

smoothness, and amorphous film-forming morphologies [139]. Due to the electron-donating nature of the nitrogen atom in arylamines, they act as hole-transport materials widely used in organic optoelectronic devices [140]. Liquid crystalline HBC derivatives display extremely high charge carrier mobilities along the one dimensional □ -stacks [141]. Therefore, a candidate for efficient hole transport, HBC-amine (Chart 4.5), was designed, where HBC is peripherally attached with arylamine moieties. This compound may exhibit high charge carrier mobility in one dimension while columnar stacking occurs due to the strong π-π interaction between the HBC aromatic cores, and thus allows "coaxial" hole transport approaches, via HBC columns and via arylamine units [82]. In order to gain more insight into the behaviour of these molecules for potential further applications in organic electronics, thin layers of this compound were investigated at the solid-liquid interface via STM.

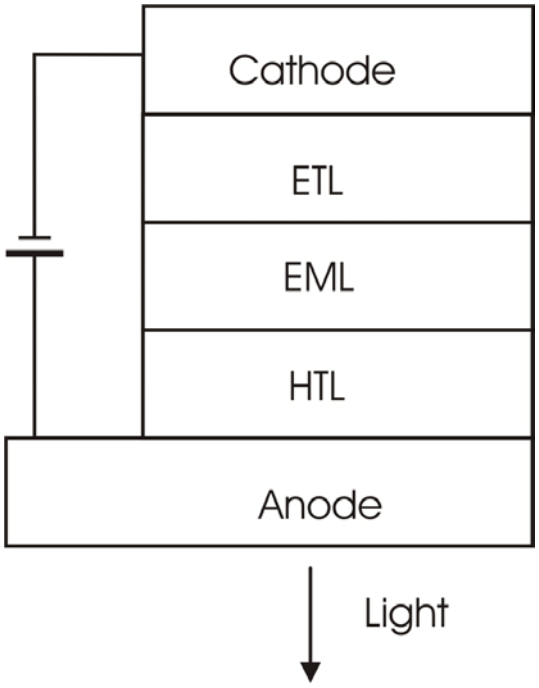

Schematic 4.1: A typical OLED structure. ETL: electron transport layer; EML: emitter layer; HTL: hole transport layer.

Figure 4.15 displays the molecular arrangement, which can be described by a unit cell with parameters of a = (2.64 ± 0.10) nm, b = (3.13 ± 0.16) nm, and $\alpha = (67 \pm 6)^{o}$ containing one molecule per unit cell. The angle between the short unit cell vector and a zig-zag-axis of the HOPG substrate was found to be $(29 \pm 4)^{o}$. The corresponding area (7.58 ± 0.45 nm^2) of a unit cell is larger than the van der Waars contour of a single molecule lying flat on HOPG (6.2 nm^2). In a high resolution STM image (Figure 4.15b), the slightly elongated objects can be assigned to □ -conjugated benzene rings and electron-rich nitrogen atoms. The dark part is

occupied by side chain and solvent molecules. The proposed packing model is depicted in Figure 4.16.

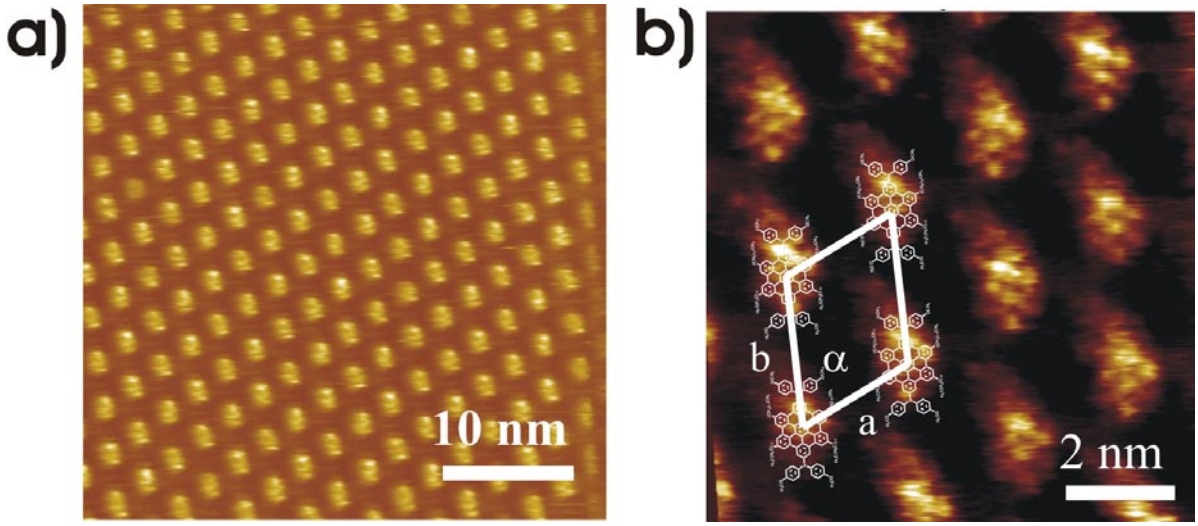

Figure 4.15: a) STM current images of a highly ordered arrangement of HBC-amine from a solution in 1,2,4-trichlorobenzene. U_s = - 0.6V, I_t = 100pA. b) High resolution STM current images of HBC-amine at U_s = - 0.6V and I_t = 100 pA.

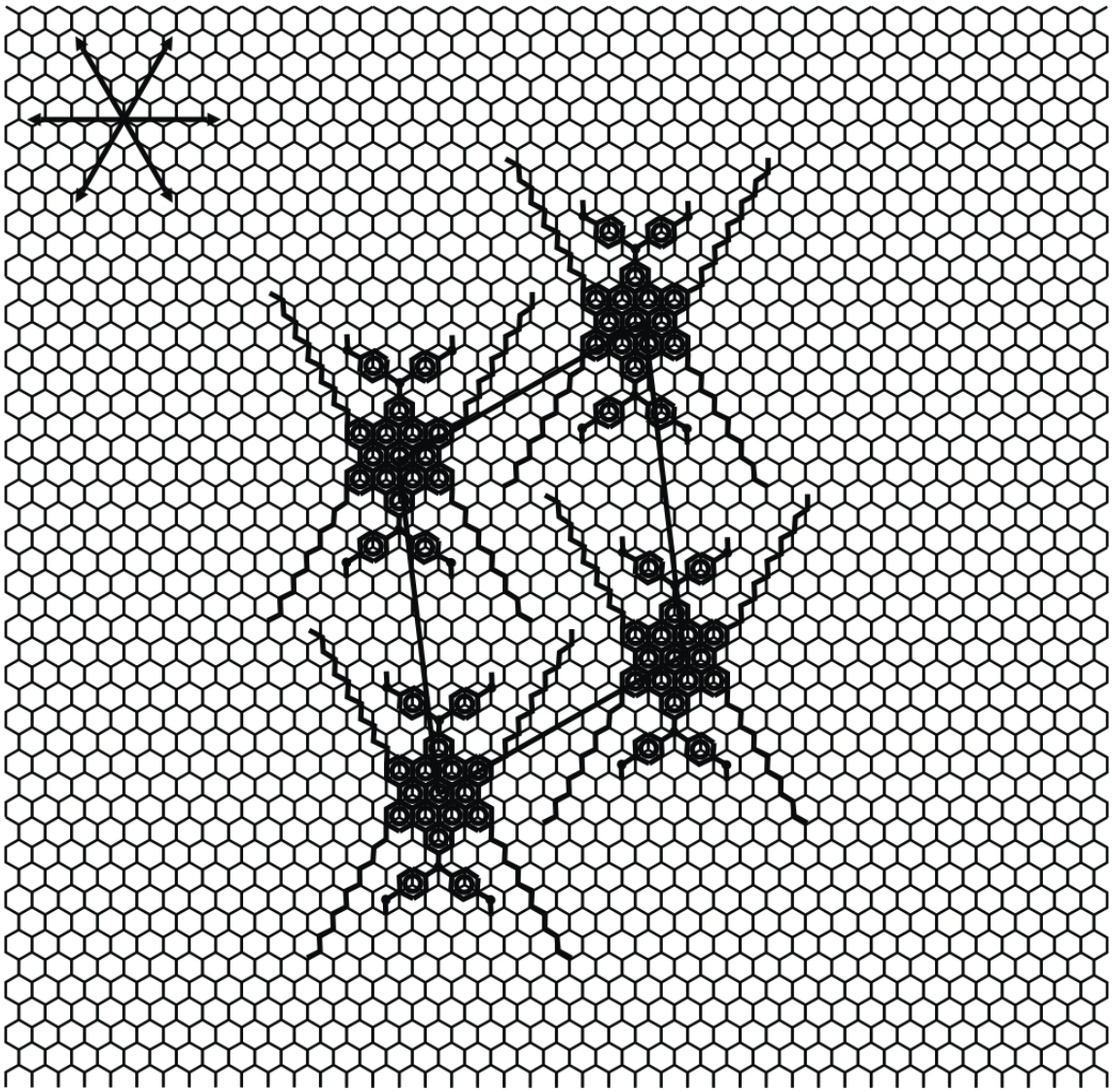

Figure 4.16: Proposed packing model for HBC-amine on HOPG.

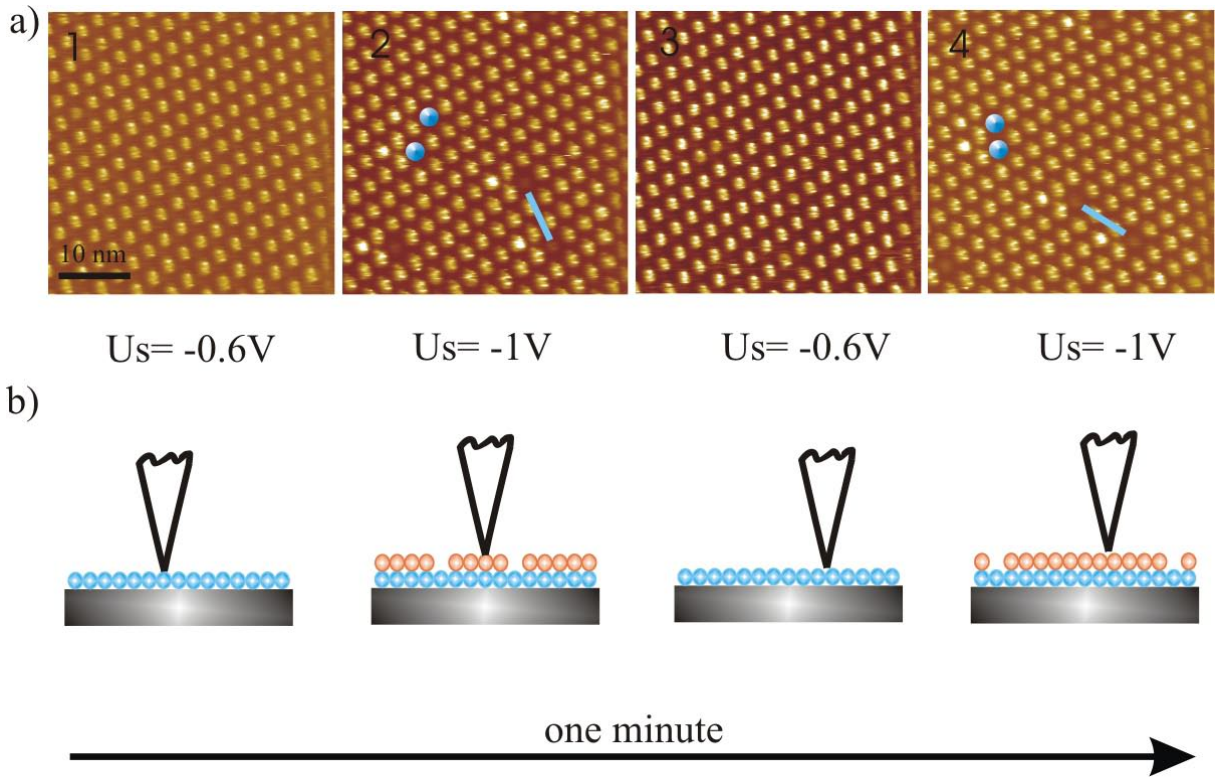

Abbildung 26: a) STM current images of HBC-amine from a solution in 1,2,4-trichlorobenzene. Tunneling parameters were (1) sample bias U_s = - 0.6V and tunneling current I_t = 100 pA, (2) U_s = - 1V, I_t = 100 pA, (3) U_s = - 0.6V, I_t = 100 pA, (4) U_s = - 1V, I_t = 100 pA. b) Schematic of images in a).

Figure 4.17 displays *in-situ* STM images recorded within one minute where the tip is moved from small to large distances to the substrate and *vice versa*. At small tunneling junction impedances (6 GΩ) in Figure 4.17a periodic nanostructures are displayed. The crystalline layer is highly perfect with the bright spots attributed to the conjugated molecular cores. At large tunneling junction impedances (10 GΩ), some weakly bright dots are indicated by the blue dots in Figure 4.17a. However, the positions of the weakly bright spots are inequivalent, as indicated by the blue bars. From the STM height image in Figure 4.18a, the depths between the bright spots and the voids are about 0.25 nm, which is shown in the cross-section profile of Figure 4.18b. Therefore, the dense molecular layer is attributed to the first layer at the small tunneling junction impedances. The less dense layer with some defects belongs to the second layer, where there are smaller interfacial forces exerted by the basal plane of the substrate, causing the molecules to be more mobile. The parameters of the unit cell in both layers are identical within the experimental accuracy. The different position of the defects in the second and the fourth image of Figure 4.17 occur, because the second layer is disturbed by the scanning tip, when imaging the first layer, and it recrystallizes when imaging the second layer. This molecular dynamics occurs on the time scale of a minute.

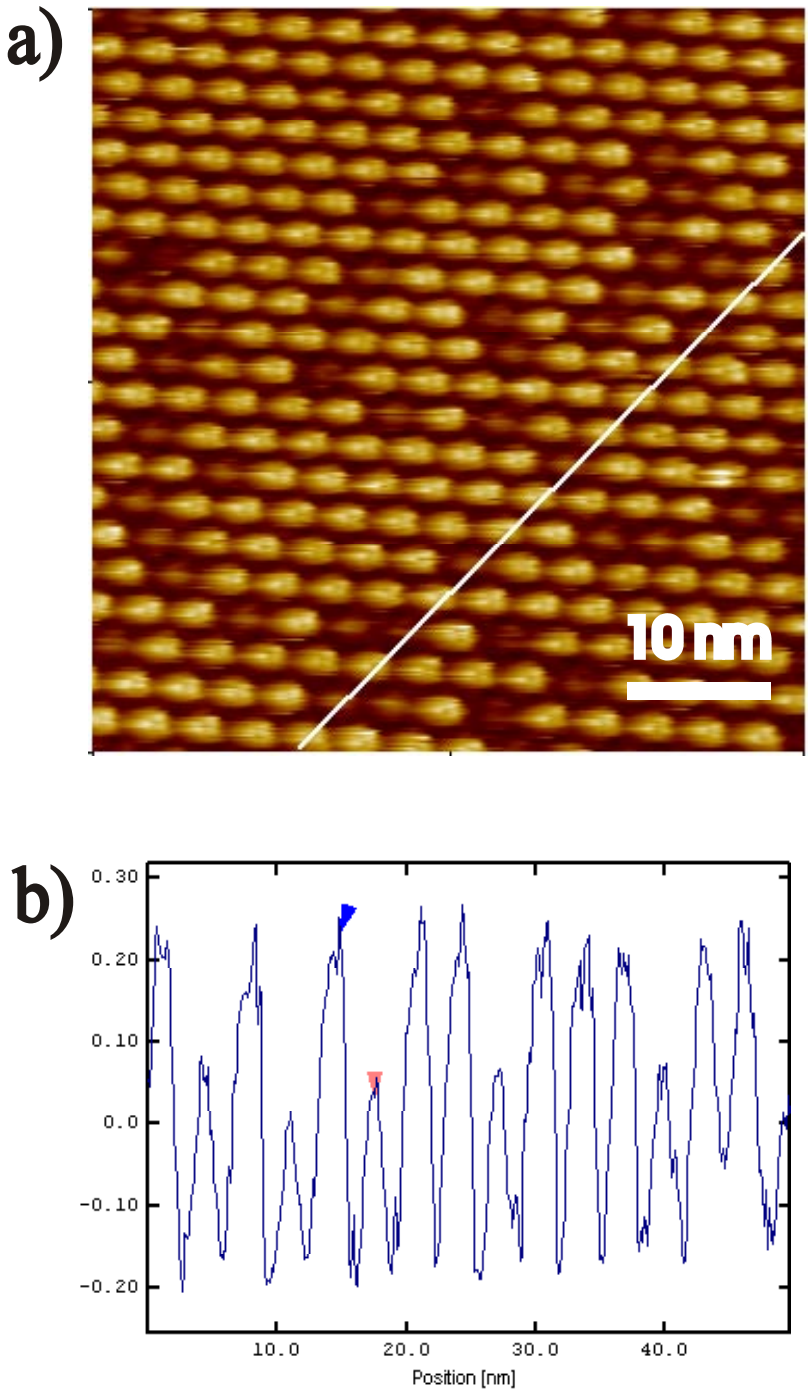

Figure 4.18: (a) STM height image of HBC-amine. U_s = - 1V ; I_t = 100 pA; Loop gain: 6%. (b) Cross-sectional profile along the line in (a).

In summary, the compound with a hole-transport enhancing amine and HBC moieties self-assembled into bilayers at the HOPG-solution in 1,2,4-trichlorobenzen. The phenomenon is determined by the interplay of intermolecular and interfacial forces on. The tendency to self-assemble on the time scale of less than a minute is observed by perturbing the second layer with the STM-tip.

4.3.2 Star-shaped nanographene derivative ordering with solvent

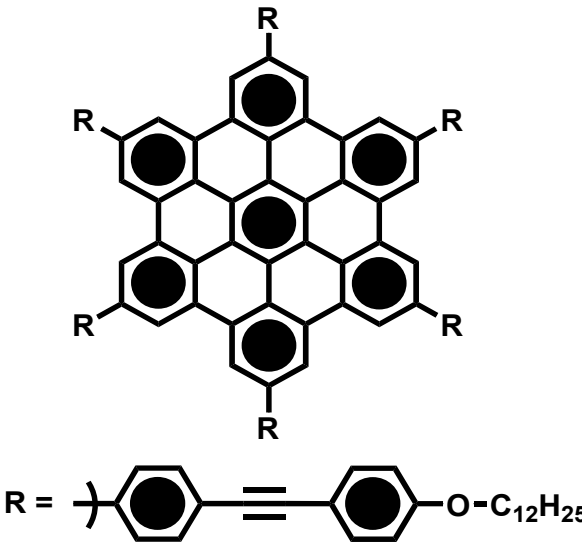

Chart 4.6: Chemical structure of HBC-star molecule.

Two- and three-dimensional architectures of well-defined molecular building blocks [142] are of major interest in the fields of microporous materials [143], molecular electronics [144,145,146,147] and molecular machines [148]. Their fabrication often relies on self-assembly processes using non-covalent intermolecular forces such as metal-ligand-complexation [143], hydrogen bonding [149,150,151,152], π-π-stacking [153,154], and interfacial forces [89]. At solid-solution interfaces the resulting architectures have been extensively studied by means of scanning tunneling microscopy [89,118,155]. However, little is known on the inclusion of solvents in these architectures [156,157].

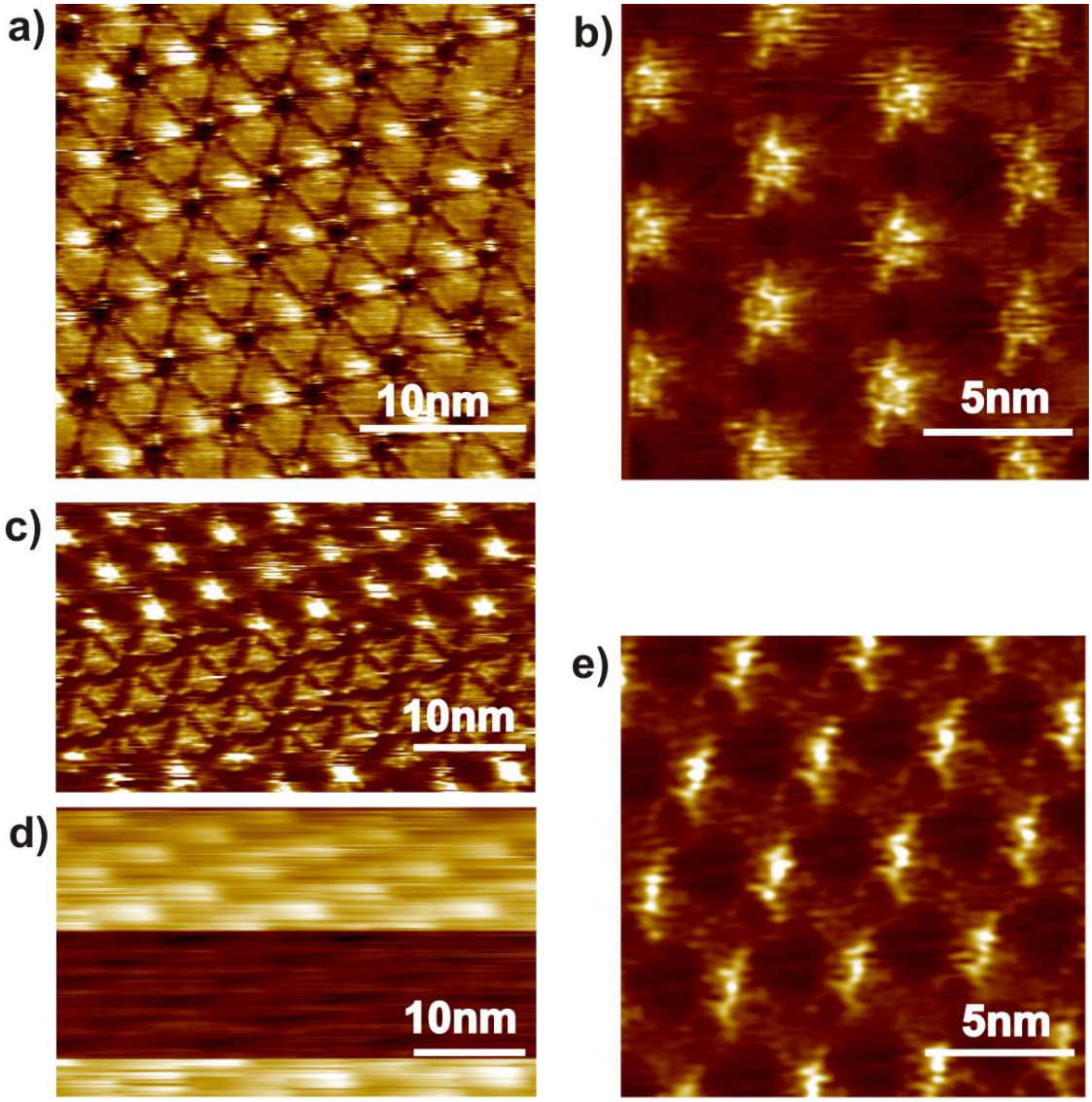

Abbildung 27: STM current images of HBC-star from a solution in 1,2,4-trichlorobenzene (a) in the first layer, (b) in the second layer and (c) simultaneously imaged first and second layer; (d) STM height image simultaneously recorded with (c) and (e). (e) STM current image of a monolayer of HBC-star from a solution in 1-phenyloctane. Tunneling parameters were: (a) sample bias U_s = -0.4 V and average tunneling current I_t = 500 pA, (b) U_s = -1.15 V, I_t = 100 pA, (b,c) U_s = -1.0 V, I_t = 200 pA and (e) U_s = -1.0 V, I_t = 80 pA [158].

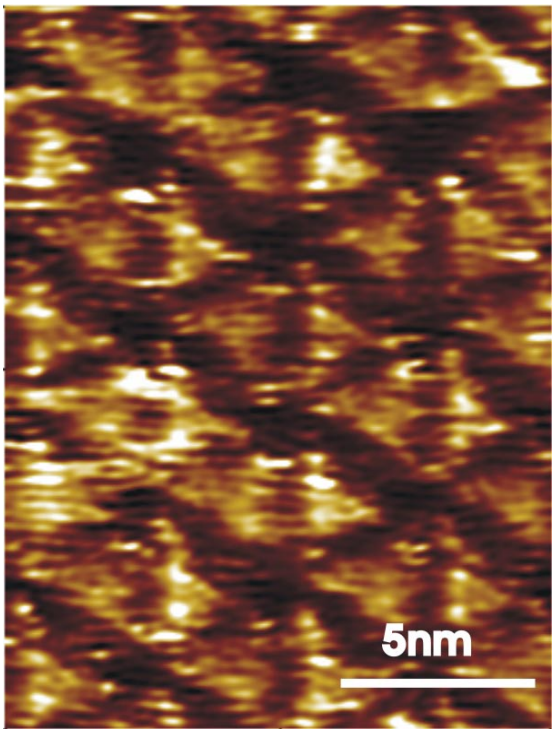

Figure 4.20: STM current images of HBC-star from a solution in 1,3-dichlorobenzene in the first layer [158].

Here an STM study is reported on the graphite-solution interface of an HBC-derivative (HBC-star, Chart 4.6) whose star-shaped molecular design provides cavities at the disk's periphery, which can be filled by smaller molecules. These voids hamper a dense packing of the molecules at the interface and they also allow for a fine-tuning of the supramolecular architectures' structure by applying solvents with different affinity to fill the voids [76].

Figure 4.19a displays an STM current image obtained from a solution of HBC-star in 1,2,4-trichlorobenzene at an average tunneling junction impedance of 0.8 GΩ. A regular pattern of triangles with large tunneling probability is visualized at both sample bias polarities. The dark (low tunneling probability) areas, in between the triangles reflect perfectly the size and shape of HBC-star molecules. The bright areas are attributed to solvent molecules filling the voids. The contrast implies that the current through the solvent filled areas is larger than through the nanographenes. The two-dimensional arrangement can be described by a unit cell ($a = (4.94 \pm 0.09)$ nm, $b = (5.05 \pm 0.07)$ nm, and $\alpha = (62 \pm 3)°$) containing two triangles, with an angle between the short unit cell vector and a zig-zag-axis of the HOPG substrate of $(6 \pm 4)°$. Upon increasing the tip-sample separation (average impedance of 11.5 GΩ) a different structure is observed (Figure 4.19b). Now, the nanographenes cause larger tunneling currents than the surrounding areas, which can be attributed to the low HOMO-LUMO-gap of HBC [72,121].

The parameters of the unit cell are identical to those determined for the structure observed at lower junction impedance.

Occasionally, the two different contrasts can be observed in the same image (Figure 4.19c), and the simultaneously recorded height image (Figure 4.19d) reveals a decrease in tip-sample separation for the structure consisting of triangles. From solutions of HBC-star in 1,3-dichlorobenzene (Figure 4.20) the same structures are observed within the experimental accuracy as from 1,2,4-trichlorobenzene solutions. Figure 4.19e displays an STM current image of the arrangement obtained from solutions of HBC-star in 1-phenyloctane. Here, exclusively one structure is found in which the star-shaped molecules can be recognized as bright features. The corresponding unit cell ($a = (4.27 \pm 0.14)$ nm, $b = (4.23 \pm 0.24)$ nm and $\alpha = (60 \pm 3)°$) is significantly smaller than the one observed from the solutions of HBC-star in the chlorinated benzenes.

In the chlorinated solvents the observed structures depend on the junction impedance, indicating double layer formation since the two structures are visualized at different tip-sample-separations [132]. Given that at even smaller impedances of ~0.1 GΩ the substrate itself is visualized we attribute the two different contrasts to a first and second layer, respectively. The, within the experimental accuracy, identical lattice constants of the two layers underline the epitaxial nature of the self-assembly process. Apparently, the interactions between the two layers are strong enough to allow for the visualization of the second layer at larger junction impedance. The large size of the unit cell and its shrinkage upon replacing the chlorinated benzenes by 1-phenyloctane suggests that only the smaller solvent molecules fill readily the voids provided by the star-shape of the molecules. The larger current through the areas filled with chlorinated benzenes is surprising since an orientation of the polar molecules in the electrical field of the STM would actually increase the tunneling barrier. However, lowering of tunneling barriers due to polar molecules, i.e. water, have previously been observed and investigated theoretically [159,160,161]. Explanations being discussed differ from the usually applied resonant tunneling models [102,121]; they include effects of the solvent on electrode work-functions and solvent supported resonant structures which let the effective barrier depend on the detailed structure and order of the polar layers [159,161,162].

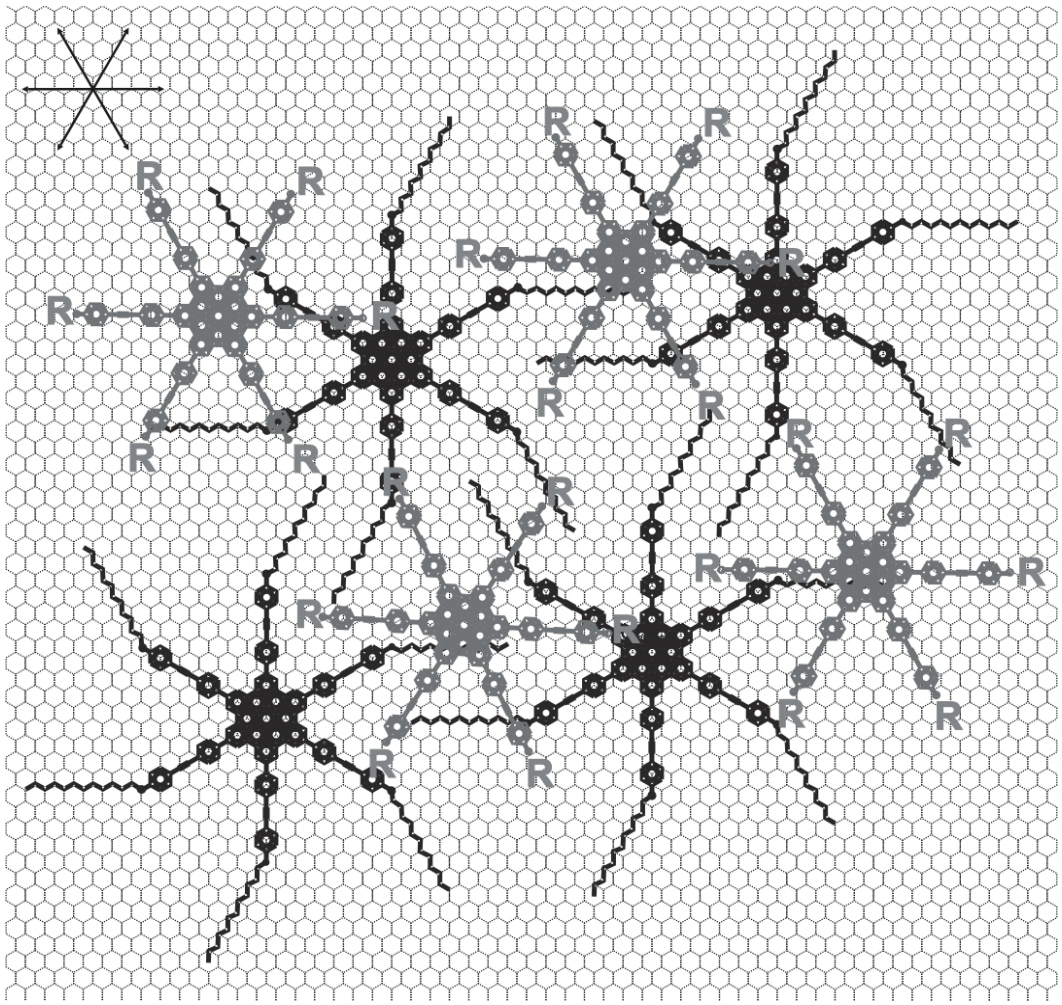

Figure 4.21: Packing model suggested for the double layer structure observed for HBC-star from solutions in 1,2,4-trichlorobenzene. The molecules in the first layer are depicted in black, those in the second in gray. The alkyl chains in the second layer have been replaced by R since their orientation is unknown [158].

Figure 4.21 displays a packing model for the observed double layer structure. It is constructed such that in the first layer the stars are placed at the sites of low tunneling current between the triangles and that the unit cell is reproduced within the experimental accuracy (a = 4.92 nm, b = 5.01 nm, α = 64°, and an angle of 7° with respect to HOPG in the model). If we assume an adsorption of the conjugated part onto the graphite in an A-B-type stacking, and an orientation of the alkyl chains along the zigzag axis of HOPG, a 30°-angle between the 'arms' of the star and the alkyl chains is found. Co-adsorbed solvent molecules are not shown since no detailed information on their adsorption geometry is available. The precise positions of the molecules in the second layer with respect to the first can be determined from images as shown in Fig. 1 d) or from images of the first layer on which a weak contrast modulation due to the second layer is observed (no images shown). The orientation of the arms in the second layer can be determined from high resolution images such as displayed in Figure 4.19b.

In conclusion, an STM study is presented of an epitaxially grown two-dimensional molecular scaffold of star-shaped nanographenes, stabilized by interfacial forces and liquid guests. The nature of the liquid allows to tune the structure which on the other hand may serve as model system to study in the same experiment the dependence of electron tunneling on order, mobility and polarity of different molecular adsorbates.

4.3.3 Alkylated phenyl-HBC nanostructure at an interface and on a surface

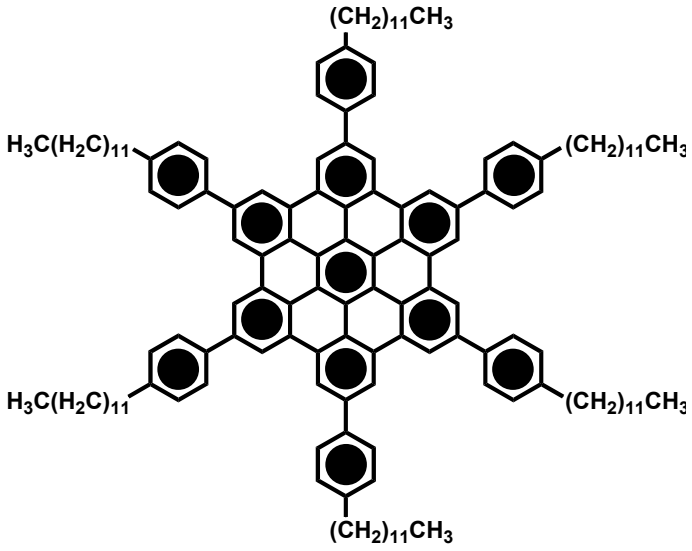

HBC-PhC$_{12}$

Chart 4.7: Chemical structure of HBC-PhC$_{12}$.

The good solubility and the high aggregation tendency of hexa(*para*-n-dodecylphenyl)hexabenzocoronene (HBC-PhC$_{12}$) molecules (Chart 4.7) have made them suitable candidates for novel electronic devices [61]. Recently, highly ordered HBC-PhC$_{12}$ films have been obtained by means of electrical fields [54]. The field was used to induce a dipole moment along the planar core of the HBC-PhC$_{12}$ molecules. As a consequence, the HBC-PhC$_{12}$ molecules orient their aromatic discs along the direction of the field lines and, due to the strong aggregation tendency, form columns perpendicularly aligned to the external electrical field. The HBC-PhC$_{12}$ cores, assembling in columnar aggregates, create an angle with the surface of 90°, defined as edge-on arrangement, which seems to be, independently from the presence of an external electrical field, the most stable HBC-PhC$_{12}$ packing on a glass surface [54].

The assembly behavior of HBC-PhC_{12} molecules at the interface of a solution in 1,2,4-trichlorobenzene with HOPG was investigated by *in-situ* STM. HBC-PhC_{12} molecules were physisorbed at the interface between the HOPG and a solution in 1,2,4-trichlorobenzene.

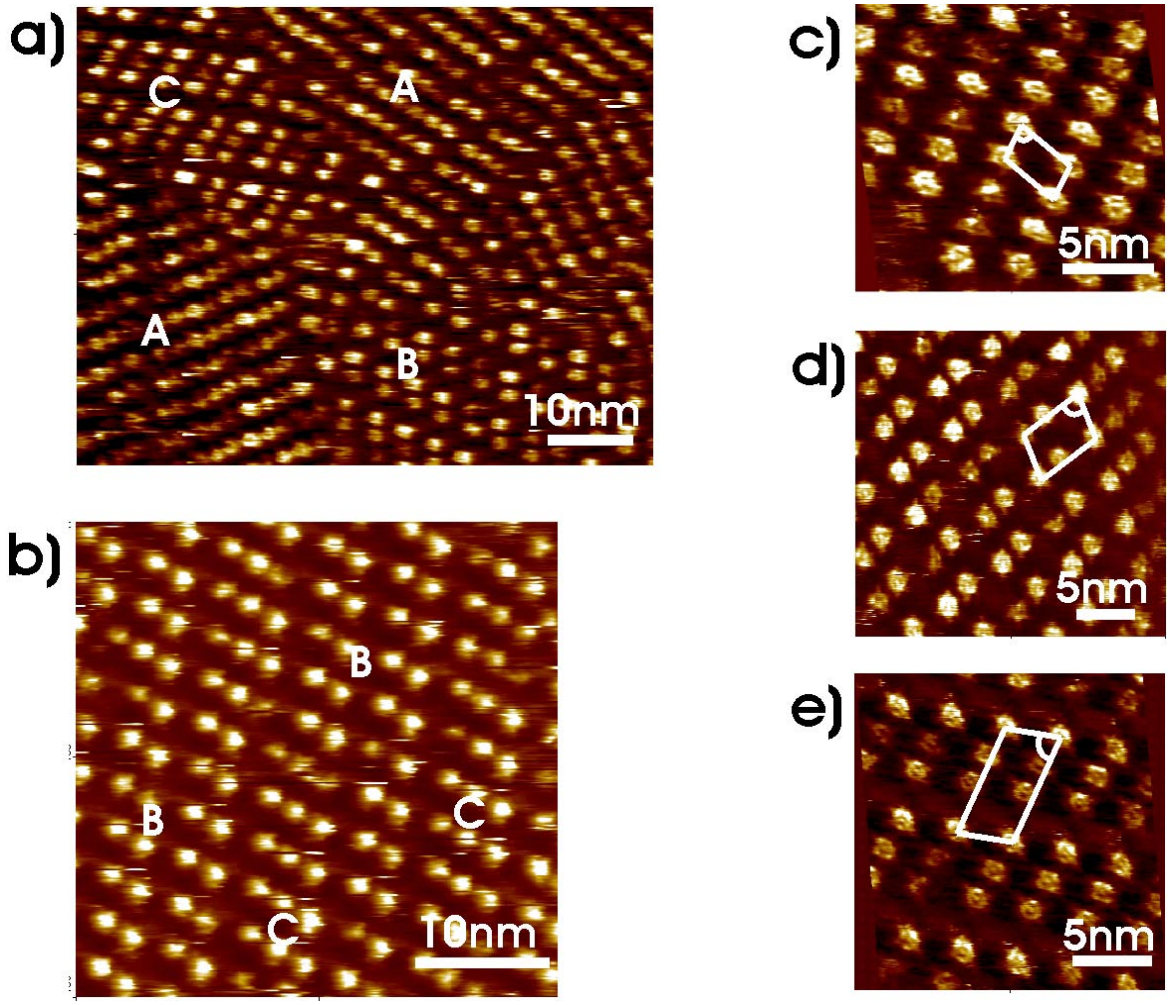

Figure 4.22: STM current images of HBC-PhC_{12} at the HOPG-solution interface. Sample bias U_s= 1 V; average tunneling current I_t = 0.1 nA. a) Large scale images with three patterns marked by A, B and C. b) B and C patterns. c) Oblique structure, ascribed to pattern A. d) Dimer structure B. e) Trimer structure C [55].

In the STM current images (Figure 4.22), the monolayer nanostructures are displayed, where the bright features (corresponding to high tunneling probability) can be attributed to π-conjugated aromatic rings. The aliphatic side chains, which are attributed to the dark parts of the images, could not be resolved.

Three different types of the 2D unit cells are presented in Figure 4.22, marked with A, B and C. The two-dimensional lattice A (Figure 4.22c) is an oblique structure described by a unit

cell with parameters a = (2.01 ± 0.11) nm, b = (3.30 ± 0.17) nm, and α = (76 ± 4)°. In case B (Figure 4.22d), the 2D unit cell is a dimeric structure (a = (3.41 ± 0.05) nm, b = (5.54 ± 0.19) nm, and α = (74 ± 1)°). The lattice constant of the trimer C, containing three molecules in a unit cell, is a = (3.48 ± 0.04) nm, b = (7.50 ± 0.34) nm, and α = (75 ± 2)°. Most abundant is the oblique pattern, while the trimer structure is the rarest.

Interestingly, a random distribution of two dissimilar contrasts of the aromatic core in all of the three domains at the HOPG-liquid interface is recorded [123]. It could possibly be attributed to a conformational change of the HBC core with the lateral phenyls from planar to nonplanar, which causes a change in the electronic properties of the HBC cores, resulting in different contrasts in the STM images. Another interpretation would be different positions of the HBC cores with respect to the STM-tip and the substrate. In fact, the asymmetric position of the molecules between tip and substrate influences the contrast in STM current images, in accord with tunneling spectroscopy.

The morphology of the field-oriented thick HBC-PhC_{12} films on HOPG surface was additionally investigated by SFM in tapping mode (Figure 4.23a and b).

Two kinds of domains can be recognized in the film, indicated by A and B. In the zoomed image (Figure 4.23b) the domain A exhibits narrow parallel stripes with a distance of (3.43 ± 0.12) nm. In the domain B, wider stripes (6.42 ± 0.09) nm are visible. Both stripe patterns are on average oriented perpendicularly with respect to the direction of the formerly applied electric field (marked by the white arrow and $\bar{E}$). The width of the narrow stripes in domain A is in agreement with the size of a HBC-PhC_{12} molecule with totally stretched alkyl chains (3.46 nm). In domain B, the width of the wide stripes is about twice that in domain A. As for field-oriented HBC-PhC_{12} molecules on a glass surface [54], the stripes of 3.4 nm width can be attributed to HBC-PhC_{12} molecules, oriented in the field direction and assembled in unidirectionally aligned columns (Figure 4.23c). The 6.4 nm bright stripes may be formed by ordered dimers of HBC-PhC_{12}, which are schematized in Figure 4.23d.

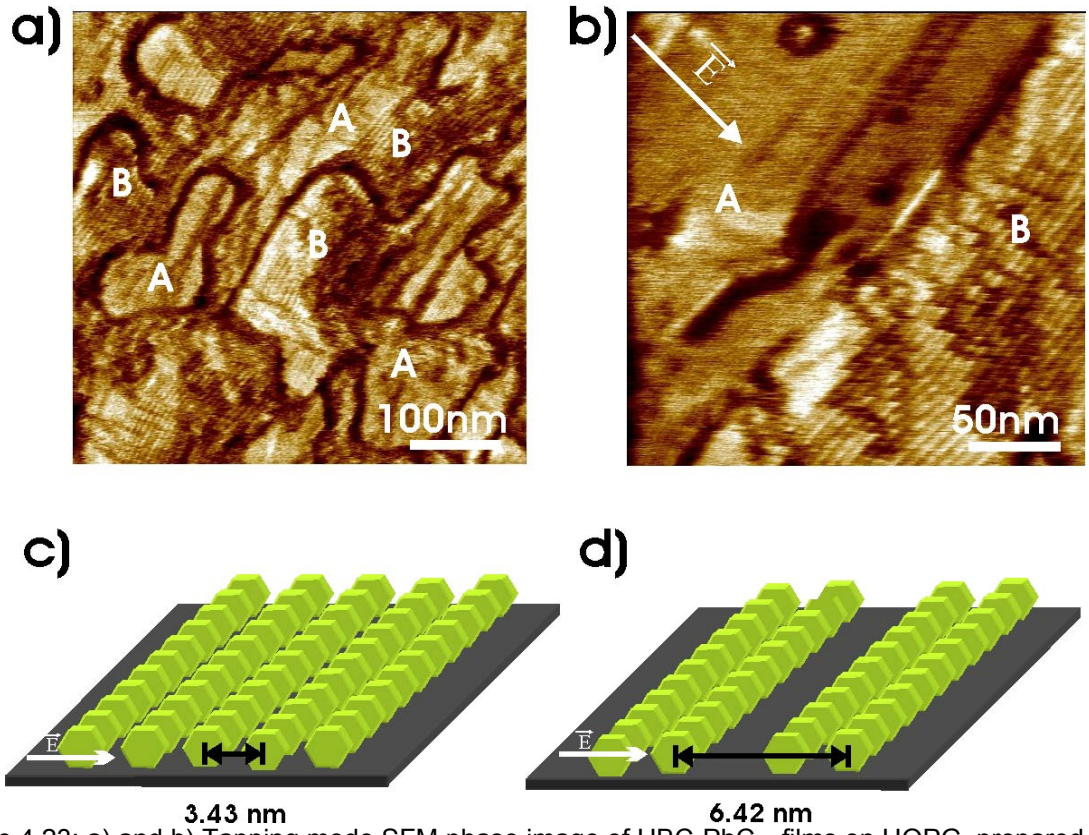

Figure 4.23: a) and b) Tapping mode SFM phase image of HBC-PhC$_{12}$ films on HOPG, prepared within electric fields. c) Schematic of single HBC-PhC$_{12}$ columns. d) Schematic of the stripes formed by two HBC-PhC$_{12}$ columns [55].

The formation of the wide stripes can be attributed to the high tendency of the HBC-PhC$_{12}$ molecules to assemble into dimer structures in 1,2,4-trichlorobenzene solvent, as the STM images of the molecules at the solid-liquid interface already proved (Figure 4.22).

The conclusion is drawn that this work demonstrates the three types of regular monolayer arrangements of face-on compound HBC-PhC$_{12}$ exhibit at the interface between the atomically flat basal plane of HOPG and solution. In addition, the order and the arrangement in thin films of HBC-PhC$_{12}$ on a HOPG surface are influenced by the external electrical fields. The presence of tilted edge-on molecules creating unidirectionally aligned domains demonstrates that electrical fields can be used to influence the strong interactions between HOPG and HBC-PhC$_{12}$, avoiding the epitaxial growth of thin films of these molecules in face-to-face arrangements parallel to the substrate. As morphology, crystal structure and molecular ordering of the first organic monolayers are essential determinants of carrier transport phenomena [163], the results of this investigation could be helpful for the basic understanding of novel electronic devices such as field effect transistors. The monolayers

obtained by the STM experiment at the solid-liquid interface help to explain the nanostructures from the thick film.

5 Conclusions and Outlooks

The STM investigations have revealed that derivatized nanographenes self-assemble quite generally as physisorbed mono-, bi- and multilayers at the interface between organic solutions and the basal plane of HOPG via inter-, intra-molecules and interfacial interactions.

In monolayers, various molecular patterns can be obtained from a great variety of nanographene derivatives. Firstly, zigzag and flower-like patterns can be formed from HBC derivatives, controlled by the symmetry of the alkyl substitution of HBC. Secondly, large C_3 symmetric conjugated PAHs substituted by bulky alkylated phenylene side chains self-assemble into highly regular honeycomb nanostructures, which is attributed to nanophase separation between the side chains and the PAH cores. The length and number of alkyl chains in *para*-position of the phenylene on the PAH cores play a key role for the self-assembly of honeycomb networks: for instance shorter side chains cause more defects in the network. Modified end groups of side chains influence the self-assembly of C_3 symmetric trizigzagHBC derivatives: a) When carboxyl groups are introduced, no molecular nanostructures were visualized, probably due to strong hydrogen bonding between carboxyl groups, which creates networks in solution, rather than forming molecular monolayers on HOPG. b) Honeycomb arrangements are observed if an electron donor moiety is attached to the end of the side chains. The electron donor moieties are found to be suspended in the solution, rather adsorbed on the basal plane of HOPG, indicating a weak interaction with the HOPG surface. c) Disordered nanostructures are found for nanographenes with an acceptor side group, since the electron acceptors may form charge transfer complexes with the PAH cores, counteracting the formation of honeycombs.

Two different molecules in the solution allow forming highly ordered mixed monolayers at the solid-liquid interface. Firstly, a mixed system of novel D_{3h} symmetric electron donors and alkylated acceptors reveals that the donors, which are not adsorbed as neat systems, are coadsorbed with the acceptors to form a monolayer on HOPG. This can be explained by a weak non-covalent donor-acceptor intermolecular interaction within the same layer (“parallel interaction”). Secondly, the cavities of honeycomb patterns are formed by C_3 symmetric conjugated PAHs with ester-end groups of their alkyl side chains. They can accommodate a guest molecule such as coronene. It is indicated that this kind of molecules may be used to trap single molecules for applications in molecular electronics or in sensors by appropriate

chemical modification in the peripheries of suitable PAHs. Based on the results that a stable and robust honeycomb architecture has been obtained, and by functionalizing the end groups of its alkyl side chains, one has the capability of a honeycomb forming PAH to host a nanometer-sized guest molecule at the interface between an organic solution and HOPG. This method may be used to host single switchable moieties to tune the dipole moment for applications in molecular electronics.

Bilayers can be formed from star-shaped nanographene derivatives due to solvent molecules, which can be incorporated in the supramolecular architecture. Another bilayer is self-assembled by the compound with hole-transporting amine and HBC moieties, controlled by the interplay of intermolecular and interfacial forces on HOPG. Moreover, some repair or self-assembly can be followed on the time scale of less than a minute. The self-assembled bilayers have potential application in nanowires.

Multilayers are produced in thin films of HBC-PhC_{12} on a HOPG surface within external electrical fields, providing "edge-on" arrangements on the surface. However, without external electrical fields, the molecules order in "face-on" patterns on HOPG. The presence of tilted edge-on molecules creating unidirectionally aligned domains demonstrates that electrical fields can be used to influence the strong interactions between HOPG and HBC-PhC_{12}. This prevents the epitaxial growth of thin films of these molecules in face-to-face arrangements parallel to the substrate. The "edge-on" morphology could be used for organic electronic devices such as organic field effect transistors.

The work presented in this thesis raises a number of new questions. For instance, it would be interesting now to investigate the electronic properties of the various PAHs in the different structures by STS and corresponding theoretical calculations, in order to device molecular systems with optimized functionalities for molecular and organic electronics. Particularly, the electronic properties of nanographene derivatives in bilayers bear a large potential in that regard. If the *I-V* characteristics of the molecules determined by STS are identical in the first and second layer, this indicates that the PAH disks in the two layers are lying face to face, and exhibit a small lateral offset [164]. However, when the *I-V*s are extremely different, it means that large lateral offset and edge-to-head overlap exists between the two disks within the bilayers [47]. Both situations may be employed in electronic devices.

On the theoretical side, molecular mechanics calculations could provide useful information for the interpretation of the different experimentally observed arrangements of the PAH derivatives on the basal plane of graphite. These studies should allow assignments of the observed submolecular contrast in the experimental images to specific parts of the molecules.

6 References

[1] Zaumseil, J. und Sirringhaus, H. (2007): Electron and ambipolar transport in organic field-effect transistors, Chemical Reviews 107 ,1296-1323. URL: ISI:000245600000011
[2] Walzer, K.; Maennig, B.; Pfeiffer, M. und Leo, K. (2007): Highly efficient organic devices based on electrically doped transport layers, Chemical Reviews 107 ,1233-1271. URL: ISI:000245600000009
[3] Hoppe, H. und Sariciftci, N. S. (2004): Organic solar cells: An overview, Journal of Materials Research 19 ,1924-1945. URL: ISI:000222418200004
[4] Berggren, M.; Dodabalapur, A.; Slusher, R. E. und Bao, Z. (1997): Organic lasers based on Forster transfer, Synthetic Metals 91 ,65-68. URL: ISI:000071756200014
[5] Mullen, K und Rabe, J. P (2008): Nanographenes as active components of single-molecule electronics and how a scanning tunneling microscope puts them to work, Accounts of Chemical Research 41 ,511.
[6] Binnig, G.; Rohrer, H.; Gerber, C. und Weibel, E. (1982): Tunneling Through A Controllable Vacuum Gap, Applied Physics Letters 40 ,178-180. URL: ISI:A1982NA28300030
[7] Binnig, G.; Rohrer, H.; Gerber, C. und Weibel, E. (1983): 7X7 Reconstruction on Si(111) Resolved in Real Space, Physical Review Letters 50 ,120-123. URL: ISI:A1983PW72600010
[8] Shirakawa, H. (2001): The discovery of polyacetylene film: The dawning of an era of conducting polymers (Nobel lecture), Angewandte Chemie-International Edition 40 ,2575-2580. URL: ISI:000169988300001
[9] Lo, S. C. und Burn, P. L. (2007): Development of dendrimers: Macromolecules for use in organic light-emitting diodes and solar cells, Chemical Reviews 107 ,1097-1116. URL: ISI:000245600000006
[10] Tang, C. W. und Vanslyke, S. A. (1987): Organic Electroluminescent Diodes, Applied Physics Letters 51 ,913-915. URL: ISI:A1987J991800015
[11] Koch, N. (2007): Organic electronic devices and their functional interfaces, Chemphyschem 8 ,1438-1455. URL: ISI:000248251100001
[12] Ebisawa, F.; Kurokawa, T. und Nara, S. (1983): Electrical-Properties of Polyacetylene Polysiloxane Interface, Journal of Applied Physics 54 ,3255-3259. URL: ISI:A1983QU28800054
[13] Horowitz, G.; Fichou, D.; Peng, X. Z.; Xu, Z. G. und Garnier, F. (1989): A Field-Effect Transistor Based on Conjugated Alpha-Sexithienyl, Solid State Communications 72 ,381-384. URL: ISI:A1989AW81700014
[14] Rotzoll, R.; Mohapatra, S.; Olariu, V.; Wenz, R.; Grigas, M.; Dimmler, K.; Shchekin, O. und Dodabalapur, A. (2006): Radio frequency rectifiers based on organic thin-film transistors, Applied Physics Letters 88 . URL: ISI:000236250100112
[15] Zhou, L. S.; Wanga, A.; Wu, S. C.; Sun, J.; Park, S. und Jackson, T. N. (2006): All-organic active matrix flexible display, Applied Physics Letters 88 . URL: ISI:000235553300083
[16] Tang, C. W. (1986): 2-Layer Organic Photovoltaic Cell, Applied Physics Letters 48 ,183-185. URL: ISI:A1986AXV0300035
[17] Gunes, S.; Neugebauer, H. und Sariciftci, N. S. (2007): Conjugated polymer-based organic solar cells, Chemical Reviews 107 ,1324-1338. URL: ISI:000245600000012

[18] Knox, W. H.; Fork, R. L.; Downer, M. C.; Stolen, R. H.; Schank, C. V. und Valdmanis, J. A. (1985): Optical pulse-compression to 8 fs at a 5-kHz repetition rate, Applied Physics Letters 46 ,1120.
[19] Samuel, I. D. W. und Turnbull, G. A. (2007): Organic semiconductor lasers, Chemical Reviews 107 ,1272-1295. URL: ISI:000245600000010
[20] Curtis, M. D.; Cao, J. und Kampf, J. W. (2004): Solid-state packing of conjugated oligomers: from pi-stacks to the herringbone structure, Journal of the American Chemical Society 126 ,4318-4328. URL: ISI:000220637100060
[21] Jaiswal, M. und Menon, R. (2006): Polymer electronic materials: a review of charge transport, Polymer International 55 ,1371-1384. URL: ISI:000242503100004
[22] Mann, B. und Kuhn, H. (1971): Tunneling Through Fatty Acid Salt Monolayers, Journal of Applied Physics 42 ,4398-&. URL: ISI:A1971K595900043
[23] Aviram, A. und Ratner, M. A. (1974): Molecular Rectifiers, Chemical Physics Letters 29 ,277-283. URL: ISI:A1974U851400031
[24] Vulillaume, D. (2008): Molecular-scale electronics, Comptes Rendus Physique 9 ,78-94. URL: ISI:000254650000009
[25] Barth, J. V.; Costantini, G. und Kern, K. (2005): Engineering atomic and molecular nanostructures at surfaces, Nature 437 ,671-679. URL: ISI:000232157900041
[26] Redl, F. X.; Cho, K. S.; Murray, C. B. und O'Brien, S. (2003): Three-dimensional binary superlattices of magnetic nanocrystals and semiconductor quantum dots, Nature 423 ,968-971. URL: ISI:000183753900044
[27] Rotzoll, R.; Mohapatra, S.; Olariu, V.; Wenz, R.; Grigas, M.; Dimmler, K.; Shchekin, O. und Dodabalapur, A. (2006): Radio frequency rectifiers based on organic thin-film transistors, Applied Physics Letters 88 . URL: ISI:000236250100112
[28] Warburton, R. J.; Schaflein, C.; Haft, D.; Bickel, F.; Lorke, A.; Karrai, K.; Garcia, J. M.; Schoenfeld, W. und Petroff, P. M. (2000): Optical emission from a charge-tunable quantum ring, Nature 405 ,926-929. URL: ISI:000087732700043
[29] Michler, P.; Kiraz, A.; Becher, C.; Schoenfeld, W. V.; Petroff, P. M.; Zhang, L. D.; Hu, E. und Imamoglu, A. (2000): A quantum dot single-photon turnstile device, Science 290 ,2282-+. URL: ISI:000165995800036
[30] Burkard, G.; Loss, D.; DiVincenzo, D. P. und Smolin, J. A. (1999): Physical optimization of quantum error correction circuits, Physical Review B 60 ,11404-11416. URL: ISI:000083554800029
[31] Xie, X. N.; Chung, H. J.; Sow, C. H. und Wee, A. T. S. (2006): Nanoscale materials patterning and engineering by atomic force microscopy nanolithography, Materials Science & Engineering R-Reports 54 ,1-48. URL: ISI:000243844700001
[32] Rosei, F. und Raiteri, P. (2002): Stress induced surface melting during the growth of the Ge wetting layer on Si(001) and Si(111), Applied Surface Science 195 ,16-19. URL: ISI:000177458900003
[33] Chen, W. und Wee, A. T. S. (2007): Self-assembly on silicon carbide nanomesh templates, Journal of Physics D-Applied Physics 40 ,6287-6299. URL: ISI:000249983900014
[34] Theobald, J. A.; Oxtoby, N. S.; Phillips, M. A.; Champness, N. R. und Beton, P. H. (2003): Controlling molecular deposition and layer structure with supramolecular surface assemblies, Nature 424 ,1029-1031. URL: ISI:000184984200036
[35] Silly, F.; Shaw, A. Q.; Porfyrakis, K.; Briggs, G. A. D. und Castell, M. R. (2007): Pairs and heptamers of C-70 molecules ordered via PTCDI-melamine supramolecular networks, Applied Physics Letters 91 . URL: ISI:000251908100076

[36] Griessl, S. J. H.; Lackinger, M.; Jamitzky, F.; Markert, T.; Hietschold, M. und Heckl, W. M. (2004): Room-temperature scanning tunneling microscopy manipulation of single C-60 molecules at the liquid-solid interface: Playing nanosoccer, Journal of Physical Chemistry B 108 ,11556-11560. URL: ISI:000223002400044
[37] Stepanow, S.; Lingenfelder, M.; Dmitriev, A.; Spillmann, H.; Delvigne, E.; Lin, N.; Deng, X. B.; Cai, C. Z.; Barth, J. V. und Kern, K. (2004): Steering molecular organization and host-guest interactions using two-dimensional nanoporous coordination systems, Nature Materials 3 ,229-233. URL: ISI:000220747700016
[38] Zhang, Y. F.; Zhu, N. und Komeda, T. (2008): Programming of a Mn-coordinated 4-4 '-biphenyl dicarboxylic acid nanosystem on Au(111) and investigation of the non-covalent binding of C60 molecules, Surface Science 602 ,614-619. URL: ISI:000253277900031
[39] Huang, H.; Chen, W.; Chen, L.; Zhang, H. L.; Sen Wang, X.; Bao, S. N. und Wee, A. T. S. (2008): "Zigzag" C-60 chain arrays, Applied Physics Letters 92 . URL: ISI:000252470900084
[40] Zhang, Y. F.; Zhu, N. und Komeda, T. (2008): Programming of a Mn-coordinated 4-4 '-biphenyl dicarboxylic acid nanosystem on Au(111) and investigation of the non-covalent binding of C60 molecules, Surface Science 602 ,614-619. URL: ISI:000253277900031
[41] Schull, G.; Douillard, L.; Fiorini-Debuisschert, C.; Charra, F.; Mathevet, F.; Kreher, D. und Attias, A. J. (2006): Single-molecule dynamics in a self-assembled 2D molecular sieve, Nano Letters 6 ,1360-1363. URL: ISI:000238973100011
[42] Furukawa, S.; Tahara, K.; De Schryver, F. C.; Van der Auweraer, M.; Tobe, Y. und De Feyter, S. (2007): Structural transformation of a two-dimensional molecular network in response to selective guest inclusion, Angewandte Chemie-International Edition 46 ,2831-2834. URL: ISI:000245904700010
[43] Novoselov, K. S.; Geim, A. K.; Morozov, S. V.; Jiang, D.; Katsnelson, M. I.; Grigorieva, I. V.; Dubonos, S. V. und Firsov, A. A. (2005): Two-dimensional gas of massless Dirac fermions in graphene, Nature 438 ,197-200. URL: ISI:000233133500042
[44] Meyer, J. C.; Geim, A. K.; Katsnelson, M. I.; Novoselov, K. S.; Booth, T. J. und Roth, S. (2007): The structure of suspended graphene sheets, Nature 446 ,60-63. URL: ISI:000244525600036
[45] McCann, E. und Fal'ko, V. I. (2006): Landau-level degeneracy and quantum hall effect in a graphite bilayer, Physical Review Letters 96 . URL: ISI:000235736200060
[46] Watson, M. D.; Fechtenkotter, A. und Mullen, K. (2001): Big is beautiful - "Aromaticity" revisited from the viewpoint of macromolecular and supramolecular benzene chemistry, Chemical Reviews 101 ,1267-1300. URL: ISI:000168684700008
[47] Jackel, F.; Watson, M. D.; Mullen, K. und Rabe, J. P. (2004): Prototypical single-molecule chemical-field-effect transistor with nanometer-sized gates, Physical Review Letters 92 . URL: ISI:000221277900068
[48] Palermo, V.; Morelli, S.; Simpson, C.; Mullen, K. und Samori, P. (2006): Self-organized nanofibers from a giant nanographene: effect of solvent and deposition method, Journal of Materials Chemistry 16 ,266-271. URL: ISI:000234887700015
[49] van de Craats, A. M.; Stutzmann, N.; Bunk, O.; Nielsen, M. M.; Watson, M.; Mullen, K.; Chanzy, H. D.; Sirringhaus, H. und Friend, R. H. (2003): Meso-epitaxial solution-growth of self-organizing discotic liquid-crystalline semiconductors, Advanced Materials 15 ,495-499. URL: ISI:000182120000007

[50] Schmidt-Mende, L.; Fechtenkotter, A.; Mullen, K.; Moons, E.; Friend, R. H. und MacKenzie, J. D. (2001): Self-organized discotic liquid crystals for high-efficiency organic photovoltaics, Science 293 ,1119-1122. URL: ISI:000170432600054
[51] van de Craats, A. M.; Warman, J. M.; Mullen, K.; Geerts, Y. und Brand, J. D. (1998): Rapid charge transport along self-assembling graphitic nanowires, Advanced Materials 10 ,36-+. URL: ISI:000071781100004
[52] van de Craats, A. M.; Warman, J. M.; Mullen, K.; Geerts, Y. und Brand, J. D. (1998): Rapid charge transport along self-assembling graphitic nanowires, Advanced Materials 10 ,36-+. URL: ISI:000071781100004
[53] Tracz, A.; Jeszka, J. K.; Watson, M. D.; Pisula, W.; Mullen, K. und Pakula, T. (2003): Uniaxial alignment of the columnar super-structure of a hexa (alkyl) hexa-peri-hexabenzocoronene on untreated glass by simple solution processing, Journal of the American Chemical Society 125 ,1682-1683. URL: ISI:000181088000001
[54] Cristadoro, A.; Lieser, G.; Rader, H. J. und Mullen, K. (2007): Field-force alignment of disc-type pi systems, Chemphyschem 8 ,586-591. URL: ISI:000245057900014
[55] Cristadoro, A.; Ai, M.; Rader, H. J.; Rabe, J. P und Mullen, K (2008): Electrical field-induced alignment of nonpolar hexabenzocoronene molecules into columnar structures on highly oriented pyrolitic graphite investigated by STM and SFM, Journal of Physical Chemistry C 112 ,5563.
[56] Shklyarevskiy, I. O.; Jonkheijm, P.; Stutzmann, N.; Wasserberg, D.; Wondergem, H. J.; Christianen, P. C. M.; Schenning, A. P. H. J.; de Leeuw, D. M.; Tomovic, Z.; Wu, J. S.; Mullen, K. und Maan, J. C. (2005): High anisotropy of the field-effect transistor mobility in magnetically aligned discotic liquid-crystalline semiconductors, Journal of the American Chemical Society 127 ,16233-16237. URL: ISI:000233445900051
[57] Reitzel, N.; Hassenkam, T.; Balashev, K.; Jensen, T. R.; Howes, P. B.; Kjaer, K.; Fechtenkotter, A.; Tchebotareva, N.; Ito, S.; Mullen, K. und Bjornholm, T. (2001): Langmuir and Langmuir-Blodgett films of amphiphilic hexa-peri-hexabenzocoronene: New phase transitions and electronic properties controlled by pressure, Chemistry-A European Journal 7 ,4894-4901. URL: ISI:000172434500015
[58] Steinhart, M.; Wendorff, J. H.; Greiner, A.; Wehrspohn, R. B.; Nielsch, K.; Schilling, J.; Choi, J. und Gosele, U. (2002): Polymer nanotubes by wetting of ordered porous templates, Science 296 ,1997-1997. URL: ISI:000176273300043
[59] Pisula, W.; Tomovic, Z.; El Hamaoui, B.; Watson, M. D.; Pakula, T. und Mullen, K. (2005): Control of the homeotropic order of discotic hexa-peri-hexabenzocoronenes, Advanced Functional Materials 15 ,893-904. URL: ISI:000229708700001
[60] Liu, C. Y.; Fechtenkotter, A.; Watson, M. D.; Mullen, K. und Bard, A. J. (2003): Room temperature discotic liquid crystalline thin films of hexa-peri-hexabenzocoronene: Synthesis and optoelectronic properties, Chemistry of Materials 15 ,124-130. URL: ISI:000180368000021
[61] Schmidt-Mende, L.; Fechtenkotter, A.; Mullen, K.; Moons, E.; Friend, R. H. und MacKenzie, J. D. (2001): Self-organized discotic liquid crystals for high-efficiency organic photovoltaics, Science 293 ,1119-1122. URL: ISI:000170432600054
[62] Clar, E.; Ironside, C. T. und Zander, M. (1959): The Electronic Interaction Between Benzenoid Rings in Condensed Aromatic Hydrocarbons - 1,12-2,3-4,5-6,7-8,9-10,11-Hexabenzocoronene, 1,2-3,4-5,6-10,11-Tetrabenzoanthanthrene, and 4,5-6,7-11,12-13,14-Tetrabenzoperopyrene, Journal of the Chemical Society ,142-147. URL: ISI:A1959WK68200028

[63] Scholl, R. und Seer, C. (1912): The secession of aromatic bounded hydrogenn and the attachment of aromatic nuclei through aluminium chloride, Justus Liebigs Annalen der Chemie 394 ,111-177. URL: ISI:000200689900008
[64] Clar, E. und Stewart, D. G. (1953): Aromatic Hydrocarbons .65. Triangulene Derivatives, Journal of the American Chemical Society 75 ,2667-2672. URL: ISI:A1953UB52400035
[65] Clar, E. und Schmidt, W. (1979): Localized Vs Delocalized Molecular-Orbitals in Aromatic-Hydrocarbons, Tetrahedron 35 ,2673-2680. URL: ISI:A1979HZ65000010
[66] Halleux, A.; Martin, R. H. und King, G. S. D. (1958): Syntheses Dans la Serie des Derives Polycycliques Aromatiques Hautement Condenses - Lhexabenzo-1,12-2,3-4,5-6,7-8,9-10,11-Coronene, Le Tetrabenzo-4,5-6,7-11,12-13,14-Peropyrene et Le Tetrabenzo-1,2-3,4-8,9-10,11-Bisanthene, Helvetica Chimica Acta 41 ,1177-1183. URL: ISI:A1958WH77500001
[67] Muller, M.; Kubel, C. und Mullen, K. (1998): Giant polycyclic aromatic hydrocarbons, Chemistry-A European Journal 4 ,2099-2109. URL: ISI:000076896400002
[68] Hyatt, J. A. (1991): Synthesis of A Hexaalkynylhexaphenylbenzene, Organic Preparations and Procedures International 23 ,460-463. URL: ISI:A1991GE02100016
[69] Herwig, P.; Kayser, C. W.; Mullen, K. und Spiess, H. W. (1996): Columnar mesophases of alkylated hexa-peri-hexabenzocoronenes with remarkably large phase widths, Advanced Materials 8 ,510-&. URL: ISI:A1996UX58600012
[70] Fechtenkotter, A.; Saalwachter, K.; Harbison, M. A.; Mullen, K. und Spiess, H. W. (1999): Highly ordered columnar structures from hexa-peri-hexabenzocoronenes - Synthesis, X-ray diffraction, and solid-state heteronuclear multiple-quantum NMR investigations, Angewandte Chemie-International Edition 38 ,3039-3042. URL: ISI:000083248100011
[71] Kuebel, C.; Eckhardt, K.; Enkelmann, V.; Wegner, G. und Mullen, K. (2000): Synthesis and crystal packing of large polycyclic aromatic hydrocarbons: hexabenzo[bc,ef,hi,kl,no,qr]coronene and dibenzo[fg,ij]phenanthro[9,10,1,2,3-pqrst]pentaphene, Journal of Materials Chemistry 10 ,879-886. URL: ISI:000086049300010
[72] Mitchell, T. N. (1992): Palladium-Catalyzed Reactions of Organotin Compounds, Synthesis-Stuttgart ,803-815. URL: ISI:A1992JN48800001
[73] Stabel, A.; Heinz, R.; DeSchryver, F. C. und Rabe, J. P. (1995): Ostwald Ripening of 2-Dimensional Crystals at the Solid-Liquid Interface, Journal of Physical Chemistry 99 ,505-507. URL: ISI:A1995QB56800009
[74] Miyaura, N. und Suzuki, A. (1995): Palladium-Catalyzed Cross-Coupling Reactions of Organoboron Compounds, Chemical Reviews 95 ,2457-2483. URL: ISI:A1995TD89200007
[75] Takahashi, S.; Kuroyama, Y.; Sonogashira, K. und Hagihara, N. (1980): A Convenient Synthesis of Ethynylarenes and Diethynylarenes, Synthesis-Stuttgart ,627-630. URL: ISI:A1980KC96700012
[76] Wu, J. H.; Watson, M. D. und Mullen, K. (2003): The versatile synthesis and self-assembly of star-type hexabenzocoronenes, Angewandte Chemie-International Edition 42 ,5329-5333. URL: ISI:000186612600012
[77] Lambert, C. und Noll, G. (1998): One- and two-dimensional electron transfer processes in triarylamines with multiple redox centers, Angewandte Chemie-International Edition 37 ,2107-2110. URL: ISI:000075532600017

[78] Lambert, C. und Noll, G. (2002): Optically and thermally induced electron transfer pathways in hexakis[4-(N,N-diarylamino)phenyl]benzene derivatives, Chemistry-A European Journal 8 ,3467-3477. URL: ISI:000177387500018
[79] Wolfe, J. P. und Buchwald, S. L. (1997): Room temperature catalytic amination of aryl iodides, Journal of Organic Chemistry 62 ,6066-6068. URL: ISI:A1997XT05100070
[80] Hartwig, J. F.; Kawatsura, M.; Hauck, S. I.; Shaughnessy, K. H. und Alcazar-Roman, L. M. (1999): Room-temperature palladium-catalyzed amination of aryl bromides and chlorides and extended scope of aromatic C-N bond formation with a commercial ligand, Journal of Organic Chemistry 64 ,5575-5580. URL: ISI:000081766500034
[81] Ito, S.; Wehmeier, M.; Brand, J. D.; Kubel, C.; Epsch, R.; Rabe, J. P. und Mullen, K. (2000): Synthesis and self-assembly of functionalized hexa-peri-hexabenzocoronenes, Chemistry-A European Journal 6 ,4327-4342. URL: ISI:000165768700009
[82] Wu, J. S.; Baumgarten, M.; Debije, M. G.; Warman, J. M. und Mullen, K. (2004): Arylarnine-substituted hexa-peri-hexabenzocoronenes: Facile synthesis and their potential applications as "coaxial" hole-transport materials, Angewandte Chemie-International Edition 43 ,5331-5335. URL: ISI:000224592400007
[83] Brown, S. P.; Schnell, I.; Brand, J. D.; Mullen, K. und Spiess, H. W. (1999): An investigation of pi-pi packing in a columnar hexabenzocoronene by fast magic-angle spinning and double-quantum H-1 solid-state NMR spectroscopy, Journal of the American Chemical Society 121 ,6712-6718. URL: ISI:000081603000021
[84] Feng, X. L.; Wu, J. S.; Ai, M.; Pisula, W.; Zhi, L. J.; Rabe, J. P. und Mullen, K. (2007): Triangle-shaped polycyclic aromatic hydrocarbons, Angewandte Chemie-International Edition 46 ,3033-3036. URL: ISI:000246139400015
[85] Feng, X. L.; Wu, J. S.; Enkelmann, V. und Mullen, K. (2006): Hexa-peri-hexabenzocoronenes by efficient oxidative cyclodehydrogenation: The role of the oligophenylene precursors, Organic Letters 8 ,1145-1148. URL: ISI:000236048300034
[86] Atkins, P. W. (2006): Physical Chemistry, Oxford University Press, Oxford.
[87] Schreiber, F. (2000): Structure and growth of self-assembling monolayers, Progress in Surface Science 65 ,151-256. URL: ISI:000166558700001
[88] Rabe, J. P. und Buchholz, S. (1991): Commensurability and Mobility in 2-Dimensional Molecular-Patterns on Graphite, Science 253 ,424-427. URL: ISI:A1991FY28800033
[89] Rabe, J. P. und Buchholz, S. (1991): Direct Observation of Molecular-Structure and Dynamics at the Interface Between A Solid Wall and An Organic Solution by Scanning Tunneling Microscopy, Physical Review Letters 66 ,2096-2099. URL: ISI:A1991FH36600012
[90] Cyr, D. M.; Venkataraman, B. und Flynn, G. W. (1996): STM investigations of organic molecules physisorbed at the liquid-solid interface, Chemistry of Materials 8 ,1600-1615. URL: ISI:A1996VC73200010
[91] Samori, P.; Severin, N.; Mullen, K. und Rabe, J. P. (2000): Macromolecular fractionation of rod-like polymers at atomically flat solid-liquid interfaces, Advanced Materials 12 ,579-582. URL: ISI:000086831600013
[92] De Feyter, S.; Gesquiere, A.; Abdel-Mottaleb, M. M.; Grim, P. C. M.; De Schryver, F. C.; Meiners, C.; Sieffert, M.; Valiyaveettil, S. und Mullen, K. (2000): Scanning tunneling microscopy: A unique tool in the study of chirality, dynamics, and

reactivity in physisorbed organic monolayers, Accounts of Chemical Research 33 ,520-531. URL: ISI:000088922200002
[93] Ulman, A. (1996): Formation and structure of self-assembled monolayers, Chemical Reviews 96 ,1533-1554. URL: ISI:A1996UU36100017
[94] Love, J. C.; Estroff, L. A.; Kriebel, J. K.; Nuzzo, R. G. und Whitesides, G. M. (2005): Self-assembled monolayers of thiolates on metals as a form of nanotechnology, Chemical Reviews 105 ,1103-1169. URL: ISI:000228412800003
[95] Buriak, J. M. (2002): Organometallic chemistry on silicon and germanium surfaces, Chemical Reviews 102 ,1271-1308. URL: ISI:000175550000001
[96] Schreiber, F. (2000): Structure and growth of self-assembling monolayers, Progress in Surface Science 65 ,151-256. URL: ISI:000166558700001
[97] Diebold, U. (2003): The surface science of titanium dioxide, Surface Science Reports 48 ,53-229. URL: ISI:000186523100001
[98] Wiesendanger, R. (1994): Scanning Probe Microscopy and Spectroscopy, Cambridge University Press, Cambridge.
[99] Fischer; Kugler, M.; Maggio-Aprile, I.; Berthod, C. und Renner, C. (2007): Scanning tunneling spectroscopy of high-temperature superconductors, Reviews of Modern Physics 79 ,353.
[100] Fishcer; Kugler, M.; Maggio-Aprile, I.; Berthod, C. und Renner, C. (2007): Scanning tunneling spectroscopy of high-temperature superconductors, Reviews of Modern Physics 79 ,353.
[101] Hofer, W. A.; Foster, A. S. und Shluger, A. L. (2003): Theories of scanning probe microscopes at the atomic scale, Reviews of Modern Physics 75 ,1287-1331. URL: ISI:000186757200006
[102] Mizutani, W.; Shigeno, M.; Kajimura, K. und Ono, M. (1992): Tunneling Through A Deformed Potential, Ultramicroscopy 42 ,236-241. URL: ISI:A1992JL73700037
[103] Spong, J. K.; Mizes, H. A.; LaCom, L. J.; Dovek, M. M.; Frommer, J. E. und Foster, J. S. (1989): Contrast mechanism for resolving organic molecules with tunnelling microscopy, Nature 338 ,173.
[104] Villagomez, C. J.; Zambelli, T.; Gauthier, S.; Gourdon, A.; Stojkovic, S. und Joachim, C. (2009): STM images of a large organic molecule adsorbed on a bare metal substrate or on a thin insulating layer: Visualization of HOMO and LUMO, Surface Science 603 ,1526.
[105] Isrealachvili, J. N (1992): Intermolecular and surface forces, London.
[106] Law, B. M. und Rieutord, F. (2002): Electrostatic forces in atomic force microscopy, Physical Review B 66 . URL: ISI:000177338500098
[107] Giessibl, F. J. (2003): Advances in atomic force microscopy, Reviews of Modern Physics 75 ,949-983. URL: ISI:000185026100007
[108] Stifter, T.; Marti, O. und Bhushan, B. (2000): Theoretical investigation of the distance dependence of capillary and van der Waals forces in scanning force microscopy, Physical Review B 62 ,13667-13673. URL: ISI:000165556400053
[109] Kittel, C. (1971): Introduction to Solid State Physics, New York.
[110] Askadskaya, L.; Boeffel, C. und Rabe, J. P. (1993): Molecular-Structure and Dynamics Within Self-Assembled Hexakisalkoxy-Triphenylene Monolayers and Alkane Wetting Films, Berichte der Bunsen-Gesellschaft-Physical Chemistry Chemical Physics 97 ,517-521. URL: ISI:A1993KY59000046
[111] vandeCraats, A. M.; Warman, J. M.; deHaas, M. P.; Adam, D.; Simmerer, J.; Haarer, D. und Schuhmacher, P. (1996): The mobility of charge carriers in all four phases of the columnar discotic material hexakis(hexylthio)triphenylene: Combined

TOF and PR-TRMC results, Advanced Materials 8 ,823-&. URL: ISI:A1996VM08200010
[112] Lazzaroni, R.; Calderone, A.; Bredas, J. L. und Rabe, J. P. (1997): Electronic structure of molecular van der Waals complexes with benzene: Implications for the contrast in scanning tunneling microscopy of molecular adsorbates on graphite, Journal of Chemical Physics 107 ,99-105. URL: ISI:A1997XG24400012
[113] Adam, D.; Schuhmacher, P.; Simmerer, J.; Haussling, L.; Siemensmeyer, K.; Etzbach, K. H.; Ringsdorf, H. und Haarer, D. (1994): Fast Photoconduction in the Highly Ordered Columnar Phase of A Discotic Liquid-Crystal, Nature 371 ,141-143. URL: ISI:A1994PF19100058
[114] Scott, L. T.; Boorum, M. M.; McMahon, B. J.; Hagen, S.; Mack, J.; Blank, J.; Wegner, H. und de Meijere, A. (2002): A rational chemical synthesis of C-60, Science 295 ,1500-1503. URL: ISI:000173981300045
[115] van de Craats, A. M. und Warman, J. M. (2001): The core-size effect on the mobility of charge in discotic liquid crystalline materials, Advanced Materials 13 ,130-133. URL: ISI:000166930100008
[116] Tahara, K.; Furukawa, S.; Uji, I.; Uchino, T.; Ichikawa, T.; Zhang, J.; Mamdouh, W.; Sonoda, M.; De Schryver, F. C.; De Feyter, S. und Tobe, Y. (2006): Two-dimensional porous molecular networks of dehydrobenzo[12]annulene derivatives via alkyl chain interdigitation, Journal of the American Chemical Society 128 ,16613-16625. URL: ISI:000242941600065
[117] De Feyter, S.; Hofkens, J.; Van der Auweraer, M.; Nolte, R. J. M.; Mullen, K. und De Schryver, F. C. (2001): Nanometer space resolved photochemistry, Chemical Communications ,585-592. URL: ISI:000168009700001
[118] De Feyter, S. und De Schryver, F. C. (2005): Self-assembly at the liquid/solid interface: STM reveals, Journal of Physical Chemistry B 109 ,4290-4302. URL: ISI:000227629700002
[119] Barth, J. V.; Weckesser, J.; Lin, N.; Dmitriev, A. und Kern, K. (2003): Supramolecular architectures and nanostructures at metal surfaces, Applied Physics A-Materials Science & Processing 76 ,645-652. URL: ISI:000181806100001
[120] Samori, P.; Yin, X. M.; Tchebotareva, N.; Wang, Z. H.; Pakula, T.; Jackel, F.; Watson, M. D.; Venturini, A.; Mullen, K. und Rabe, J. P. (2004): Self-assembly of electron donor-acceptor dyads into ordered architectures in two and three dimensions: Surface patterning and columnar "double cables", Journal of the American Chemical Society 126 ,3567-3575. URL: ISI:000220286400054
[121] Lazzaroni, R.; Calderone, A.; Bredas, J. L. und Rabe, J. P. (1997): Electronic structure of molecular van der Waals complexes with benzene: Implications for the contrast in scanning tunneling microscopy of molecular adsorbates on graphite, Journal of Chemical Physics 107 ,99-105. URL: ISI:A1997XG24400012
[122] Jackel, F. (2005): Humboldt University.
[123] Samori, P.; Jackel, F.; Unsal, O.; Godt, A. und Rabe, J. P. (2001): Ordered nanostructures of a [2]catenane through self-assembly at surfaces - An STM study with sub-molecular resolution, Chemphyschem 2 ,461-464. URL: ISI:000169976000010
[124] Barth, J. V.; Weckesser, J.; Lin, N.; Dmitriev, A. und Kern, K. (2003): Supramolecular architectures and nanostructures at metal surfaces, Applied Physics A-Materials Science & Processing 76 ,645-652. URL: ISI:000181806100001
[125] Gearba, R. I.; Lehmann, M.; Levin, J.; Ivanov, D. A.; Koch, M. H. J.; Barbera, J.; Debije, M. G.; Piris, J. und Geerts, Y. H. (2003): Tailoring discotic mesophases:

Columnar order enforced with hydrogen bonds, Advanced Materials 15 ,1614-+. URL: ISI:000186000400008
[126] Murphy, A. R. und Frechet, J. M. J. (2007): Organic semiconducting oligomers for use in thin film transistors, Chemical Reviews 107 ,1066-1096. URL: ISI:000245600000005
[127] Facchetti, A. (2007): Semiconductors for organic transistors, Materials Today 10 ,28-37. URL: ISI:000244597300017
[128] Roncali, J. (1997): Synthetic principles for bandgap control in linear pi-conjugated systems, Chemical Reviews 97 ,173-205. URL: ISI:A1997WG46400007
[129] Pisula, W.; Kastler, M.; Wasserfallen, D.; Robertson, J. W. F.; Nolde, F.; Kohl, C. und Mullen, K. (2006): Pronounced supramolecular order in discotic donor-acceptor mixtures, Angewandte Chemie-International Edition 45 ,819-823. URL: ISI:000234987600031
[130] Fleming, A. J.; Coleman, J. N.; Dalton, A. B.; Fechtenkotter, A.; Watson, M. D.; Mullen, K.; Byrne, H. J. und Blau, W. J. (2003): Optical spectroscopy of isolated and aggregate hexabenzocoronene derivatives: A study of self-assembling molecular nanowires, Journal of Physical Chemistry B 107 ,37-43. URL: ISI:000180254900008
[131] Walzer, K.; Sternberg, M. und Hietschold, M. (1998): Formation and characterization of coronene monolayers on HOPG(0001) and MoS2(0001): a combined STM/STS and tight-binding study, Surface Science 415 ,376-384. URL: ISI:000076730300028
[132] Samori, P.; Severin, N.; Simpson, C. D.; Mullen, K. und Rabe, J. P. (2002): Epitaxial composite layers of electron donors and acceptors from very large polycyclic aromatic hydrocarbons, Journal of the American Chemical Society 124 ,9454-9457. URL: ISI:000177358600043
[133] Jackel, F.; Watson, M. D.; Mullen, K. und Rabe, J. P. (2006): Tunneling through nanographene stacks, Physical Review B 73 . URL: ISI:000235009700121
[134] Hoger, S.; Bonrad, K.; Mourran, A.; Beginn, U. und Moller, M. (2001): Synthesis, aggregation, and adsorption phenomena of shape-persistent macrocycles with extraannular polyalkyl substituents, Journal of the American Chemical Society 123 ,5651-5659. URL: ISI:000169338400006
[135] Grave, C.; Lentz, D.; Schafer, A.; Samori, P.; Rabe, J. P.; Franke, P. und Schluter, A. D. (2003): Shape-persistant macrocycles with terpyridine units: Synthesis, characterization, and structure in the crystal, Journal of the American Chemical Society 125 ,6907-6918. URL: ISI:000183359300027
[136] Kalsani, V.; Ammon, H.; Jackel, F.; Rabe, J. P. und Schmittel, M. (2004): Synthesis and self-assembly of a rigid exotopic bisphenanthroline macrocycle: Surface patterning and a supramolecular nanobasket, Chemistry-A European Journal 10 ,5481-5492. URL: ISI:000224783800023
[137] Mena-Osteritz, E. und Bauerle, P. (2001): Self-assembled hexagonal nanoarrays of novel macrocyclic oligothiophene-diacetylenes, Advanced Materials 13 ,243-+. URL: ISI:000167413000002
[138] Griessl, S. J. H.; Lackinger, M.; Jamitzky, F.; Markert, T.; Hietschold, M. und Heckl, W. M. (2004): Room-temperature scanning tunneling microscopy manipulation of single C-60 molecules at the liquid-solid interface: Playing nanosoccer, Journal of Physical Chemistry B 108 ,11556-11560. URL: ISI:000223002400044
[139] Kulkarni, A. P.; Tonzola, C. J.; Babel, A. und Jenekhe, S. A. (2004): Electron transport materials for organic light-emitting diodes, Chemistry of Materials 16 ,4556-4573. URL: ISI:000225078600017

[140] Thelakkat, M. (2002): Star-shaped, dendrimeric and polymeric triarylamines as photoconductors and hole transport materials for electro-optical applicatoins, Macromolecular Materials Engneering 287 ,442.
[141] van de Craats, A. M.; Warman, J. M.; Fechtenkotter, A.; Brand, J. D.; Harbison, M. A. und Mullen, K. (1999): Record charge carrier mobility in a room-temperature discotic liquid-crystalline derivative of hexabenzocoronene, Advanced Materials 11 ,1469-1472. URL: ISI:000084184800014
[142] Lehn, J. M. (1995): Supramolecular Chemistry - Concept and Perspectives, VCH, Weinheim.
[143] Kitagawa, S.; Kitaura, R. und Noro, S. (2004): Functional porous coordination polymers, Angewandte Chemie-International Edition 43 ,2334-2375. URL: ISI:000221307200005
[144] Joachim, C.; Gimzewski, J. K. und Aviram, A. (2000): Electronics using hybrid-molecular and mono-molecular devices, Nature 408 ,541-548. URL: ISI:000165548600107
[145] Carroll, R. L. und Gorman, C. B. (2002): The genesis of molecular electronics, Angewandte Chemie-International Edition 41 ,4379-4400. URL: ISI:000179752500001
[146] Maruccio, G.; Cingolani, R. und Rinaldi, R. (2004): Projecting the nanoworld: Concepts, results and perspectives of molecular electronics, Journal of Materials Chemistry 14 ,542-554. URL: ISI:000220224100013
[147] Nitzan, A. und Ratner, M. A. (2003): Electron transport in molecular wire junctions, Science 300 ,1384-1389. URL: ISI:000183181800033
[148] Collier, C. P.; Mattersteig, G.; Wong, E. W.; Luo, Y.; Beverly, K.; Sampaio, J.; Raymo, F. M.; Stoddart, J. F. und Heath, J. R. (2000): A [2]catenane-based solid state electronically reconfigurable switch, Science 289 ,1172-1175. URL: ISI:000088866600036
[149] Desiraju, G. R. (1995): Supramolecular Synthons in Crystal Engineering - A New Organic-Synthesis, Angewandte Chemie-International Edition in English 34 ,2311-2327. URL: ISI:A1995TF90400001
[150] EichhorstGerner, K.; Stabel, A.; Moessner, G.; Declerq, D.; Valiyaveettil, S.; Enkelmann, V.; Mullen, K. und Rabe, J. P. (1996): Self-assembly of a two-component hydrogen-bonded network: Comparison of the two-dimensional structure observed by scanning tunneling microscopy and the three-dimensional crystal lattice, Angewandte Chemie-International Edition in English 35 ,1492-1495. URL: ISI:A1996VC67100010
[151] Clair, S.; Pons, S.; Seitsonen, A. P.; Brune, H.; Kern, K. und Barth, J. V. (2004): STM study of terephthalic acid self-assembly on Au(III): Hydrogen-bonded sheets on an inhomogeneous substrate, Journal of Physical Chemistry B 108 ,14585-14590. URL: ISI:000223922500052
[152] Lackinger, M.; Griessl, S.; Heckl, W. A.; Hietschold, M. und Flynn, G. W. (2005): Self-assembly of trimesic acid at the liquid-solid interface - a study of solvent-induced polymorphism, Langmuir 21 ,4984-4988. URL: ISI:000229243800035
[153] Samori, P.; Francke, V.; Mullen, K. und Rabe, J. P. (1998): Growth of solution cast macromolecular pi-conjugated nanoribbons on mica, Thin Solid Films 336 ,13-15. URL: ISI:000078141900004
[154] Engelkamp, H.; Middelbeek, S. und Nolte, R. J. M. (1999): Self-assembly of disk-shaped molecules to coiled-coil aggregates with tunable helicity, Science 284 ,785-788. URL: ISI:000080056200040

[155] Rabe, J. P.; Buchholz, S. und Askadskaya, L. (1993): Scanning Tunneling Microscopy of Several Alkylated Molecular Moieties in Monolayers on Graphite, Synthetic Metals 54 ,339-349. URL: ISI:A1993KT78600042
[156] vandeCraats, A. M.; Warman, J. M.; deHaas, M. P.; Adam, D.; Simmerer, J.; Haarer, D. und Schuhmacher, P. (1996): The mobility of charge carriers in all four phases of the columnar discotic material hexakis(hexylthio)triphenylene: Combined TOF and PR-TRMC results, Advanced Materials 8 ,823-&. URL: ISI:A1996VM08200010
[157] Gyarfas, B. J.; Wiggins, B.; Zosel, M. und Hipps, K. W. (2005): Supramolecular structures of coronene and alkane acids at the Au(111)-solution interface: A scanning tunneling microscopy study, Langmuir 21 ,919-923. URL: ISI:000226614200019
[158] Jackel, F.; Ai, M.; Wu, J. S.; Mullen, K. und Rabe, J. P. (2005): Solvent molecules in an epitaxially grown scaffold of star-shaped nanographenes, Journal of the American Chemical Society 127 ,14580-14581. URL: ISI:000232780900026
[159] Pan, J.; Jing, T. W. und Lindsay, S. M. (1994): Tunneling Barriers in Electrochemical Scanning-Tunneling-Microscopy, Journal of Physical Chemistry 98 ,4205-4208. URL: ISI:A1994NH49000001
[160] Hugelmann, M. und Schindler, W. (2003): Tunnel barrier height oscillations at the solid/liquid interface, Surface Science 541 ,L643-L648. URL: ISI:000184970600001
[161] Nitzan, A. (2001): Electron transmission through molecules and molecular interfaces, Annual Review of Physical Chemistry 52 ,681-750. URL: ISI:000169246500024
[162] Hugelmann, M. und Schindler, W. (2003): Tunnel barrier height oscillations at the solid/liquid interface, Surface Science 541 ,L643-L648. URL: ISI:000184970600001
[163] Sheraw, C. D.; Jackson, T. N.; Eaton, D. L. und Anthony, J. E. (2003): Functionalized pentacene active layer organic thin-film transistors, Advanced Materials 15 ,2009-2011. URL: ISI:000187431300006
[164] Watson, M. D.; Jackel, F.; Severin, N.; Rabe, J. P. und Mullen, K. (2004): A hexa-peri-hexabenzocoronene cyclophane: An addition to the toolbox for molecular electronics, Journal of the American Chemical Society 126 ,1402-1407. URL: ISI:000188834900036

A Acknowledgements

To finish the whole work of the thesis, the help of professors, colleagues and friends was not absent.

I am extremely grateful to my supervisor, Prof. J. P. Rabe, who offered me the opportunity to a fantastic single macromolecule world. During my work, he has provided his patient educating, continual encouragement and scientific guidance. His clear understanding of nano and surface science, sharp insight through varieties of encountered problems and generously sharing his advice and ideas were very helpful and the main source to stimulate and propel the whole work. In the daily life, I really appreciate for his understanding and help.

Working in Prof. Rabe's group has given me the chance to work (and play) with a number of people. In particular, I would like to thank a former member of the group, Dr. Frank Jäckel, for teaching me to use the home-built STM, sharing his experience and discussing. I also want to thank Dr. Stefan Kirstein, Dr. Nikolai Severin and Prof. Dr. Norbert Koch for their invaluable advice. To the expertise of the technical and administrative support stuff, Sabine Schönherr, Lothar Geyer, Evi Problenz, Martina Sae-Chew and Claudia Stephan, I am very much obligated. I cannot express enough thanks to Jörn-Oliver Vogel, Hua Liang, Rolf Kniprath, Benjamin Bröker, Dr. Peng Wu, Dr. Jian Zhang, Omar Al-khatib, Steffen Duhm, Stefan Eilers, Hendrik Glowatzki, Carsten Jost, Philipp Lange, Tobias Liebig, Ingo Salzmann and Barner Jörg for their warm help in discussing in the projects and getting useful information for a foreigner in Germany.

I owe my appreciation to Prof. Klaus Müllen and some members from his group from the Max-Planck-Institute for Polymer Research in Mainz in Germany who provided high quality synthetic materials and always discussed results. I am particularly indebted to Dr. Jishan Wu, Dr. Xinliang Feng, Dr. Anna Cristadoro, Xi Dou for sharing ideas besides the molecular synthesis.

I acknowledged the financial support from the European Union through MAC-MES and from the SFB 658.

Finally, special thanks go to my husband, Wei Zhuang, my little boy, Aichen Zhuang, my parents and my sister family for their secretarial help, patience, understanding, endless encouragement and love. Without their love and endurance it would not have been possible to complete the long journey of time for doctorate works.

B Lebenslauf

Der Lebenslauf wird aus Datenschutzgründen nicht im Internet veröffentlicht.

C Publications

- M. Ai, S. Groeper, W. Zhuang, X. Dou, X. Feng, K. Müllen, J. P. Rabe,"Optical switching study of an azobenzene rigidly linked to a hexa-*peri*-hexabenzocoronene derivative in solution and at a solid-liquid interface", *Applied Physics A, Material Science and Processing* **2008**, 93, 277-283.
- A. Cristadoro, M. Ai, H. J. Räder, J. P. Rabe, K. Müllen, "Electrical Field-Induced Alignment of Non Polar Hexabenzocoronene Molecules into Columnar Structures on Highly Oriented Pyrolitic Graphite Investigated by STM and SFM", *J.Phys.Chem. C.* **2008**, 112, 5563-5566.
- X. Feng, W. Pisula, M. Ai, S. Gröper, J. P. Rabe, K. Müllen, "Unusual Symmetry Effect on Hexa-peri-hexabenzocoronene", *Chem. Mater.* **2008**, 20, 1191-1193.
- X. Feng, J. Wu, M. Ai, W. Pisola, L. Zhi, J. P. Rabe, K. Müllen, "Triangle-shaped Polycyclic Aromatic Hydrocarbons", *Angew. Chem. Int. Ed.* **2007**, 46, 3033-3036.
- F. Jäckel, M. Ai, J. Wu, K. Müllen, J. P. Rabe, "Solvent Molecules in an Epitaxially Grown Scaffold of Star-shaped Nanographenes" *J. Am. Chem. Soc.* **2005**, 127, 14580-14581.
- M. Ai, X. Feng, W. Zhuang, F. Jäckel, K. Müllen, J. P. Rabe, " Various peripheries of the trizigzagHBC derivatives influence on self-organization at the solid-liquid interfaces", manuscript in preparation.
- M. Ai, F. Jäckel, X. Feng, W. Zhuang, J. Wu, K. Müllen, J. P. Rabe, "Electron donor assembled at the solid-liquid interfaces via intermolecular donor-acceptor interaction within the same layer", manuscript in preparation.

D Erklärung

Hiermit erkläre ich, die Dissertation selbständig und nur unter Verwendung der angegebenen Hilfen und Hilfsmittel angefertigt zu haben.

Ich habe mich anderwärts nicht um einen Doktorgrad beworben und besitze einen entsprechenden Doktorgrad nicht.

Ich erkläre die Kenntnisnahme der dem Verfahren zugrunde liegenden Promotionsordnung der Mathematisch-Naturwissenschaftlichen Fakultät I der Humboldt-Universität zu Berlin.

Min Ai